UNIVERSITÀ
DEGLI STUDI
DI BRESCIA

DOTTORATO DI RICERCA IN **TECHNOLOGY FOR HEALTH**
Dipartimento di Ingegneria dell'Informazione

MED/36 - DIAGNOSTICA PER IMMAGINI E RADIOTERAPIA

CICLO XXXV

# SURGICAL NAVIGATION AND AUGMENTED REALITY FOR MARGINS CONTROL IN HEAD AND NECK CANCER


DOTTORANDO:

Dott. Marco Ferrari

SUPERVISORI

Ch.mo Prof. Roberto Maroldi, Università degli Studi di Brescia
Ch.mo Prof. Alberto Signoroni, Università degli Studi di Brescia
Ch.mo Prof. Alberto Deganello, Università degli Studi di Milano

# Index

# Riassunto (in Italian)

## USO DI SISTEMI DI NAVIGAZIONE CHIRURGICA E REALTÀ AUMENTATA PER OTTIMIZZARE IL CONTROLLO DEI MARGINI DI RESEZIONE NELLA CHIRURGIA ONCOLOGICA DEL DISTRETTO TESTA COLLO

I tumori maligni del distretto testa-collo rappresentano un insieme di lesioni dalle diverse caratteristiche patologiche, epidemiologiche e prognostiche. Per una porzione considerevole di tali patologie, l'intervento chirurgico finalizzato all'asportazione completa del tumore rappresenta l'elemento chiave del trattamento, quand'anche esso includa altre modalità quali la radioterapia e la terapia sistemica.

La qualità dell'atto chirurgico ablativo è pertanto essenziale al fine di garantire le massime chance di cura al paziente. Nell'ambito della chirurgia oncologica, la qualità delle ablazioni viene misurata attraverso l'analisi dello stato dei margini di resezione. Nello specifico, il pezzo operatorio risultante dall'asportazione chirurgica e/o i limiti del difetto risultante dall'asportazione stessa vengono studiati ad un livello microscopico (*i.e.*, tramite tecniche istologiche) per identificare la presenza di tessuto o cellule neoplastiche a livello dei margini di resezione. Quest'ultimo termine viene impiegato per far riferimento al piano di separazione tra il tessuto che viene asportato e il tessuto che rimane a costituire i limiti del difetto chirurgico. Qualora vengano identificate delle cellule neoplastiche in corrispondenza di un margine, la resezione sarà considerata incompleta, poiché si assumerà che una componente della neoplasia residui nei tessuti del paziente (*i.e.*, a livello del letto di resezione). Oltre a rappresentare un surrogato della qualità della resezione chirurgica, lo stato dei margini di resezione ha notevoli implicazioni da un punto di vista clinico e prognostico. Infatti, il coinvolgimento dei margini di resezione da parte della neoplasia rappresenta invariabilmente un fattore prognostico sfavorevole, oltre che implicare la necessità di intensificare i trattamenti postchirurgici (*e.g.*, ponendo indicazione alla chemioradioterapia adiuvante), comportando una maggiore tossicità per il paziente.

La proporzione di resezioni con margini positivi (*i.e.*, coinvolti dalla neoplasia) nel distretto testa-collo è tra le più elevate in ambito di chirurgia oncologica. La complessità anatomica di tale distretto, nonché la densità considerevole di strutture neurovascolari vitali, rappresentano le ragioni più frequentemente chiamate in causa per spiegare tale dato. L'intervento chirurgico ablativo avviene infatti in regioni dall'alta complessità morfologica, in cui il team chirurgico dispone, per poter eseguire l'atto terapeutico, dei propri sensi (vista, tatto), dell'ausilio di ottiche endoscopiche ad elevata magnificazione nel contesto di cavità naturali (*e.g.*, la cavità nasale, la cavità orale/orofaringea) e dello studio dettagliato degli esami radiologici preoperatori. Di conseguenza, la chirurgia oncologica del distretto testa-collo rappresenta un ambito super-specialistico di una certa attrattività in termini di implementazione tecnologica, con particolare riferimento alle tecnologie in grado di potenziare la capacità del chirurgo di visualizzare in tempo reale l'estensione della patologia.

In tale contesto si pone l'obiettivo del dottorato di cui questa tesi riporta i risultati. Le due tecnologie di cui si è analizzata l'utilità in termini di ottimizzazione dello stato dei margini di resezione sono la navigazione chirurgica con rendering tridimensionale e la realtà aumentata basata sulla videoproiezione di

immagini. Le sperimentazioni sono state svolte parzialmente presso l'Università degli Studi di Brescia, parzialmente presso l'Azienda Ospedale Università di Padova e parzialmente presso l'University Health Network (Toronto, Ontario, Canada).

I sistemi di navigazione chirurgica sono ampiamente diffusi nelle sale operatorie degli ospedali terziari e non-terziari. Tuttavia, l'impiego di tale tecnologia è comunemente rivolto alla prevenzione di eventi avversi intraoperatori, mentre i dati in merito all'impiego dei sistemi di navigazione per l'ottimizzazione dello stato dei margini di resezione sono scarsi e frammentari. Nel contesto dell'attività di ricerca di questo dottorato, un sistema di navigazione chirurgica con rendering tridimensionale è stato impiegato a partire da sperimentazioni precliniche su modello tumorale in plastica, per poi passare a modelli più complessi e realistici su cadavere e, infine, alla sperimentazione clinica. Nell'ambito della sperimentazione preclinica è emerso che l'impiego della tecnologia in studio migliora la qualità dei margini di resezione a prescindere dall'esperienza del chirurgo, con particolare riferimento ai margini costituiti interamente da tessuti molli. È inoltre risultato possibile applicare la metodica della navigazione finalizzata a delineare i margini di resezione alle tecniche endoscopiche grazie all'impiego del rendering di endoscopia virtuale. Nell'ambito clinico è stato organizzato uno studio prospettico single-arm con reclutamento nel periodo Marzo-Giugno 2021, nel contesto del quale sono stati analizzati *in primis* la fattibilità dell'implementazione della navigazione chirurgica per l'ottimizzazione dei margini di resezione e *in secundis* i benefici oncologici risultanti da tale implementazione. L'applicazione clinica delle tecniche di navigazione chirurgica studiate precedentemente in ambito preclinico è risultata logisticamente fattibile senza un sostanziale impatto sulle tempistiche perioperatorie, né l'evidenza di eventi avversi maggiori. Si è osservato inoltre un sostanziale vantaggio in termini di stato dei margini di resezione. Seppur con un follow-up eccessivamente breve per poter osservare dei vantaggi significativi da un punto di vista prognostico, tale studio dimostra che l'impiego della navigazione chirurgica con rendering tridimensionale conferisce dei sostanziali benefici in termini di ottimizzazione dello stato dei margini di resezione.

La seconda tecnologia studiata nell'ambito di questo dottorato è stata la realtà aumentata basata sull'impiego di un videoproiettore co-registrato con un sistema di navigazione chirurgica. Un sistema comprendente entrambe le tecnologie (*i.e.*, navigazione chirurgica e realtà aumentata basata sulla videoproiezione) è stato sviluppato presso il Guided Therapeutics Laboratory dell'University Health Network (Toronto, Ontario, Canada). Tale sistema è stato quindi testato in ambito preclinico su modelli di piccolo animale e modelli antropomorfi in plastica. Nell'ambito di tale sperimentazione è stato dimostrato che l'impiego di metodiche di realtà aumentata con videoproiezione non conferisce sostanziali vantaggi in termini di ottimizzazione dei margini di resezione rispetto alla navigazione chirurgica, specialmente laddove l'immagine videoproiettata a livello del campo operatorio sia rappresentata dalla superficie della neoplasia. Al contrario, la proiezione di linee di osteotomia predeterminate è risultata come una metodica particolarmente promettente, seppur non sostitutiva della navigazione chirurgica in termini di ottimizzazione dei margini di resezione. In base a tali risultati, si è concluso che la realtà aumentata con videoproiezione può rappresentare una metodica intraoperatoria utile a delineare le linee osteotomiche nel contesto di resezioni complesse del distretto craniocefalico. Di per sé, tuttavia, tale tecnologia non è risultata associata ad un franco miglioramento

dello stato dei margini di resezione rispetto alla navigazione chirurgica. Pertanto, si ritiene che la traslazione clinica di tale tecnologia debba avvenire in modo complementare a quella della navigazione chirurgica con rendering tridimensionale e con obiettivi non esclusivamente consistenti nell'ottimizzazione dello stato dei margini di resezione.

# Background

## Novel approaches in surgical management: how to assess surgical margins. Frail biological basis with promising future perspectives

*Ferrari et al. (2021), In: Vermorken et al. (eds) Critical Issues in Head and Neck Oncology; doi: 10.1007/978-3-030-63234-2_7*

**Introduction**

Understanding the physical interface between tumor and host is a fascinating topic, as it dictates our current ability to appreciate the mechanisms of local growth of tumor and plan a resection with an adequate cuff of surrounding normal tissues. Despite many uncertainties regarding the definition of "adequate margins" that should be achieved by surgeons, there is strong evidence that positivity of surgical margins is one of the main predictors of local control and overall survival in carcinomas of the upper aerodigestive tract. As a consequence, the presence of positive margins together with extranodal extension are the main factors supporting the use of chemotherapy in association with radiotherapy in the adjuvant setting.[1,2]

The present chapter provides a basic historical, biological, and practical background on the concept of margins, which is essential to appreciate the importance of future perspectives in the field of margin control for tumors of the head and neck.

**Historical Background: The Concept of "Margin"**

The concept of margin in oncologic surgery is almost 6 centuries younger than the word "cancer", which was coined by Hippocrates in view of the appearance of blood vessels surrounding a tumor and resembling the claws of a crab.[3,4] Thereafter, cancer was considered mostly as a "humoral disease", which was consequently deemed as non-curable through simple surgical excision. Galen should be credited for being the first to hypothesize that cancer can infiltrate surrounding tissue even beyond the sensitivity of the naked eye, an intuition driven by the observation that tumors tend to regrow in scars.[5] This assumption led to conclude that cancer should be removed together with a cuff of apparently normal tissue, which still remains the pillar of surgical oncology. Although the contribute of Galen in understanding cancer is considered as controversial,[6] the observation that a tumor can early return in areas adjacent to where it was completely excised can be considered as the first insight into the concept of margins. Thus, it can be estimated that the concept of "surgical margins" was born in the second century, which means almost six hundred years after Hippocrates. In the 19$^{th}$ century, Virchow and Lebert observed that a cancer is formed by "cancer cells", which have the ability to invade neighboring tissues in small groups, yet not producing macroscopic changes in the early phases.[5] This new understanding of cancer provided an essential explanation to the observation of Galen, thus corroborating that cancer can be theoretically cured through excision of adjacent tissues. Despite its ancient birth, the concept of surgical margins first settled in oncologic surgery at the end of the 19$^{th}$ century, with Halsted being one of the most distinguished oncologic surgeons to concretely apply this thought to surgical practice.[7] Although biological comprehension of cancer has seen a large number of steps forward since then, the basic concept of surgical margins has remained unchanged, namely removing enough tissue to ensure that all cancer cells are

included in the surgical specimen. On the other hand, the contemporary understanding of cancer biology suggests that cancer cells dissemination occurs from even early-stage tumors (also at a systemic level), thus rising some doubts on the belief that "removing all cancer cells" is the actual mechanism through which cancer is cured.[8]

**Current Biological Rationale of Margins in Head and Neck Surgery**

The recommendation to leave a margin of normal tissue surrounding the visible tumor stands in the awareness that tumor cells can subtly extend far beyond the macroscopic boundary of the tumor. In the head and neck, oral squamous cell carcinoma represents the most frequently analyzed cancer to assess the pattern of growth towards adjacent tissues. The histologic morphology of the interface between tumor and surrounding soft tissues has been classified in 5 patterns with increasing degree of aggressiveness (Figure 1).[9] Type 1 pattern is defined as "broad pushing front", meaning that the tumor grows expansively and does not release groups of cells beyond its surface. Type 2 is described as "finger-like" as the tumor front displays some appendices irregularly protruding towards neighboring tissues. From type 3 to type 5, non-contiguous groups of cells with heterogeneous shape and distance from the tumor front are observed. In the type 3 front, only tumor islands, which look like "fingers" that grow up to the point of detaching from the tumor, are observed. Smaller cell groups, strands, or even single cells located within 1 mm from the main tumor surface fall under the definition of type 4 front. Type 5 front of invasion, finally, displays the so-called "satellites", which consist of either a cell or a group of cells located 1 mm beyond the tumor front. The ability to subclinically infiltrate surrounding soft tissues such as fat, striated muscles, fascial structures, and loose connective areas intuitively increases with the type of invasion front. Oral cancer was also used to analyze the pattern of invasion of bone, with special reference to the mandible. Two modalities of extension towards bone have been observed: in the erosive pattern, the tumor causes bone resorption by activating osteoclasts along a broad front of invasion; in the infiltrative pattern, tumor cells grow between bony trabecula by partially maintaining the microscopic and macroscopic bony architecture.[10] Some authors surmised that the infiltrative pattern might represent a later phase of invasion of bone compared to the erosive pattern. Parallel to these mechanisms of infiltration of adjacent tissues, cancers can acquire the ability to grow along nerves and/or vessels, which all together provides tumor cells with a dense network of pathways to move distantly from the clinically appreciable mass.[11–13]


**Figure 1**. Patterns of local invasion of soft tissues according to Brandwein-Gensler *et al*.[9]

**Special Elements of Challenge in the Head and Neck Area**

The head and neck probably represents one of the most challenging areas of the human body to achieve adequately and homogeneously wide margins.

Although a number of factors contribute to the challenge, the need to preserve several vital functions most commonly compete with the delineation of a wide margin all along the tumor surface (Figure 2A). In fact, the head and neck are dense in neurovascular structures and essential effector organs such as the brain, eyes, tongue, and larynx, which constantly place the surgeon and multidisciplinary team in front of dilemmas on resectability versus non-resectability or preservation versus ablation.

The density of neural and vascular structures also provides cancers with a dense network of potential escape routes (Figure 2B). This further complicates the management of tumors displaying perineural and lymphovascular spread, as the vectors of microscopic growth of the disease might be numerous, thus making the genuine extension of the tumor deeply counterintuitive compared to the macroscopic shape of the lesion.

Biological heterogeneity is another element of complexity characterizing tumors of the head and neck. Besides the well-known variety of cancer types that exquisitely affect specific areas (*i.e.*, sinonasal tract, salivary glands), several degrees of biological aggressiveness have been observed within a single histology (Figure 2C). There is evidence that tumors pertaining to the same histological category can display widely different propensity to grow beyond the macroscopic boundaries of the lesion through budding, satellitosis, pagetoid growth, perineural spread, permeative bone invasion, or other mechanisms.[14–21] This fact poses an additional challenge, since a tumor, even though labelled with a reliable preoperative diagnosis, might potentially be amenable to a "close-margin" excision (*i.e.*, when microscopic local extension is limited) or could instead require a "wide-margin" resection (*i.e.*, when microscopic groups of cells deeply invade adjacent tissues) as far as is known prior to surgery.

The 3-dimensional shape of the tumor also hinders adequate and regular delineation of margins (Figure 2D). While often resembling a plaque or a sphere in the early phases of growth, advanced tumors of the head and neck acquire a 3-dimensional morphology that mirrors the complexity of subsite anatomy. This translates into a substantially increased chance of misorienting the plane of dissection with respect to one or other components of the tumor.[22]

The deep location of a tumor, which means that the lesion is located underneath an uninvolved epithelial plane, is not a rarity in the head and neck (Figure 2E). It can result from either the origin of the tumor (*e.g.*, salivary cancers, mesenchymal tumors), its growth pattern (*i.e.*, submucosal growth in mucosal carcinomas), or tumor history (*e.g.*, deep or nodal recurrences). Cancers with no superficial components force surgeons to infer the 3-dimensional configuration of the lesion based on imaging, palpation, and knowledge of anatomy, yet with a non-negligible risk for the resection to be misled.

Finally, improvement and implementation of non-surgical strategies bring to the operating theater an increasing number of patients with a tumor recurring within an irradiated and/or medically treated area (Figure 2F). Similarly, refinements in surveillance strategies allow identification of post-surgical recurrences that are often suitable for surgical re-excision. Post-treatment presentation frequently implies a cancer that is

multifocally dispersed within uninvolved yet deeply altered tissues, thus remarkably increasing the chance of leaving microscopic residual disease irrespective of the attention posed towards margin delineation.

These elements being considered altogether, surgical margins have been unsurprisingly a hot topic in head and neck oncology over the last decades.

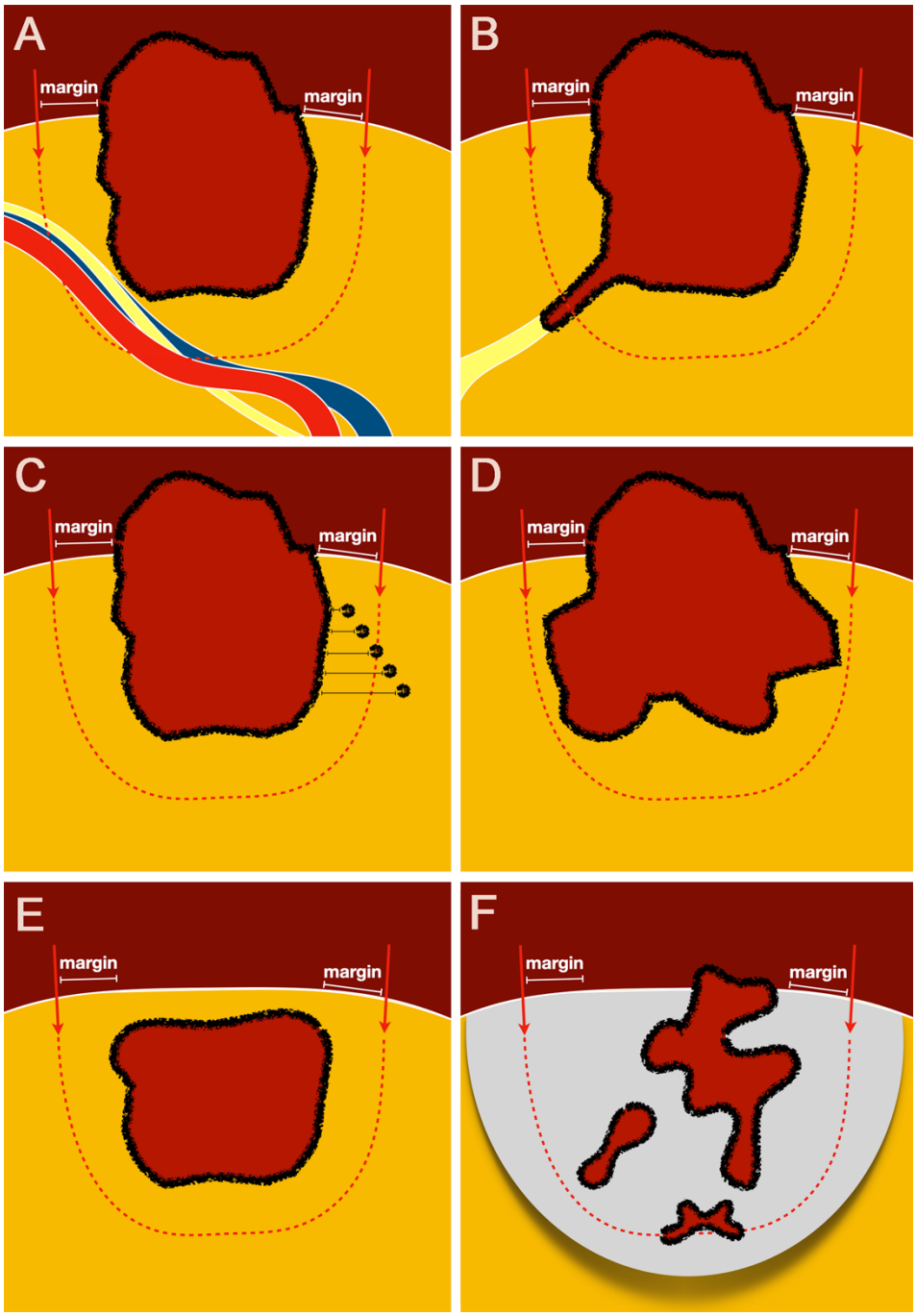


**Figure 2**. Special elements of challenge in the management of margins in cancers of the head and neck. **A**. Adjacency to critical neurovascular structures. **B**. High density of nerves and vessels providing cancer with a network of escape routes. **C**. Heterogeneous propensity towards subclinical extension into adjacent tissues. **D**. Complex 3-dimensional shape. **E**. Deep location of the tumor. **F**. Multifocal tumor dispersed into previously treated tissues

**Practical Determinants of Margin**

Owing to the aforesaid elements of complexity, oncologic surgeons have developed strategies to optimize margin delineation. Similar to the principles guiding elective treatment of lymph node levels, these strategies are probabilistic in nature, meaning that they are intended to maximize the probability to also include the occult portion of the disease in the resection. This, however, has the cost to unnecessarily resect uninvolved tissue in some patients, or to remove an insufficient thickness of microscopically involved tissue in others.

Three main theoretical approaches have supported the establishment of surgical rules to properly delineate margins.

The "metric approach" consists of the identification of a spatial cut-off that ensures all tumor cells are included in the resection in the majority of cases.[23] This can be objectively measured at definitive pathology. Since the distance between tumor and specimen surface shrinks during intraoperative cutting and throughout post-surgical processing, the actual margin thickness needs to be estimated. In oral cancer, for instance, since a 5 mm pathologic margin was identified as a prognostic cut-off in several studies, a shrinkage rate of the surgical specimen accounting for 21-32% and varying with tissue type and size, at least a 1-cm actual margin is precautionarily recommended.[24,25] Main argumentations against the metric approach are that a universal cut-off can be adequate, excessive, or insufficient depending upon histology and tumor-specific biology, and that 1 cm margin is hardly ever achievable in some head and neck sites (*i.e.*, sinonasal tract, skull base).

The "barrier approach" is based on the assumption that tumor expansion is contained by some anatomical structures, which usually consist of fascial layers, muscles, or bones.[23] This approach leads surgeons to identify and follow specific anatomical planes that surround the tumor, even though it implies to delineate the dissection plane with an irregular distance from the tumor surface. The main flaws of this approach are in the poor recognizability of some of these barrier-structures at definitive pathology, alongside the scarce demonstrability that they actually serve as barriers against tumor local progression.

The "compartment approach", finally, is based on the surmise that tumor cells tend to follow specific anatomical structures or vectors dictated by tissue architecture.[26] Though sounding similar to the barrier approach, this way of conceiving tumor progression is less optimistic on the capability of some structures to prevent local cancer progression. Rather, cancer cells would expand owing to a "pressure growth" that pushes cancers towards the pathways of least resistance (*e.g.*, between muscular fibers or fascicles).

As for all competing theoretical models aimed at explaining a biological phenomenon, the reality probably lies somewhere in the middle. Most likely, cancers progress through preferential pathways (either because of least resistance or due to a biological gain of function such as perineural spread), while also stochastically infiltrating surrounding tissues with some tissues (*e.g.*, bone, cartilage) probably serving as physical barriers against tumor expansion. Moreover, distribution between these modalities of local expansion can obviously vary among malignancies.

A paradoxical fact on recommendations for margin width lies in the technique-dependent threshold defining "clear margins". A cancer of the upper aerodigestive tract would be defined as radically resected with a threshold of 5 mm of pathologically uninvolved tissue if operated on with open surgery, 2-5 mm if through transoral robotic surgery, 0.5-2 mm if via transoral laser surgery, and regardless of metric measurements

provided that adjacent structures are not infiltrated in case endoscopic transnasal resection has been performed.[27–36] On the one hand, this difference is understandable as it expresses the need to define as either "adequate" or "inadequate" a resection performed with a given technique. On the other, it reflects that the definition of margin is currently far from being biology driven.[37]

**"Frailty" of Cutting Through Healthy Tissue**

The concept of "free margin" grounds on the belief that tissue uninvolved by cancer is healthy. However, evidence dating back to the 1990s suggested that tissues surrounding mucosal cancers bear molecular alterations typically found in malignancies.[38] These observations are in agreement with the multistep model that explains cancer development and progression. In fact, precancerous cells that gradually accumulate all the mutations necessary to become cancer also proliferate, thus giving rise to a number of cells that are preconditioned towards malignant transformation. This might also explain the propensity of cancers induced by long-term exposure to a risk factor (*i.e.*, tobacco smoking) towards recurrence, field cancerization, and synchronous/metachronous malignancies. Consequently, instead of conceiving cancer as a well-defined mass, preconditioning of the surrounding mucosa contributes to make it more comparable to an ill-defined "cloud" of genetic alterations centered around the visible disease and variably extending to the adjacent mucosa (Figure 3).

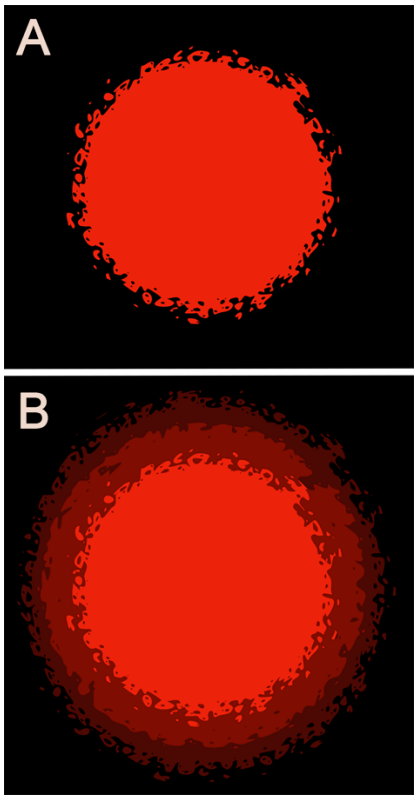


**Figure 3**. Discrepancy between the common representation of cancer (A) and actual distribution of precancerous alterations in adjacent tissues (B).

**Current Intraoperative Margin Evaluation**

For mucosal cancers, which represent the majority of head and neck malignant tumors, delineation of margins is required on both the superficial aspect, meaning that the surgeon has to decide how far from the visible tumor the mucosa has to be cut, and during dissection of deep tissues. For superficial delineation of margins, surgeons rely on sight and palpation, with some technologies (*e.g.*, narrow band imaging) augmenting the ability to identify altered tissues mostly owing to optical changes.[39,40] Delineation of deep margins is based on palpation, imaging interpretation, and the consequent 3-dimensional configuration that the surgeon creates in his/her mind. Sight is currently excluded from the ideal strategies to define the deep margin of resection, as it would imply the deep portion of the tumor to be exposed, which is a suboptimal scenario as opposed to leaving the tumor surrounded by a cuff of normal tissue.

Frozen sections allow intraoperative microscopic assessment of resection margins. Two main approaches to perform frozen sections for margin assessment are traditionally available: the defect-driven (also defined as patient-driven) technique consists of sampling the surgical bed, whereas in the specimen-driven technique tissues to be analyzed are harvested from the surgical specimen. There is no consensus on which technique yields the best accuracy in terms of intraoperative margin evaluation. Some evidence suggests that specimen-driven frozen sections might provide a higher chance of achieving wide negative margins as compared to defect-driven approach.[41] Moreover, positive frozen sections on the surgical specimen may also represent an independent negative prognostic factor, whereas defect-driven frozen sections have not been demonstrated to carry any relevant prognostic information.[42] This could be explained by the fact that sampling on the surgical specimen leads the surgeon to address the most critical margin relative to the palpable mass, whereas analysis of the surgical bed requires inferring the initial situation of the tumor. However, some authors have reported that circumferential sampling of the surgical bed has an almost excellent negative predictive value, though with suboptimal positive predictive value.[43] Irrespective of the specific technique employed to sample tissue to be sent for frozen section analysis, a meta-analysis demonstrated that achieving negative margins by extending the resection based on a positive frozen section does not equate to an initially negative margin, nor does it significantly increase the local control rate.[44] These data should not be misinterpreted as suggesting uselessness of achieving negative margins through additional resection following a positive frozen section. In fact, in the same meta-analysis, local recurrence-free survival of patients with positive margins is reported being close-to-significantly ($p=0.055$) worse compared to those with negative margins achieved through additional specimens on a positive frozen section.[44] As a consequence, one can conclude that obtaining negative margins upfront represents the best case scenario from a prognostic standpoint, but radicalization on a positive frozen section is still to be recommended based on the currently available data.

**Future Directions: "Know Your Enemy"**

Borrowing the aphorism of Sun Tzu from "The art of war", the first step to improve our ability to locally control cancer should consist of "knowing cancer". In particular, it is a common observation that every head and neck cancer has its own specificity in terms of local progression, which is not reliably expressed by the current systems of classifying and describing tumors.

For instance, it has been demonstrated that tongue squamous cell carcinoma has a particular propensity to subclinically invade the so-called "T-N tract", which roughly corresponds to the connective space including the sublingual area up to the level IB.[45] This confirms that tongue cancer can grow eccentrically with respect to the epicenter of clinically appreciable disease, which has not been observed in other oral cavity subsites whose cancerization shares analogous epidemiological and histopathological characteristics. This data being acquired, a modification of the surgical technique defined as "compartmental tongue surgery" has been implemented by some groups, aiming at addressing this particular characteristic of tongue cancer. Indeed, based on preliminary and retrospective data, compartmental tongue resection seems to provide improved oncologic outcomes compared to standard wide-margin resection.[26,46] These findings possibly confirm that focusing attention on the most probable escaping route of tumor might translate into better control of cancer.

Another example of deepening the understanding of cancer local behavior is the relationship between histologic growth pattern and topographic gross extension. For instance, it has been revealed that perineural and lymphovascular invasion substantially drive local extension of cancers of the maxillary sinus regardless of their histology.[47] In particular, tumors displaying lymphovascular invasion tend to grow with a caudal direction and give nodal metastases, while those with perineural invasion more frequently invade superior, medial, and posterior structures. Should detection of perineural and lymphovascular invasion be reliably detectable before surgery, the resection could be extended accordingly towards the most critical areas.

In view of this evidence, head and neck oncologic surgeons should be avid in knowing the local behavior of cancers with a histology-, site-, and possibly biology-level precision. Therefore, future research on local tumor extension in the head and neck should primarily assess the relationship between the cancer's specificities and escape routes, in order to guide surgeons towards the most critical areas and possibly improve outcomes.

**Future Directions: Enhanced Tumor Visualization**

Another strategy to improve local control is to augment the way cancer is "seen" during ablation. The most promising and accessible technology to support this refinement is represented by surgical navigation systems. Although most frequently employed to minimize intraoperative complications and optimize precision of reconstruction, cross-sectional imaging-based navigation could also provide the surgical team with a more precise image of tumor extension. This has been shown in a preclinical setting, where the employment of navigation with 3-dimensional rendering of the tumor extension significantly increased the adequacy of margin delineation in models of advanced cancers variably extending within the craniomaxillofacial skeleton.[22] Over a total of 381 simulated osteotomies, the use of surgical navigation decreased the rate of gross margin involvement from 18.1% to 0.0%. Moreover, some groups have published their experience in using navigation to improve the margin status of resections of advanced cancers of the head and neck, showing encouraging results.[48–50] Despite the limited number of patients reported in these preliminary experiences (24 overall), the employment of navigation led to obtain free margins in a high percentage of patients affected by locally advanced cancer of the head and neck.

By basing the 3-dimensional representation of the tumor on radiologic data, navigation-guided resections might also benefit from incorporating relevant information into cancer rendering. For instance, the

tumor can be rendered together with an isotropic expansion to provide a visual representation of a metric margin. Moreover, cancer rendering could also include fusion of functional and cross-sectional imaging, possibly increasing the accuracy of tumor mapping.[50] In this sense, whichever future methodology is capable of better depicting the actual tumor extension could be incorporated in the representation of tissue to be resected through surgical navigation.

However, the accuracy of surgical navigation is constrained by precise and lasting registration alongside the presence of a bony framework that limits motions of soft tissue. For this reason, navigation is most likely useful in the setting of tumors strictly attached to the craniomaxillofacial skeleton, whereas cancers invading mostly soft tissues would be less accurately rendered.

**Future Directions: Augmented Mapping of the Surgical Bed**

The latest and most promising advent in the field of surgical margins control is application of bio-optical imaging technologies to search for tumor localizations that would otherwise be undetectable by the naked eye.[51] Employment of this technology to improve delineation of the superficial margin of resection has been already demonstrated to be beneficial. On the contrary, optical imaging to detect potential residues of the tumor into the surgical bed and accordingly guide frozen section is still an ever-changing field. The most promising optical imaging modalities which could meet this need are fluorescence-based imaging, hyperspectral imaging, and Raman spectroscopy. Fluorescence-based imaging relies on either natural (*i.e.*, autofluorescence imaging) or targeted fluorescence (*i.e.*, through biological probes attached to fluorophores) of cancer tissue. Hyperspectral imaging consists of dividing electromagnetic waves beyond the 3-band division of the human eye and even beyond the spectrum of visible light. By collecting and elaborating this optical information, it is possible to infer biological information of a tissue under analysis. Raman spectroscopy is able to depict the molecular fingerprint of a tissue by taking advantage of light scattering as a consequence of vibration of intramolecular bonds. All these imaging modalities rely on the common principle of collecting bio-optical characteristics of tissues and render them in a way that is appreciable to the surgeon's eye.

Recently, van Keulen *et al*. published a series of 20 patients who were operated on for head and neck squamous cell carcinoma by targeted fluorescence-surgery.[52] All patients were injected with panitumumab, an anti-epidermal growth factor receptor (EGFR) monoclonal antibody, conjugated to the fluorophore IRDye800CW. The surgeon could therefore visualize in real time the distribution of EGFR through a hand-held camera prior to incise tissues. The authors demonstrated that tumor-to-background ratio, which represents the ability to distinguish the tumor from surrounding tissues, was satisfactory irrespective of age, gender, tumor size and site, and EGFR expression. Though preliminary in nature, these data are encouraging, as they demonstrate feasibility of the workflow and suggest that targeted-fluorescence imaging is reliable. Analysis of the actual benefit of this technology in terms of intraoperative margin status evaluation will represent an essential future step.

Halicek *et al*. published a study on 293 fresh specimens obtained from resection of head and neck squamous cell carcinomas in 102 patients and analyzed with reflectance-based hyperspectral imaging.[53] The authors found that hyperspectral imaging could distinguish squamous cell carcinoma from uninvolved tissue

with an area-under-curve ranging between 0.80 and 0.90 compared to histopathological microscopic evaluation. The time span required to obtain hyperspectral-based evaluation of the surgical specimen was estimated to be around 2 minutes. This study provided promising data on the classification performance of hyperspectral imaging calculated from a large dataset. However, application of this methodology to the surgical bed would require optimization for potential confounders such as blood and cauterized tissues.

Barroso *et al*. have demonstrated the utility of Raman spectroscopy in identifying positive margins on 26 mandibulectomy specimens, with diagnostic accuracy as high as 95%.[54] Yu *et al*. achieved a 99.3% sensitivity and 94.3% specificity in distinguishing tongue squamous cell carcinoma with respect to normal tissue by applying a deep learning method to Raman spectral data obtained from 24 fresh specimens.[55]

The above-mentioned references represent just selected publications among a large and constantly increasing number of studies demonstrating and progressively refining the diagnostic performance of bio-optical imaging techniques on fresh tissues harboring cancer. The following step will probably be to apply these technologies intraoperatively and quantify the actual benefit they can confer to outcomes.

## Conclusions

Adequate control of margins is an urgent need in head and neck surgical oncology. Our current understanding of local progression of cancer is still inadequate, especially considering the variety of histologies and biological behaviors characterizing the head and neck area. Consensus should be reached to obtain a solid and biology-driven definition of “adequate margins”, which could be transversally applied to a given cancer irrespective of the surgical technique employed to excise it. On the other hand, technologies such as surgical navigation and bio-optical imaging will probably be implementing our current way of ablating cancers, possibly translating into better delineated surgical specimens and improved outcomes.

## References


1. Bernier J, Domenge C, Ozsahin M, et al. Postoperative Irradiation with or without Concomitant Chemotherapy for Locally Advanced Head and Neck Cancer. N Engl J Med. 2004;350(19):1945-1952. doi:10.1056/NEJMoa032641
2. Cooper JS, Pajak TF, Forastiere AA, et al. Postoperative Concurrent Radiotherapy and Chemotherapy for High-Risk Squamous-Cell Carcinoma of the Head and Neck. N Engl J Med. 2004;350(19):1937-1944+2019. doi:10.1056/NEJMoa032646
3. Deeley TJ. A brief history of cancer. Clin Radiol. 1983;34(6):597-608. doi:10.1016/S0009-9260(83)80405-X
4. di Lonardo A, Nasi S, Pulciani S. Cancer: We should not forget the past. J Cancer. 2015;6(1):29-39. doi:10.7150/jca.10336
5. Fonseca R. Oral and Maxillofacial Surgery.; 2017. doi:10.1016/B978-0-323-26278-1.00011-8
6. Faguet GB. A brief history of cancer: Age-old milestones underlying our current knowledge database. Int J Cancer. 2015;136(9):2022-2036. doi:10.1002/ijc.29134
7. Halsted WS. The results of operations for the cure of cancer of the breast performed at the Johns Hopkins Hospital from June, 1889, to January, 1894. Ann Surg. 1894;20(5):497-555. doi:10.1097/00000658-189407000-00075
8. Wolf GT. Surgical margins in the genomic era: The Hayes Martin lecture, 2012. Arch Otolaryngol - Head Neck Surg. 2012;138(11):1001-1013. doi:10.1001/2013.jamaoto.82
9. Brandwein-Gensler M, Teixeira MS, Lewis CM, et al. Oral squamous cell carcinoma: Histologic risk assessment, but not margin status, is strongly predictive of local disease-free and overall survival. Am J Surg Pathol. 2005;29(2):167-178. doi:10.1097/01.pas.0000149687.90710.21
10. Shaw RJ, Brown JS, Woolgar JA, Lowe D, Rogers SN, Vaughan ED. The influence of the pattern of mandibular invasion on recurrence and survival in oral squamous cell carcinoma. Head Neck. 2004;26(10):861-869. doi:10.1002/hed.20036
11. Aleskandarany MA, Sonbul SN, Mukherjee A, Rakha EA. Molecular Mechanisms Underlying Lymphovascular Invasion in Invasive Breast Cancer. Pathobiology. 2015;82(3-4):113-123. doi:10.1159/000433583

12. Marchesi F, Piemonti L, Mantovani A, Allavena P. Molecular mechanisms of perineural invasion, a forgotten pathway of dissemination and metastasis. Cytokine Growth Factor Rev. 2010;21(1):77-82. doi:10.1016/j.cytogfr.2009.11.001
13. Amit M, Na'Ara S, Gil Z. Mechanisms of cancer dissemination along nerves. Nat Rev Cancer. 2016;16(6):399-408. doi:10.1038/nrc.2016.38
14. Maffeis V, Cappellesso R, Galuppini F, et al. Tumor budding is an adverse prognostic marker in intestinal-type sinonasal adenocarcinoma and seems to be unrelated to epithelial-mesenchymal transition. Virchows Arch. 2020. doi:10.1007/s00428-020-02748-1
15. Garden AS, Weber RS, Morrison WH, Ang KK, Peters LJ. The influence of positive margins and nerve invasion in adenoid cystic carcinoma of the head and neck treated with surgery and radiation. Int J Radiat Oncol Biol Phys. 1995;32(3):619-626. doi:10.1016/0360-3016(95)00122-F
16. Liu S-A, Wang C-C, Jiang R-S, Lee F-Y, Lin W-J, Lin J-C. Pathological features and their prognostic impacts on oral cavity cancer patients among different subsites - A singe institute's experience in Taiwan. Sci Rep. 2017;7(1):7451. doi:10.1038/s41598-017-08022-w
17. Martins-Andrade B, Dos Santos Costa SF, Sant'ana MSP, et al. Prognostic importance of the lymphovascular invasion in head and neck adenoid cystic carcinoma: A systematic review and meta-analysis. Oral Oncol. 2019;93:52-58. doi:10.1016/j.oraloncology.2019.04.014
18. Adel M, Kao H-K, Hsu C-L, et al. Evaluation of Lymphatic and Vascular Invasion in Relation to Clinicopathological Factors and Treatment Outcome in Oral Cavity Squamous Cell Carcinoma. Medicine (Baltimore). 2015;94(43):e1510. doi:10.1097/MD.0000000000001510
19. Ho YY, Wu TY, Cheng HC, Yang CC, Wu CH. The significance of tumor budding in oral cancer survival and its relevance to the eighth edition of the American Joint Committee on Cancer staging system. Head Neck. 2019;41(9):2991-3001. doi:10.1002/hed.25780
20. King R, Page RN, Googe PB, Mihm MC. Lentiginous melanoma: A histologic pattern of melanoma to be distinguished from lentiginous nevus. Mod Pathol. 2005;18(10):1397-1401. doi:10.1038/modpathol.3800454
21. Takahashi Y, Takahashi E, Nakakura S, Kitaguchi Y, Mupas-Uy J, Kakizaki H. Risk Factors for Local Recurrence or Metastasis of Eyelid Sebaceous Gland Carcinoma After Wide Excision With Paraffin Section Control. Am J Ophthalmol. 2016;171:67-74. doi:10.1016/j.ajo.2016.08.028
22. Ferrari M, Daly MJ, Douglas CM, et al. Navigation-guided osteotomies improve margin delineation in tumors involving the sinonasal area: A preclinical study. Oral Oncol. 2019;99. doi:10.1016/j.oraloncology.2019.104463
23. Upile T, Fisher C, Jerjes W, et al. The uncertainty of the surgical margin in the treatment of head and neck cancer. Oral Oncol. 2007;43(4):321-326. doi:10.1016/j.oraloncology.2006.08.002
24. Pangare TB, Waknis PP, Bawane SS, Patil MN, Wadhera S, Patowary PB. Effect of Formalin Fixation on Surgical Margins in Patients With Oral Squamous Cell Carcinoma. J Oral Maxillofac Surg. 2017;75(6):1293-1298. doi:10.1016/j.joms.2016.11.024
25. Johnson RE, Sigman JD, Funk GF, Robinson RA, Hoffman HT. Quantification of surgical margin shrinkage in the oral cavity. Head Neck. 1997;19(4):281-286. doi:10.1002/(sici)1097-0347(199707)19:4<281::aid-hed6>3.3.co;2-4
26. Calabrese L, Bruschini R, Giugliano G, et al. Compartmental tongue surgery: Long term oncologic results in the treatment of tongue cancer. Oral Oncol. 2011;47(3):174-179. doi:10.1016/j.oraloncology.2010.12.006
27. Nichols AC, Theurer J, Prisman E, et al. Radiotherapy versus transoral robotic surgery and neck dissection for oropharyngeal squamous cell carcinoma (ORATOR): an open-label, phase 2, randomised trial. Lancet Oncol. 2019;20(10):1349-1359. doi:10.1016/S1470-2045(19)30410-3
28. Benazzo M, Canzi P, Mauramati S, et al. Transoral Robot-Assisted Surgery in Supraglottic and Oropharyngeal Squamous Cell Carcinoma: Laser Versus Monopolar Electrocautery. J Clin Med. 2019;8(12):2166. doi:10.3390/jcm8122166
29. Persky MJ, Albergotti WG, Rath TJ, et al. Positive Margins by Oropharyngeal Subsite in Transoral Robotic Surgery for T1/T2 Squamous Cell Carcinoma. Otolaryngol - Head Neck Surg (United States). 2018;158(4):660-666. doi:10.1177/0194599817742852
30. Cannon RB, Houlton JJ, Patel S, et al. Patterns of cervical node positivity, regional failure rates, and fistula rates for HPV+ oropharyngeal squamous cell carcinoma treated with transoral robotic surgery (TORS). Oral Oncol. 2018;86:296-300. doi:10.1016/j.oraloncology.2018.10.001
31. Cracchiolo JR, Roman BR, Kutler DI, Kuhel WI, Cohen MA. Adoption of transoral robotic surgery compared with other surgical modalities for treatment of oropharyngeal squamous cell carcinoma. J Surg Oncol. 2016;114(4):405-411. doi:10.1002/jso.24353
32. Vaish R, Shah S, Chaukar D. Prognostic significance of surgical margins after transoral laser microsurgery for early-stage glottic cancer. Oral Oncol. 2020;100. doi:10.1016/j.oraloncology.2019.104511
33. Peretti G, Piazza C, Cocco D, et al. Transoral CO2 laser treatment for Tis-T3 glottic cancer: The University of Brescia experience on 595 patients. Head Neck. 2010;32(8):977-983. doi:10.1002/hed.21278
34. Abdelmeguid AS, Raza SM, Su SY, et al. Endoscopic resection of sinonasal malignancies. Head Neck. 2020;42(4):645-652. doi:10.1002/hed.26047
35. Castelnuovo P, Battaglia P, Turri-Zanoni M, et al. Endoscopic endonasal surgery for malignancies of the anterior cranial base. World Neurosurg. 2014;82(6):S22-S31. doi:10.1016/j.wneu.2014.07.021

36. Nicolai P, Castelnuovo P, Villaret AB. Endoscopic resection of sinonasal malignancies. Curr Oncol Rep. 2011;13(2):138-144. doi:10.1007/s11912-011-0151-6
37. Meier JD, Oliver DA, Varvares MA. Surgical margin determination in head and neck oncology: Current clinical practice. The results of an International American Head and Neck Society member survey. Head Neck. 2005;27(11):952-958. doi:10.1002/hed.20269
38. Ball VA, Righi PD, Tejada E, Radpour S, Pavelic ZP, Gluckman JL. p53 immunostaining of surgical margins as a predictor of local recurrence in squamous cell carcinoma of the oral cavity and oropharynx. Ear, Nose Throat J. 1997;76(11):818-823. doi:10.1177/014556139707601109
39. Piazza C, Del Bon F, Peretti G, Nicolai P. Narrow band imaging in endoscopic evaluation of the larynx. Curr Opin Otolaryngol Head Neck Surg. 2012;20(6):472-476. doi:10.1097/MOO.0b013e32835908ac
40. Piazza C, Del Bon F, Paderno A, et al. The diagnostic value of narrow band imaging in different oral and oropharyngeal subsites. Eur Arch Oto-Rhino-Laryngology. 2016;273(10):3347-3353. doi:10.1007/s00405-016-3925-5
41. Amit M, Na'Ara S, Leider-Trejo L, et al. Improving the rate of negative margins after surgery for oral cavity squamous cell carcinoma: A prospective randomized controlled study. Head Neck. 2016;38:E1803-E1809. doi:10.1002/hed.24320
42. Buchakjian MR, Ginader T, Tasche KK, Pagedar NA, Smith BJ, Sperry SM. Independent Predictors of Prognosis Based on Oral Cavity Squamous Cell Carcinoma Surgical Margins. Otolaryngol - Head Neck Surg (United States). 2018;159(4):675-682. doi:10.1177/0194599818773070
43. Tirelli G, Boscolo Nata F, Gatto A, et al. Intraoperative Margin Control in Transoral Approach for Oral and Oropharyngeal Cancer. Laryngoscope. 2019;129(8):1810-1815. doi:10.1002/lary.27567
44. Bulbul MG, Tarabichi O, Sethi RK, Parikh AS, Varvares MA. Does Clearance of Positive Margins Improve Local Control in Oral Cavity Cancer? A Meta-analysis. Otolaryngol - Head Neck Surg (United States). 2019;161(2):235-244. doi:10.1177/0194599819839006
45. Tagliabue M, Gandini S, Maffini F, et al. The role of the T-N tract in advanced stage tongue cancer. Head Neck. 2019;41(8):2756-2767. doi:10.1002/hed.25761
46. Piazza C, Grammatica A, Montalto N, Paderno A, Del Bon F, Nicolai P. Compartmental surgery for oral tongue and floor of the mouth cancer: Oncologic outcomes. Head Neck. 2019;41(1):110-115. doi:10.1002/hed.25480
47. Ferrari M, Ioppi A, Schreiber A, et al. Malignant tumors of the maxillary sinus: Prognostic impact of neurovascular invasion in a series of 138 patients. Oral Oncol. 2020;106. doi:10.1016/j.oraloncology.2020.104672
48. Catanzaro S, Copelli C, Manfuso A, et al. Intraoperative navigation in complex head and neck resections: indications and limits. Int J Comput Assist Radiol Surg. 2017;12(5):881-887. doi:10.1007/s11548-016-1486-0
49. Tarsitano A, Ricotta F, Baldino G, et al. Navigation-guided resection of maxillary tumours: The accuracy of computer-assisted surgery in terms of control of resection margins – A feasibility study. J Cranio-Maxillofacial Surg. 2017;45(12):2109-2114. doi:10.1016/j.jcms.2017.09.023
50. Feichtinger M, Pau M, Zemann W, Aigner RM, Kärcher H. Intraoperative control of resection margins in advanced head and neck cancer using a 3D-navigation system based on PET/CT image fusion. J Cranio-Maxillofacial Surg. 2010;38(8):589-594. doi:10.1016/j.jcms.2010.02.004
51. Wu C, Gleysteen J, Teraphongphom NT, Li Y, Rosenthal E. In-vivo optical imaging in head and neck oncology: Basic principles, clinical applications and future directions review-Article. Int J Oral Sci. 2018;10(2). doi:10.1038/s41368-018-0011-4
52. van Keulen S, Nishio N, Fakurnejad S, et al. Intraoperative Tumor Assessment Using Real-Time Molecular Imaging in Head and Neck Cancer Patients. J Am Coll Surg. 2019;229(6):560-567.e1. doi:10.1016/j.jamcollsurg.2019.09.007
53. Halicek M, Dormer JD, Little J V., et al. Hyperspectral imaging of head and neck squamous cell carcinoma for cancer margin detection in surgical specimens from 102 patients using deep learning. Cancers (Basel). 2019;11(9). doi:10.3390/cancers11091367
54. Barroso EM, ten Hove I, Bakker Schut TC, et al. Raman spectroscopy for assessment of bone resection margins in mandibulectomy for oral cavity squamous cell carcinoma. Eur J Cancer. 2018;92:77-87. doi:10.1016/j.ejca.2018.01.068
55. Yu M, Yan H, Xia J, et al. Deep convolutional neural networks for tongue squamous cell carcinoma classification using Raman spectroscopy. Photodiagnosis Photodyn Ther. 2019;26:430-435. doi:10.1016/j.pdpdt.2019.05.008

# Use of surgical navigation with three-dimensional rendering to improve the margin status of oncological ablations in the head and neck

## Development of preclinical, phantom-based craniofacial tumor models and per-single-margin theoretical benefit measurement

*Ferrari et al., Oral Oncol 2019; doi: 10.1016/j.oraloncology.2019.104463*

**Introduction**

Tumors of the sinonasal complex pose a significant challenge for head and neck surgeons. They are usually diagnosed at a locally advanced stage due to the non-specific symptoms patients exhibit during early stages. Proximity of these malignancies to critical anatomical structures such as the orbit, cavernous sinus, optic nerve and brain makes surgical treatment challenging as the goal is to ensure adequate tumor resection while minimizing morbidity to the patient.

Over the last 30 years, the development of endoscopic transnasal surgery along with improvements in radiotherapy, such as intensity-modulated radiation therapy and particle therapy, have revolutionized the management of sinonasal cancer.[1-11] A large majority are now resected endoscopically, considerably reducing the morbidity of surgery compared to the historical craniofacial resections that were once performed routinely for such cancers. However, open surgery is still necessary in the most advanced stage sinonasal cancers, often in combination with endoscopic resection (*i.e.*, cranioendoscopic resection and endoscopic-assisted maxillectomy).[1,12,13]

When an osteotomy is required for a sinonasal cancer the surgeon must plan the osteotomy sites taking into consideration tumor extension, anatomical landmarks, and reconstructive requirements. Correct orientation of the osteotomy, to ensure adequate margins, requires the surgeon to build a three-dimensional (3D) mental image of the tumor before surgery, based on the preoperative imaging. Even in the hands of highly skilled surgeons, this process is difficult as small changes in the orientation of the osteotomy can significantly affect the trajectory through soft tissues and bone. The problem is made even more complex in the skull base due to the close proximity of critical anatomical structures.

Surgical navigation in the craniomaxillofacial region has been most commonly employed to assess adequacy of reconstruction after trauma (*i.e.*, orbital walls), while application for oncological resections for osteotomy planning and determination of margins is less frequent.[14-16] However, the potential for navigation to maximize precision and avoid major complications during the ablation was considered when this technology was first described for head and neck surgical oncology.[17-19] Navigation has clearly demonstrated improved accuracy and reproducibility of craniomaxillofacial osteotomies,[20] thus translating clinically into improved outcomes.[21-24]

The aim of this preclinical study was to assess and quantify the potential benefit of 3D real-time navigation in sinonasal cancers requiring open surgery osteotomies.

## Material and methods

### *Tumor model preparation*

Three artificial skulls (Sawbones®, Washington) and a moldable material (Play-Doh®, Hasbro®, Rhode Island) mixed with acrylic glue were employed to build 7 tumor models (5 maxillary sinus tumors, 1 nasoethmoidal, and 1 superior alveolar crest tumors) (Figure 1A). Involvement of the infratemporal fossa, orbital cavity, anterior/middle skull base, and cranial cavity were reproduced to simulate locally advanced sinonasal cancers.

Anatomical areas that would have remained covered by normal tissues (premaxillary area, temporal/infratemporal fossa, orbital cavity) were covered with white medical gauze to simulate the standard visualization of the tumor, such that they were visible only through the oral and nasal cavities (Figure 1B).

Areas requiring an osteotomy were visually delineated (Figure 1B) and classified in 6 groups as follows: palate (Pa), inferior-lateral orbital rim (ILOR), zygoma (Zy), fronto-maxillary junction (FMJ), cranial vault-anterior skull base (CV-ASB), and pterygomaxillary junction-middle skull base (PMJ-MSB).

### *Image acquisition and tumor contouring*

3D images of each skull model were acquired using a prototype cone-beam computed tomography (CBCT) imaging system on a mobile C-arm.[25,26] This flat-panel imaging system is under investigation for guidance of head and neck procedures involving significant bone resection and/or complex anatomical reconstruction, and was recently deployed in a prospective patient study.[27] In this study, 3D volumes (256×256×192) covered a field of view of 20×20×15 $cm^3$ using isotropic 0.8-mm 3D voxels. Radiation doses for this CBCT system are low (<1/5$^{th}$) in comparison to nominal diagnostic CT scanning.[26]

On CBCT imaging, the sinonasal tumor models were clearly distinguishable from the artificial bone, as they showed much higher x-ray attenuation (Figure 1C). Contouring of the tumors was obtained semi-automatically using a two-step process within NIRFAST-Slicer software.[28,29] First, a global threshold was applied to provide a quick, coarse segmentation, and then manual refinement (duration: 2-3 minutes) was used to smooth the segmentation (Figure 1D). To visualize the planned surgical margin (Figure 1E), a semi-transparent wireframe was generated at a distance of 1 cm from the tumor surface using volumetric image dilation processing in MATLAB software (MathWorks, Massachusetts).

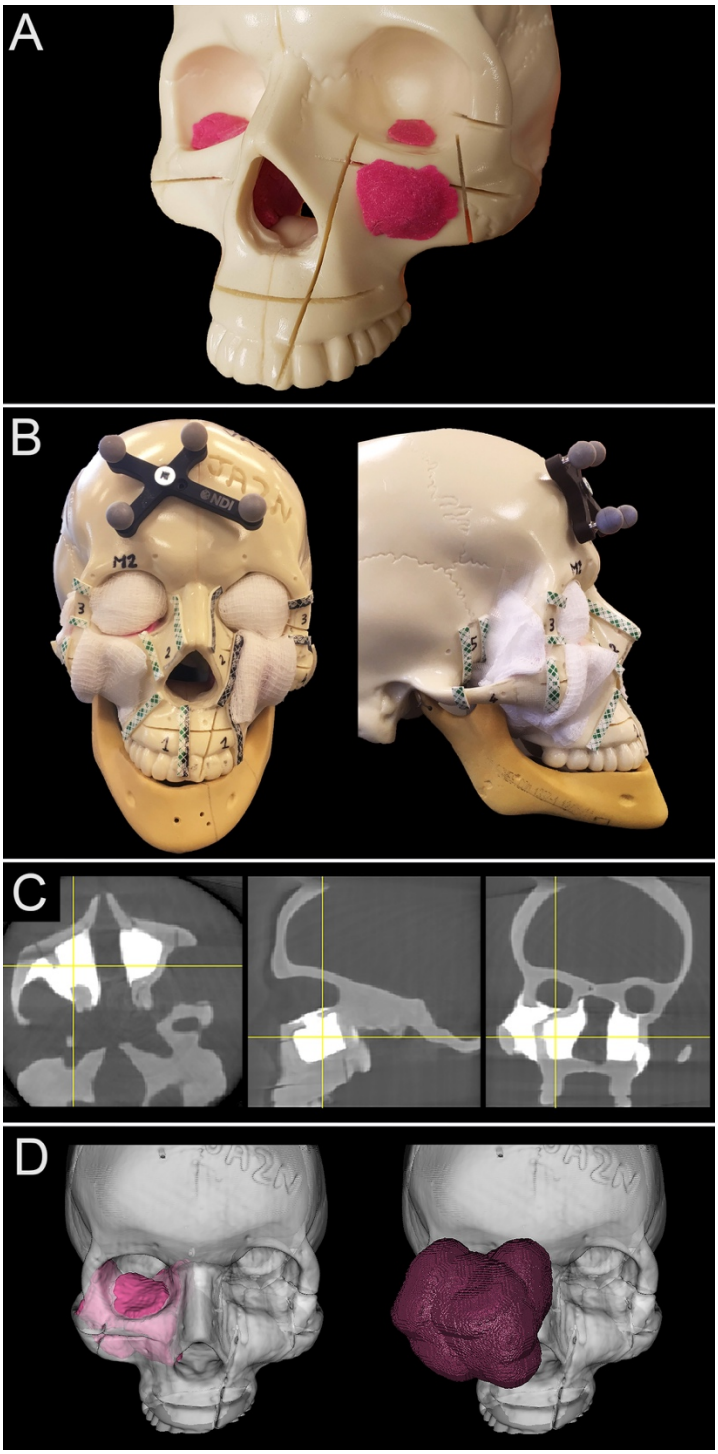


**Figure 1**. Tumor models and imaging. **A**. Moldable material and acrylic glue were used to create tumor models, positioned within skulls made of artificial bone. Tumors were shaped based on real cases. **B**. Anatomical areas that would have remained covered by normal tissues were covered with white medical gauze. Areas requiring an osteotomy were visually delineated with thick tape. A small 4-sphere reference tool was anchored to the skull. **C**. The moldable material employed to make up tumor models showed spontaneous hyperdensity with respect to the artificial bone. Involvement of adjacent areas was reproduced to simulate locally advanced sinonasal cancers. **D**. Tumors were contoured (pink volume) and semi-transparent wireframe was generated at a distance of 1 cm from the tumor surface using volumetric image dilation (purple volume).

***Navigation system***

CBCT images were displayed within an in-house navigation software package (GTx-Eyes),[30] based on the open-source Image-Guided Surgery Toolkit.[31] Tumor and margin segmentations were superimposed on tri-planar views and separately as 3D surface renderings. Surgical tool tracking in this study was provided by a stereoscopic infrared camera (Polaris Spectra, NDI, Waterloo, Ontario). Image-to-tracker registration was obtained by paired-point matching of pre-drilled divots by means of a tracked pointer. A small 4-sphere reference tool (NDI, Waterloo, Ontario) was anchored to the skull throughout registration and simulations. A registration error of 1 mm or less was considered acceptable for the navigation experiments. A 4-sphere reference (Medtronic, Jacksonville, FL) was secured to a 6-mm osteotome (Symmetry Surgical®, Antioch, Tennessee), which was then calibrated using a custom stainless-steel planar jig. Figure 2 demonstrates the use of the navigation system to guide the osteotome and avoid an intratumoral cut. According to surgeon's preferences, the entire 3D-rendering could be freely rotated and the skull rendering clipped along the virtual cutting plane (Figures 2 and 3). The intersection of bone with the cutting plane was highlighted in green to show more clearly the relation of the cutting plane with the tumor surface.

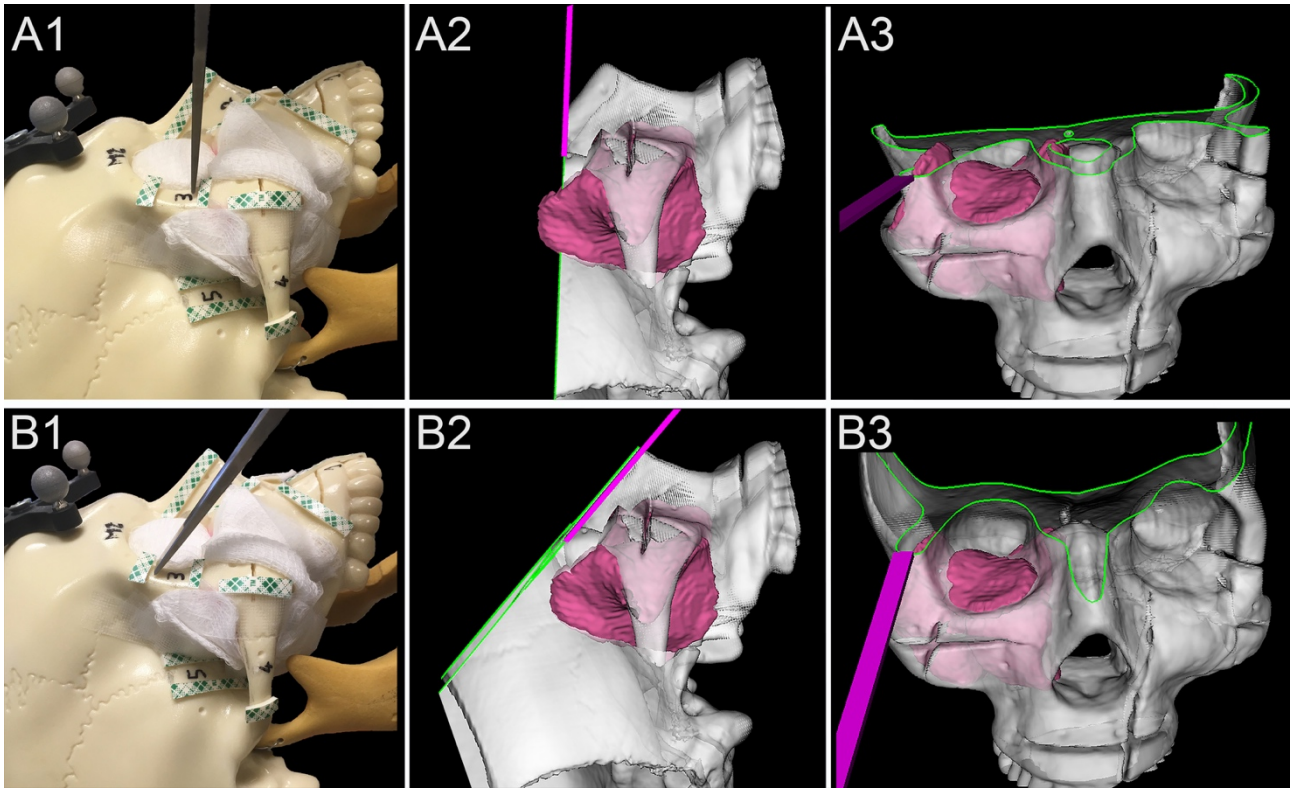


**Figure 2**. Basic principle of 3D rendering navigation for margin delineation. **A1-3**. Real lateral view, front 3D rendered view, and lateral 3D rendered view of an unguided simulation. The virtual cutting plane crosses a portion of the tumor model located into the temporal fossa, which was not fully appreciable when looking at the skull model due to the gauze simulating a cuff of healthy tissue left around the tumor. **B1-3**. Real lateral view, front 3D rendered view, and lateral 3D rendered view of a tumor-guided simulation. With real-time 3D rendering navigation, the surgeon shifted the osteotome cranially and tilted it parallel the surface of the tumor. Visualization of the cutting trajectory was facilitated by the clipping function, which provided a real-time representation of the cutting plane (green line shows the intersection between the cutting plane and bone).

***Simulation***

Surgeons from the Department of Otolaryngology – Head and Neck Surgery of the University Health Network (Toronto, Ontario, Canada) and from the Unit of Otorhinolaryngology – Head and Neck Surgery of the University of Brescia (Brescia, Italy) were recruited for the simulations.

Each surgeon received a brief explanation of the steps of the simulation and of the subsequent analysis methods. The surgical task was to position the osteotome within aforementioned delineated areas (Pa, ILOR, Zy, FMJ, CV-ASB, and PMJ-MSB) to provide a 1 cm margin from the tumor along the plane trajectory. No cutting was performed to allow reuse of the models; rather, the osteotome position and orientation were recorded when the surgeon gave vocal confirmation of their proposed cut and the analysis was performed on the virtual cutting trajectory. Three surgical techniques were compared in sequence: 1) unguided; 2) tumor-guided; and 3) margin-guided, as shown in Figure 3. First, the surgeons could only view the cross-sectional images (*i.e.*, axial, sagittal, coronal), with no access to the real-time navigation system or the 3D tumor/margin renderings (unguided simulation; Figure 3A). Second, after completing all the unguided cuts, virtual osteotomies were guided using real-time tool tracking and the 3D tumor segmentation (tumor-guided simulation; Figure 3B). Finally, real-time tracking was used again, this time with 3D visualization of both the tumor and margin segmentations (margin-guided simulation; Figure 3C). The duration of each simulation was recorded.

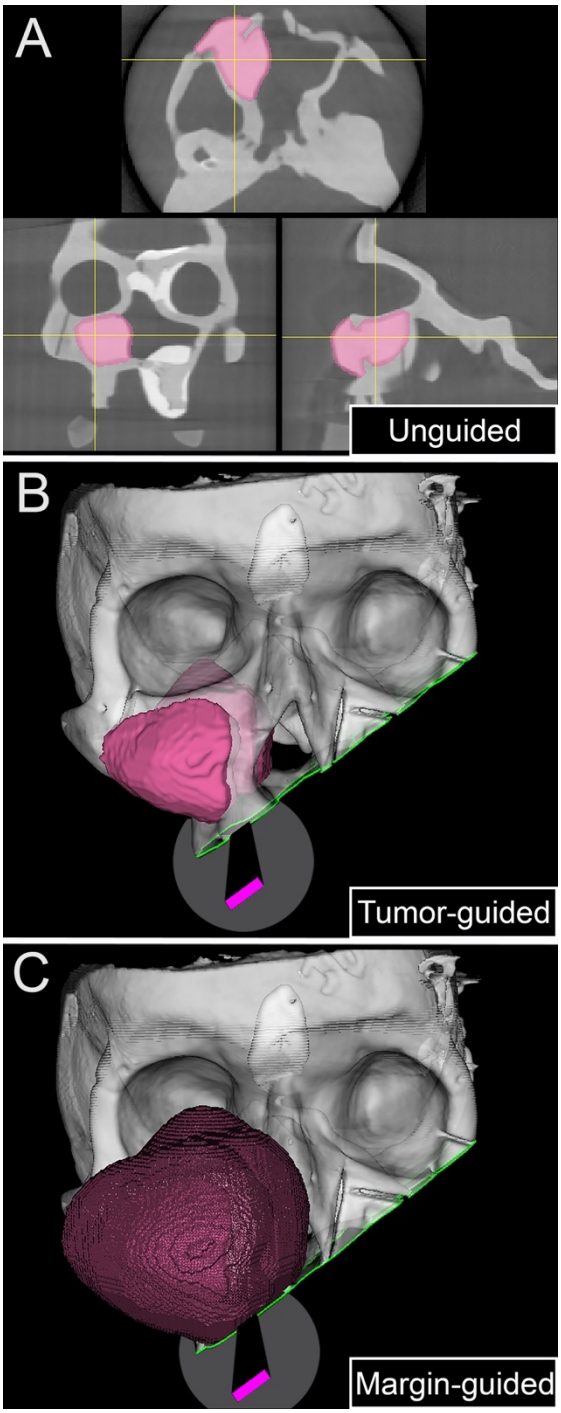


**Figure 3**. Three-step simulation. The panel summarizes the 3 steps of the simulation. **A**. First, the surgeon was asked to simulate the osteotomies based on cross-sectional images only. **B**. Then, the simulation was repeated under the guidance of the tumor rendering. **C**. Finally, the simulation was redone a third time with both tumor and margin renderings.

***Virtual cutting plane analysis***

Analysis of cutting planes was performed by means of MATLAB software (MathWorks, Massachusetts). An area of 4 cm length along the longitudinal axis of the cut and 2 cm width (1 cm on both sides with respect to the longitudinal axis) was isolated from each plane. The minimal distance with respect to the tumor surface was calculated for each point making up the isolated area and reproduced as a distribution of distances shown as a 4×2 $cm^2$ color scaled image (Figures 4 and 5). Distance from the tumor surface was classified as “intratumoral” when 0 mm or negative, “close”

when greater than 0 mm and less than or equal to 5 mm, “adequate” when greater than 5 mm and less than or equal to 15 mm, and “excessive” over 15 mm. The percentages of points at intratumoral, close, adequate, and excessive distances were calculated for each simulation plane.

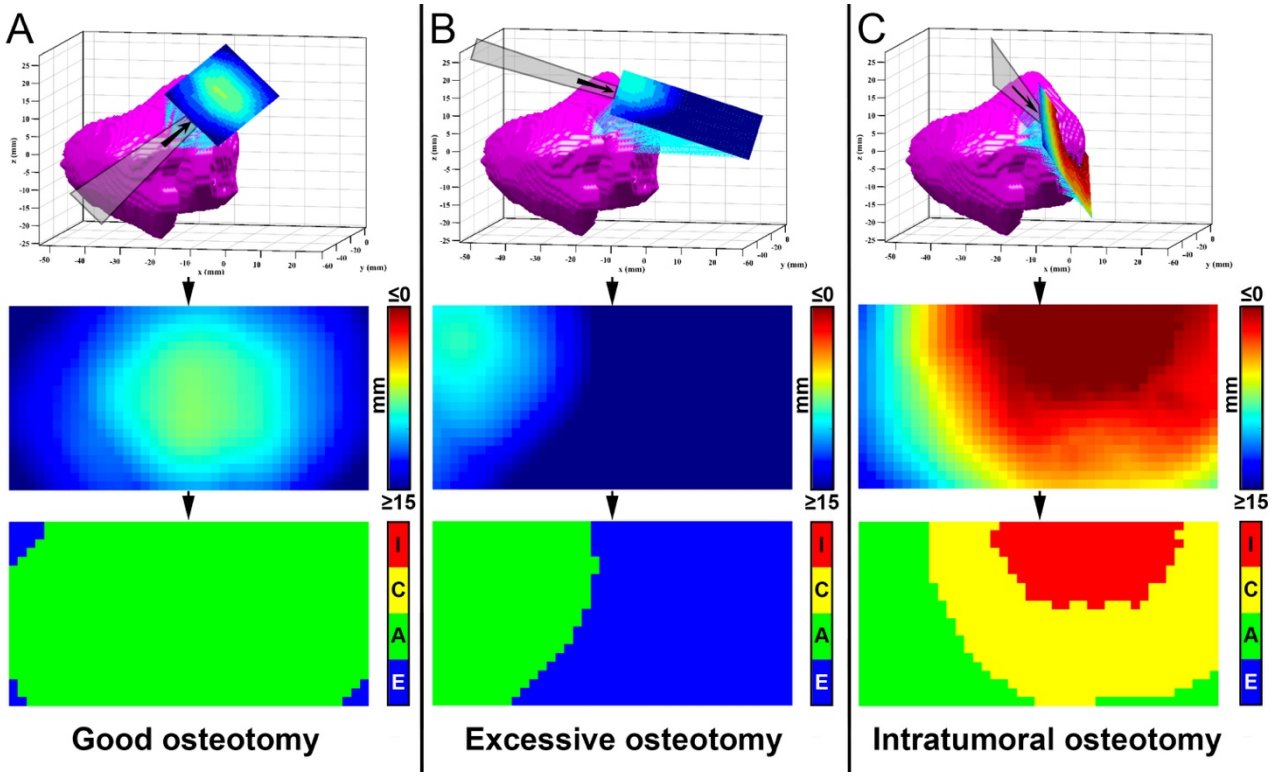


**Figure 4**. Virtual cutting plane analysis. An area of 4 cm length and 2 cm width was isolated from each plane. The minimal distance with respect to the tumor surface was calculated for each point of the isolated area and reproduced as a color scaled image. Distance from the tumor surface was classified as “Intratumoral” when 0 mm or negative (I, red), “Close” between 0 and 5 mm (C, yellow), “Adequate” between 5 and 15 mm (A, green), and “Excessive” over 15 mm (E, blue).

### *Statistical analysis*

Statistical analysis was run through XLSTAT® (Addinsoft®, New York). Simulations were grouped in three categories: unguided, tumor-guided, and margin-guided. These 3 groups were compared in terms of percentage of intratumoral, close, adequate, and excessive distances from the tumor and duration of the simulations through the bilateral Kruskal-Wallis test and Steel-Dwass-Critchlow-Fligner post-hoc test. Rate of intratumoral virtual cuts within the 3 groups was assessed with the Fisher exact test. Intraindividual differences in terms of percentage of adequate distance between the tumor-guided and unguided groups were calculated and considered the “gain” provided by the navigation with 3D rendering. The association between this value (*i.e.*, gain) and side of the skull, surgeon, and anatomical region of cut simulation was studied with the bilateral Kruskal-Wallis test and Steel-Dwass-Critchlow-Fligner post-hoc test. Level of significance was set at 0.05 for all statistical tests.

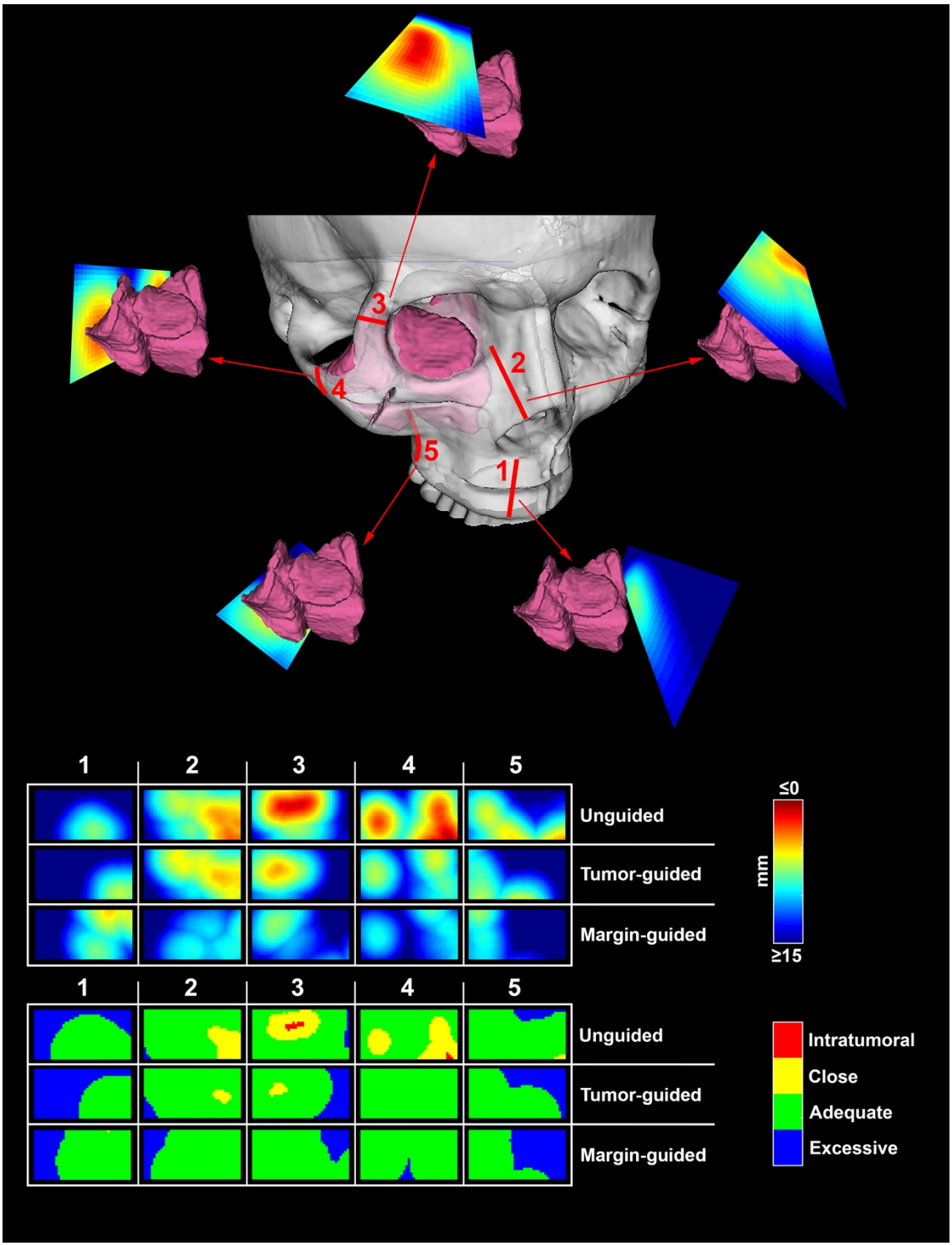


**Figure 5**. Data generation. The upper part of the panel shows the sequence of 5 cut simulations around the tumor model. The lower part of the panel depicts how the planes generated through analysis could be compared to visually assess the changes from the unguided to the tumor- and margin-guided simulations.

## Results

Eight head and neck surgeons with heterogeneous experience (ranging from 4 to 21 years of experience) in oncologic ablations participated to the study. Six surgeons have completed a head and neck fellowship training, while 2 were attending a residency training program at the time of simulations. Overall, 381 cuts were simulated, namely 127 per group (*i.e.*, unguided, tumor-guided, margin-guided). All the

surgeons confidently used the clipping function during navigation, with variable and subjective preference in terms of rotation of the 3D-rendered image. Most of the surgeons felt more confident with the tumor-guided navigation compared to the margin-guided navigation.

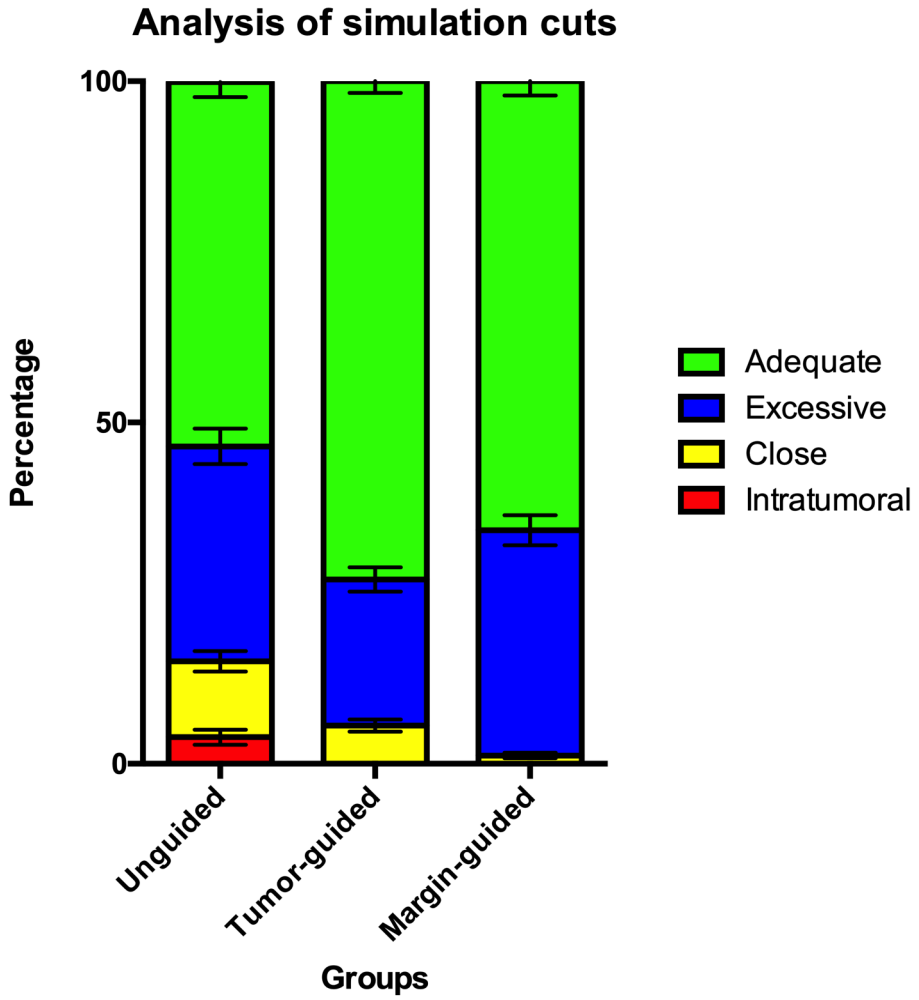


**Figure 6**. Comparison between techniques. Stacked histogram summarizing the distribution of intratumoral, close, adequate, and excessive points for the unguided and tumor- and margin-guided navigations.

Intratumoral cuts were observed in 23/127 (18.1%) unguided simulations, whereas none of the guided simulations (both tumor-guided and margin-guided) passed through the tumor ($p<0.0001$) (Table 1). When analyzing single-surgeon results, rate of intratumoral unguided cuts ranged from 10.0% to 66.7%; this variability was close to statistical significance ($p=0.051$). The percentage of points falling within the tumor volume was significantly higher in the group of unguided simulations compared to the guided ($p<0.0001$) (Table 1; Figure 6). Percentage of close points was significantly lower in margin-guided with respect to the other 2 groups ($p<0.0001$) (Table 1; Figure 6). The rate of excessively distant points was significantly lower in the tumor-guided group compared to the others ($p=0.0002$) (Table 1; Figure 6). The percentage of points at adequate distance from the tumor surface was significantly higher in the guided groups when compared to the

unguided group (p<0.0001) (Table 1; Figure 6). The time to complete the simulations was significantly shorter in the unguided group (p=0.001) (Table 1).

The gain provided by the 3D tumor rendering guidance was on average +19.6% (median: +17.4%), ranging from -48.4% to +100.0%, and was not significantly affected by any of the variables included in the study.

| Outcome | Unguided | Tumor-guided | Margin-guided | P-value |
|---|---|---|---|---|
| Intratumoral cuts (count) | 23/127 (18.1%) | 0/127 (0.0%) | 0/127 (0.0%) | <0.0001* |
| Intratumoral points (mean [IQR]) | 3.9% [0.0-0.0%]$^{A}$ | 0.0% [0.0-0.0%]$^{B}$ | 0.0% [0.0-0.0%]$^{B}$ | <0.0001** |
| Close points (mean [IQR]) | 11.1% [0.0-20.7%]$^{A}$ | 5.6% [0.0-5.9%]$^{A}$ | 1.2% [0.0-0.0%]$^{B}$ | <0.0001** |
| Excessive points (mean [IQR]) | 31.5% [4.8-50.9%]$^{A}$ | 21.4% [3.8-32.5%]$^{B}$ | 33.0% [11.7-48.1%]$^{A}$ | 0.0002** |
| Adequate points (mean [IQR]) | 53.4% [35.8-71.7%]$^{A}$ | 73.0% [61.3-86.3%]$^{B}$ | 65.8% [51.7-86.1%]$^{B}$ | <0.0001** |
| Duration (mean [IQR]) | 113.8 sec [60.5-130.7 sec]$^{A}$ | 198.9 sec [98.7-252.9 sec]$^{B}$ | 172.5 sec [112.6-210.7 sec]$^{B}$ | 0.001** |

**Table 1**. Table summarizing outcomes of the 3 simulations performed. *Fisher exact test; **Kruskal-Wallis test; $^{A,B}$Groups significantly different based on Steel-Dwass-Critchlow-Fligner post-hoc test. IQR – Interquartile range.

## Discussion

The present preclinical study demonstrates the beneficial role, in terms of margin delineation, of real-time 3D navigation in ablative surgery for advanced sinonasal tumors. The frequency of intratumoral cuts decreased from 18.1% to 0.0% when the surgeon used navigation during the simulation, and the adequacy of margin delineation improved by 19.6%. Since margin control still represents an unmet challenge in the management of such cancers, integration of real-time 3D navigation into surgical practice is a promising avenue for the future.

### *Current standard of care*

Surgery plays an important role in the management of advanced sinonasal cancer,[32,33] with non-surgical strategies being currently employed mostly in the neoadjuvant or adjuvant setting.[34-36] Achieving clear margins is paramount and is the key surgeon-controllable variable that can significantly affect patient outcome.[37-40] Consequently, optimization of margin control has been a key research focus for surgeons and researchers. To date, most of the research around this issue has been based on surgical technique, with refinements in open surgical approaches being claimed as a solution to partially improve margin control.[41-44] More recently, Deganello *et al.* demonstrated the benefit of guiding the medial and posterior margin delineation through an endoscopic transnasal approach.[13]

***Surgical navigation***

Surgical navigation guidance has been reported as a potential strategy to optimize control of margins. Feichtinger *et al.* reported their experience with positron emission tomography (PET)/CT-based navigation in a series of 6 patients with locally advanced sinonasal/oral cancer. Initial resection with navigation was demonstrated to be inadequate in 4/6 (67%) of patients, with revision of the resection obtaining adequate margins in 3/4 (75%) of the patients.[23] Likewise, Catanzaro *et al.* and Tarsitano *et al.* recently demonstrated that navigation provided a significant improvement in terms of deep margin status when added to the standard procedure for advanced maxillary, oral, or orbital cancers (*i.e.*, ablation followed by mapping of the surgical bed with frozen-section biopsies).[21,22] While these studies included only a limited number of patients (18), they were the first advocates for margin improvement using surgical navigation. One limitation of the navigation systems used in these studies is that they only provide tracking of a pointer tool, whereas in this work we investigate the use of planar cutting tool tracking (*e.g.*, osteotome, saw) along with a 3D rendering.

***Osteotomies***

Resection of tumors of the sinonasal tract requiring open surgery is based on a variable number of osteotomies made through the bones that contain the neoplasm. This requires the surgeon to position and orient the saw/osteotome according to a mental representation of the tumor with respect to specific anatomical landmarks identified throughout the dissection. Sinonasal tumors are frequently irregular in shape having invaded neighboring structures, which are characterized by unique anatomical complexity. For this reason it is not uncommon to set suboptimal cutting trajectories, which results in a high rate (21-45%) of positive margins.[13,39,40,45]

The use of 3D navigation provides the surgeon with a real time direct visualization of the tumor, thus allowing to choose the ideal position and orientation of the osteotome with respect to the tumor anatomy. This translates into the ability to find a balance between achieving sufficiently adequate margins while sparing uninvolved structures and neurovascular bundles, as already demonstrated in studies assessing this technology in pelvic tumor resection.[46,47] In this preclinical study, we observed a significant improvement in the virtual delineation of margins when 3D navigation was employed (Table 1, Figure 6). Simultaneously, the rate of excessively distant points was significantly reduced (Table 1, Figure 6). The rate of close points (*i.e.*, <5 mm distant from the tumor surface) was minimal with the addition of the margin rendering (Figure 3C), which served as a visual guide providing the surgeon with a reference of 1-cm margin. Interestingly, the margin rendering led surgeons to increase the distance of the cutting planes, thus resulting in a higher percentage of points excessively distant from the tumor surface when compared to 3D visualization of the tumor alone (Table 1, Figure 6). This finding aligns with the fact that surgeons generally preferred the tumor-guided navigation as compared to the margin-guided. Such results suggest that employment of a fixed margin rendering is of potential use, but likely requires adequate training to be properly interpreted by the surgeon while depicting the trajectory of osteotomies.

The gain in terms of margin delineation provided by surgical navigation was on average 19.6% and ranged from 10.3% to 34.3% when analyzing the single-surgeon results. Despite the heterogeneity of training and experience, which resulted in a close-to-significant variability of the rate of intratumoral unguided cuts ($p=0.051$), the improvement in adequacy of margin delineation when relying on surgical navigation was statistically independent of the surgeon. This result suggests that surgical navigation could be beneficial for both expert and novice surgeons. A possible explanation is that the 3D visualization of the tumor facilitates the margin delineation.

An area of 4x2 cm was chosen for the analysis of cutting planes. This arbitrary parameter choice was meant to reproduce the portion of the plane that would have been actually delineated in real surgery. On the longitudinal axis of the osteotome/saw, the cutting trajectory remains constant during maxillectomy. This is due to the fact that the osteotomy edges prevent freedom of movement towards the underlying bony/soft tissues. Therefore, we estimated 4 cm as an adequate approximation to render this mechanical constraint. On the tangential axis the surgeon can adjust the trajectory of osteotome/saw creating curve cuts. For this reason, the area of analysis was restricted to 1 cm on each side of the midline of the osteotome, as wider areas would not reliably simulate the possibility to curve the cutting instruments. With the intent to qualitatively describe the cutting planes, distances with respect to the tumor surface were classified as intratumoral (crossing the tumor), close (<5 mm), adequate (5-15 mm), and excessive (>15 mm). The close class follows the standard definition of "close margin" in head and neck oncology, even though it must be specified that data proving that this cutoff is meaningful in sinonasal cancer are currently lacking. A relatively wide range (from 5 to 15 mm) was adopted to define the adequate distance. This was necessary as in sinonasal oncological surgery the possibility to surround the tumor with healthy tissue varies widely according to the anatomical relationships with neighboring critical structures (*e.g.*, orbit, internal carotid artery, brain). This also reflects the variable need to adjust the margin delineation based on biological aggressiveness of diverse histologies.

Previous studies from our research group have demonstrated that real-time, 3D guidance of osteotomies in the maxillofacial skeleton is accurate and applicable to the surgical setting.[20,48] In a recent study from Hasan *et al.*, intraoperative CBCT was acquired to provide on-the-table images for navigation reflecting changes in patient anatomy (*e.g.*, mandible mobility).[27,48] However, intraoperative imaging is unavailable in the majority of centers where patients are treated for head and neck cancer. Consequently, it is of utmost importance to minimize the delay between preoperative imaging and surgery, aiming to maximize the reliability of tumor contouring. Segmentation of tumor boundaries at imaging requires enough contrast between the tumor and surrounding tissues, which is best provided by magnetic resonance imaging (MRI) due to its intrinsically high contrast resolution.[1,49] However, contrast-enhanced CT can also be employed to preoperatively or intraoperatively contour tumors, thus taking advantage from its quicker acquisition timing and higher logistical versatility. Fusion imaging combining CT, MRI, and/or PET has an even higher potential to optimize the precision of tumor contouring by merging morphological and functional information.[50]

Accuracy of registration is another essential requirement for 3D guidance of osteotomies. Under the ideal conditions of our laboratory setting, a registration error less than 1 mm was easily obtained in the present

study. Similarly, registration errors ranging between 0.3 and 1.0 mm have been reported in the surgical application of similar navigations systems, demonstrating that such spatial accuracy can also be achieved in the clinical setting.[21,48] A potential alternative way to bypass registration would be to use customized cutting guides (*i.e.*, jigs), as those employed especially in fibula free flap-based reconstruction of the mandible.[51] However, this strategy seems anatomically challenging for certain osteotomies (i.e. ILOR, Zy, FMJ, CV-ASB, and PMJ-MSB) due to the need to work in narrow spaces.

A minor drawback of the 3D rendering system presented in this study is the significant increase of time needed to complete the simulation when using navigation. In fact, the average duration of simulations increased from 114 (unguided) to 199 (tumor-guided) and 173 (margin-guided) seconds. In addition, one should also consider the time needed preoperatively to contour the tumor, which could substantially vary based on surgeon and radiologist's experience, shape complexity, and imaging quality. However, this potential time increase would be counterbalanced by the aforementioned advantages in terms of margins delineation and is likely of little relevance during a long surgical procedure. Moreover, a learning curve with subsequent time reduction is expected as already observed in other studies focusing on navigation in the sinonasal area.[16]

*Limitations of the study*

The main limitation of the present study is its preclinical nature, which makes the results potentially biased by the "ideal" conditions of the laboratory setting. However, the preliminary clinical data published in the literature so far align with the observations of the present study.[21-23] This makes the translation of such technology into clinical practice a step forward, however there must be adequate research in the clinical setting to ensure that there is measurable clinical benefit to the patient from an oncological point of view. A further limitation of the study was the order of simulations (unguided, tumor-guided, margin-guided) was not randomized. The rationale for this was based on the belief that tumor-guided and margin-guided simulations could have enhanced adequate osteotome orientation in the subsequent unguided task. Similarly, performing the margin-guided simulation before the tumor-guided could have biased the ability to delineate the cutting trajectory at an adequate distance from the tumor surface. However, the authors acknowledge that using the same order of osteotome each time may have caused a "learning effect" that is independent of whether image guidance was used or not.

As a final remark, application of surgical navigation to oncologic procedures cannot prescind from a cohesive multidisciplinary approach, which includes radiologists, engineers, technicians, nurses, and surgeons skilled in the intraoperative interpretation of cross-sectional and 3D imaging. Therefore, future clinical validation of the present results will depend on the qualifications and experience of the multidisciplinary surgical teams, and their ability to effectively implement this technology in the operating room.

**Conclusions**

This preclinical study has demonstrated the significant benefit of navigation-guided osteotomies for sinonasal tumors. At the cost of a negligible time increase, real-time 3D navigation completely prevented

intratumoral trajectories and optimized the delineation of margins. Translation into the clinical setting - with rigorous assessment from an oncological point of view - will be the proposed next step.

**References**


1. Lund VJ, Stammberger H, Nicolai Pet al. European position paper on endoscopic management of tumours of the nose, paranasal sinuses and skull base. Rhinol Suppl 2010; 22:1-143.
2. Villaret AB, Yakirevitch A, Bizzoni Aet al. Endoscopic transnasal craniectomy in the management of selected sinonasal malignancies. Am J Rhinol Allergy 2010; 24:60-65.
3. Nicolai P, Battaglia P, Bignami Met al. Endoscopic surgery for malignant tumors of the sinonasal tract and adjacent skull base: a 10-year experience. Am J Rhinol 2008; 22:308-316.
4. Lund VJ, Wei WI. Endoscopic surgery for malignant sinonasal tumours: an eighteen year experience. Rhinology 2015; 53:204-211.
5. Snyderman CH, Carrau RL, Kassam ABet al. Endoscopic skull base surgery: principles of endonasal oncological surgery. J Surg Oncol 2008; 97:658-664.
6. Nicolai P, Castelnuovo P, Bolzoni Villaret A. Endoscopic resection of sinonasal malignancies. Curr Oncol Rep 2011; 13:138-144.
7. Hanna E, DeMonte F, Ibrahim S, Roberts D, Levine N, Kupferman M. Endoscopic resection of sinonasal cancers with and without craniotomy: oncologic results. Arch Otolaryngol Head Neck Surg 2009; 135:1219-1224.
8. Lund V, Howard DJ, Wei WI. Endoscopic resection of malignant tumors of the nose and sinuses. Am J Rhinol 2007; 21:89-94.
9. Castelnuovo P, Battaglia P, Turri-Zanoni Met al. Endoscopic endonasal surgery for malignancies of the anterior cranial base. World Neurosurg 2014; 82:S22-31.
10. Moya-Plana A, Bresson D, Temam S, Kolb F, Janot F, Herman P. Development of minimally invasive surgery for sinonasal malignancy. Eur Ann Otorhinolaryngol Head Neck Dis 2016; 133:405-411.
11. Ramaekers BL, Pijls-Johannesma M, Joore MAet al. Systematic review and meta-analysis of radiotherapy in various head and neck cancers: comparing photons, carbon-ions and protons. Cancer Treat Rev 2011; 37:185-201.
12. Naunheim MR, Goyal N, Dedmon MMet al. An Algorithm for Surgical Approach to the Anterior Skull Base. J Neurol Surg B Skull Base 2016; 77:364-370.
13. Deganello A, Ferrari M, Paderno Aet al. Endoscopic-assisted maxillectomy: Operative technique and control of surgical margins. Oral Oncol 2019; 93:29-38.
14. Austin RE, Antonyshyn OM. Current applications of 3-d intraoperative navigation in craniomaxillofacial surgery: a retrospective clinical review. Ann Plast Surg 2012; 69:271-278.
15. Bell RB. Computer planning and intraoperative navigation in cranio-maxillofacial surgery. Oral Maxillofac Surg Clin North Am 2010; 22:135-156.
16. Azarmehr I, Stokbro K, Bell RB, Thygesen T. Surgical Navigation: A Systematic Review of Indications, Treatments, and Outcomes in Oral and Maxillofacial Surgery. J Oral Maxillofac Surg 2017; 75:1987-2005.
17. To EW, Yuen EH, Tsang WMet al. The use of stereotactic navigation guidance in minimally invasive transnasal nasopharyngectomy: a comparison with the conventional open transfacial approach. Br J Radiol 2002; 75:345-350.
18. Schramm A, Gellrich NC, Gutwald Ret al. Indications for computer-assisted treatment of cranio-maxillofacial tumors. Comput Aided Surg 2000; 5:343-352.
19. Schramm A, Suarez-Cunqueiro MM, Barth ELet al. Computer-assisted navigation in craniomaxillofacial tumors. J Craniofac Surg 2008; 19:1067-1074.
20. Bernstein JM, Daly MJ, Chan Het al. Accuracy and reproducibility of virtual cutting guides and 3D-navigation for osteotomies of the mandible and maxilla. PLoS One 2017; 12:e0173111.
21. Tarsitano A, Ricotta F, Baldino Get al. Navigation-guided resection of maxillary tumours: The accuracy of computer-assisted surgery in terms of control of resection margins - A feasibility study. J Craniomaxillofac Surg 2017; 45:2109-2114.
22. Catanzaro S, Copelli C, Manfuso Aet al. Intraoperative navigation in complex head and neck resections: indications and limits. Int J Comput Assist Radiol Surg 2017; 12:881-887.
23. Feichtinger M, Pau M, Zemann W, Aigner RM, Karcher H. Intraoperative control of resection margins in advanced head and neck cancer using a 3D-navigation system based on PET/CT image fusion. J Craniomaxillofac Surg 2010; 38:589-594.
24. Guo R, Guo YX, Feng Z, Guo CB. Application of a computer-aided navigation technique in surgery for recurrent malignant infratemporal fossa tumors. J Craniofac Surg 2015; 26:e126-132.
25. Siewerdsen JH, Moseley DJ, Burch Set al. Volume CT with a flat-panel detector on a mobile, isocentric C-arm: pre-clinical investigation in guidance of minimally invasive surgery. Med Phys 2005; 32:241-254.
26. Daly MJ, Siewerdsen JH, Moseley DJ, Jaffray DA, Irish JC. Intraoperative cone-beam CT for guidance of head and neck surgery: Assessment of dose and image quality using a C-arm prototype. Med Phys 2006; 33:3767-3780.

27. King E, Daly MJ, Chan Het al. Intraoperative cone-beam CT for head and neck surgery: feasibility of clinical implementation using a prototype mobile C-arm. Head Neck 2013; 35:959-967.
28. Jermyn M, Ghadyani H, Mastanduno MAet al. Fast segmentation and high-quality three-dimensional volume mesh creation from medical images for diffuse optical tomography. J Biomed Opt 2013; 18:86007.
29. Kikinis R, Pieper SD, Vosburgh KG. 3D Slicer: A Platform for Subject-Specific Image Analysis, Visualization, and Clinical Support. In: Jolesz FA, ed. *Intraoperative Imaging and Image-Guided Therapy*. New York: Springer, 2014.
30. Daly MJ, Chan H, Nithiananthan Set al. Clinical implementation of intraoperative cone-beam CT in head and neck surgery *Progress in Biomedical Optics and Imaging*. Orlando: Proceedings of SPIE, 2011.
31. Enquobahrie A, Cheng P, Gary Ket al. The image-guided surgery toolkit IGSTK: an open source C++ software toolkit. J Digit Imaging 2007; 20 Suppl 1:21-33.
32. Castelnuovo P, Turri-Zanoni M, Battaglia P, Antognoni P, Bossi P, Locatelli D. Sinonasal Malignancies of Anterior Skull Base: Histology-driven Treatment Strategies. Otolaryngol Clin North Am 2016; 49:183-200.
33. Lopez F, Lund VJ, Suarez Cet al. The Impact of Histologic Phenotype in the Treatment of Sinonasal Cancer. Adv Ther 2017; 34:2181-2198.
34. Bossi P, Saba NF, Vermorken JBet al. The role of systemic therapy in the management of sinonasal cancer: A critical review. Cancer Treat Rev 2015; 41:836-843.
35. Khoury T, Jang D, Carrau R, Ready N, Barak I, Hachem RA. Role of induction chemotherapy in sinonasal malignancies: a systematic review. Int Forum Allergy Rhinol 2019; 9:212-219.
36. Turri-Zanoni M, Lambertoni A, Margherini Set al. Multidisciplinary treatment algorithm for the management of sinonasal cancers with orbital invasion: A retrospective study. Head Neck 2019.
37. Paulino AC, Marks JE, Bricker P, Melian E, Reddy SP, Emami B. Results of treatment of patients with maxillary sinus carcinoma. Cancer 1998; 83:457-465.
38. Ozsaran Z, Yalman D, Baltalarli B, Anacak Y, Esassolak M, Haydaroglu A. Radiotherapy in maxillary sinus carcinomas: evaluation of 79 cases. Rhinology 2003; 41:44-48.
39. Bristol IJ, Ahamad A, Garden ASet al. Postoperative radiotherapy for maxillary sinus cancer: long-term outcomes and toxicities of treatment. Int J Radiat Oncol Biol Phys 2007; 68:719-730.
40. Nishio N, Fujimoto Y, Fujii Met al. Craniofacial Resection for T4 Maxillary Sinus Carcinoma: Managing Cases with Involvement of the Skull Base. Otolaryngol Head Neck Surg 2015; 153:231-238.
41. Chatni SS, Sharan R, Patel D, Iyer S, Tiwari RM, Kuriakose MA. Transmandibular approach for excision of maxillary sinus tumors extending to pterygopalatine and infratemporal fossae. Oral Oncol 2009; 45:720-726.
42. Kreeft AM, Smeele LE, Rasch CRet al. Preoperative imaging and surgical margins in maxillectomy patients. Head Neck 2012; 34:1652-1656.
43. Balm AJ, Smeele LE, Lohuis PJ. Optimizing exposure of the posterolateral maxillary and pterygoid region: the lower cheek flap. Eur J Surg Oncol 2008; 34:699-703.
44. Sun J, Shen Y, Weng YQ, Li J, Zhang ZY. Lateral lip-splitting approach for total and subtotal maxillectomy. J Oral Maxillofac Surg 2009; 67:1197-1205.
45. Qureshi SS, Chaukar DA, Talole SD, Dcruz AK. Clinical characteristics and outcome of non-squamous cell malignancies of the maxillary sinus. J Surg Oncol 2006; 93:362-367.
46. Sternheim A, Daly M, Qiu Jet al. Navigated pelvic osteotomy and tumor resection: a study assessing the accuracy and reproducibility of resection planes in Sawbones and cadavers. J Bone Joint Surg Am 2015; 97:40-46.
47. Sternheim A, Kashigar A, Daly Met al. Cone-Beam Computed Tomography-Guided Navigation in Complex Osteotomies Improves Accuracy at All Competence Levels: A Study Assessing Accuracy and Reproducibility of Joint-Sparing Bone Cuts. J Bone Joint Surg Am 2018; 100:e67.
48. Hasan W, Daly MJ, Chan HHL, Qiu J, Irish JC. Intraoperative cone-beam CT-guided osteotomy navigation in mandible and maxilla surgery. Laryngoscope 2019.
49. Maroldi R, Ravanelli M, Borghesi A, Farina D. Paranasal sinus imaging. Eur J Radiol 2008; 66:372-386.
50. Konidena A, Shekhar S, Dixit A, Patil DJ, Gupta R. Fusion imaging: a bipartite approach. Oral Radiol 2018; 34:1-9.
51. Tarsitano A, Del Corso G, Ciocca L, Scotti R, Marchetti C. Mandibular reconstructions using computer-aided design/computer-aided manufacturing: A systematic review of a defect-based reconstructive algorithm. J Craniomaxillofac Surg 2015; 43:1785-1791.

# Use of surgical navigation with three-dimensional rendering and virtual endoscopy to delineate critical margins in advanced craniofacial tumors models

*Taboni et al., Front Oncol 2021; doi: 10.3389/fonc.2021.747227*

**Introduction**

Resection of advanced maxillary sinus cancers can be particularly challenging due to anatomical proximity to surrounding neural and vascular structures. This challenge creates a dilemma for surgical treatment as one is balancing between an adequate margin of resection and potential morbidity. Over the last 3 decades, the evolution of transnasal endoscopic surgery and improvements in adjuvant treatments have been considerably impacting on the management of sinonasal cancer.[1–13] Transnasal endoscopy can be considered the standard of treatment for many adequately selected nasoethmoidal malignancies and, in addition, it can be can effectively aid delineation of critical margins of resection even in the setting of open approaches for advanced sinonasal cancers (i.e., endoscopic-assisted maxillectomy and cranioendoscopic resection).[13,14] With the era of endoscopic and minimal access surgical ablations there has been an increasing reliance on imaging for patient selection as well as for prediction of volume of ablation. The ability to increasingly employ intraoperative near real-time on-the-table surgical navigation to improve margin-negative resection is upon us.

With the advent of new technologies, particularly in the area of intraoperative imaging, the ability to increase the confidence and performance of margin-negative tumor resections while maximizing the preservation of normal anatomical structures is upon us. Specifically, determining the posterior margin (PM) of the resection during maxillectomy surgery is a challenge and has prompted researchers to propose solutions to address this problem.[13,15–19] Correct delineation of the PM of a maxillectomy requires the surgeon to build a three-dimensional (3D) mental image of the tumor based on preoperative imaging. Even in the hands of experienced surgeons, this process can be difficult and minor deviations in position and orientation of the margin can significantly affect the cut trajectory with respect to the tumor and critical anatomical structures.

Since the early 1990s, surgical navigation (SN) has emerged as useful aid and evolved parallel to transnasal endoscopic surgery, particularly with the intent to avoid complications.[20] SN in the craniomaxillofacial region has proven to be useful in the assessment of reconstruction adequacy and for the planning of osteotomies during oncologic ablations.[21–23] Moreover, SN has provided improved accuracy of craniomaxillofacial osteotomies[24,25] and proportional improvement of clinical outcomes can be hypothesized based on preliminary experiences.[26–29] Implementation of endoscopy with 3D-rendered SN with virtual endoscopy (3D-SNVE) may represent a significant step forward.

The aim of this preclinical study was to test and quantify the benefits provided by 3D-SNVE in terms of adequate delineation of the PM in models of advanced maxillary tumors that would require an open maxillectomy.

## Materials and methods

### *Tumor model preparation*

Four artificial skulls (Sawbones®, Washington) and a moldable material (Play-Doh®, Hasbro®, Rhode Island) mixed with acrylic glue were employed to build 4 models of locally advanced maxillary sinus tumors with varying degrees of posterior tumor extension. The degree of posterior extension in each model is described in terms of involvement of anatomical spaces/structures and closest distance from the internal carotid artery (ICA) (T-C distance): I) invasion of the pterygopalatine fossa (PPF), T-C distance: 14.9 mm (Model #1); II) invasion of the medial pterygoid plate, pterygoid fossa, and base of the pterygoid process, T-C distance: 10.2 mm (Model #2); III) complete invasion of the pterygoid process, T-C distance: 6.2 mm (Model #3); IV) invasion of the anterior foramen lacerum and upper parapharyngeal space, T-C distance: 3.5 mm (Model #4) (Figure 1). Each tumor model was created based on actual cases of maxillary cancers treated between January 2016 and December 2018 in the Unit of Otorhinolaryngology – Head and Neck Surgery of the University of Brescia (Brescia, Italy); the tumor models were based on preoperative magnetic resonance imaging (MRI) (Figure 1). Soft tissues in the models were simulated using medical gauzes to restrict tumor visualization to only the endoscopic and transoral views (*i.e.,* simulating tumors ulcerating into the sinonasal and/or oral cavity). The anterior third of the nasal septum was simulated with a 3-mm slice of silicon, fixed orthotopically to the skull with acrylic glue. As a result of silicon elasticity, the anterior nasal septum could be partially tilted and displaced with the scope and instruments during simulations. The ICAs in the models were created from an angio-CT which was done in a neurological work-up for an anonymized patient and were semi-automatically contoured through Mimics® (Materialise, Leuven, Belgium). First, a global threshold was applied to provide a quick gross segmentation, and then manual refinement was used to smooth the segmentation. Respective stereolithography (STL) files were generated and ICAs were 3D printed [3D Printer Dimension 1200es system (Stratasys, Eden Prairie, MN)] and painted with red dye mixed with iodine solution for CT contrast (Omnipaque, GE Healthcare). A carotid canal was manually created in the base of the artificial skulls and each ICA was fixed in the anatomical situation. The area for simulation of transnasal PM delineation was marked by horizontal lines in the phantoms and further classified into a superior and an inferior part based on the plane passing through the inferior aspect of the nasopharyngeal vault (Figure 2C).

### *Surgical pointer tool preparation*

Custom surgical pointers were designed using Autodesk Fusion 360 software (San Rafael, CA) and 3D printed on a Dimension 1200es system (Stratasys, Eden Prairie, MN). Surgeons participating in simulations were provided with color-coded pointers with different angulations (0°, 30°, 45°, 60°, and 90°) (Figure 2B and 2D). Each pointer was meant to simulate the trajectory of delineation of the PM of resection, so that the surgeon could select which trajectory best represented the way he/she would have set the PM of resection from a transnasal perspective.

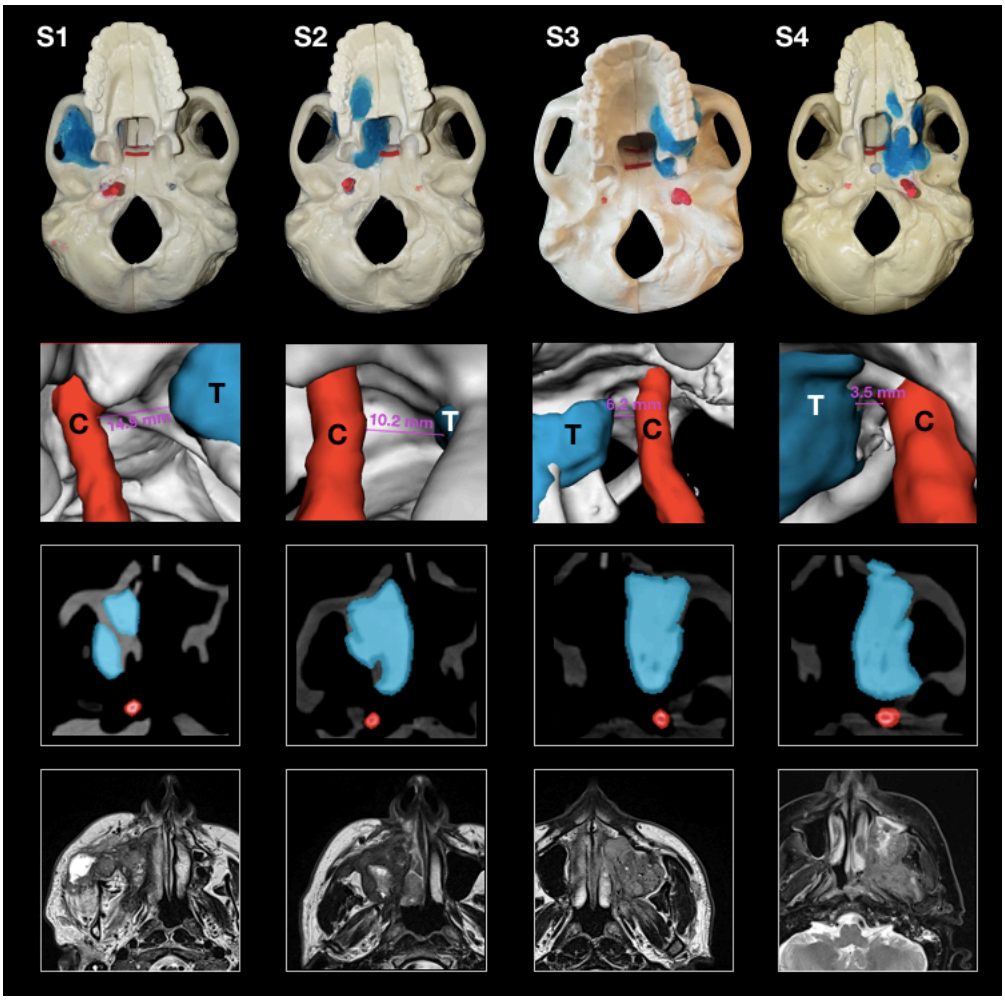


**Figure 1**. Panel with 4 phantoms, as seen from an inferior perspective (superior row); 3D rendering of the tumor and the carotid alongside with the tumor-carotid distance for each model (central row); appearance of tumors at the computed tomography imaging alongside with contouring of the tumor and the carotid (inferior row).

### *Image acquisition and tumor contouring*

3D images of each skull model were acquired using a prototype cone-beam computed tomography (CBCT) imaging system on a mobile C-arm.[30,31] The mentioned flat-panel imaging system was validated for guidance of head and neck procedures involving significant bone resection and/or complex anatomical reconstruction.[32] In this study, 3D volumes (256×256×192) covered a field of view of 20×20×15 $cm^3$ using isotropic 0.8-mm 3D voxels. On CBCT imaging, the tumor and carotid models were clearly distinguishable from the artificial bone, as they showed much higher x-ray attenuation (Figure 1 and 3). Contouring of the tumors and ICAs was obtained semi-automatically using a two-step process within NIRFAST-Slicer software.[33] First, a global threshold was applied to provide a quick, coarse segmentation, and then manual refinement was used to smooth the segmentation. To visualize a virtual surgical margin around the ICA (Figure 3), a semi-transparent wireframe was generated at 2 mm from the vessel surface using volumetric image dilation processing in MATLAB software (MathWorks, Massachusetts).

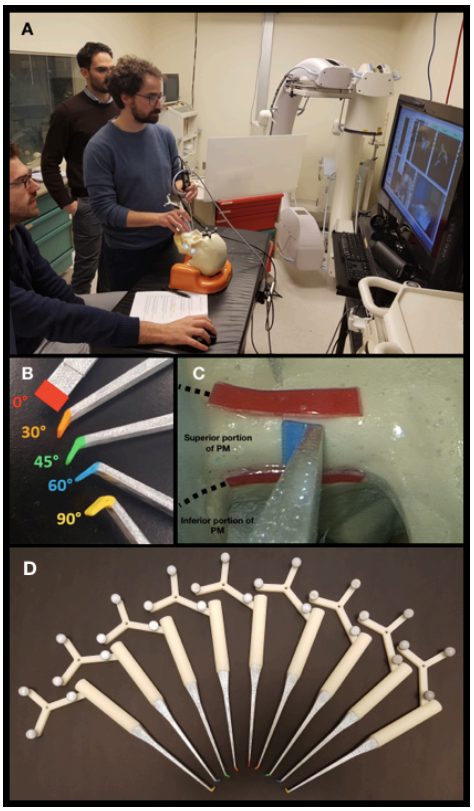


**Figure 2**. Simulation setting (**A**); pointers with different types of angled tips (**B, D**); endoscopic view with red lines indicating the superior and inferior potions of the posterior margin (**C**).

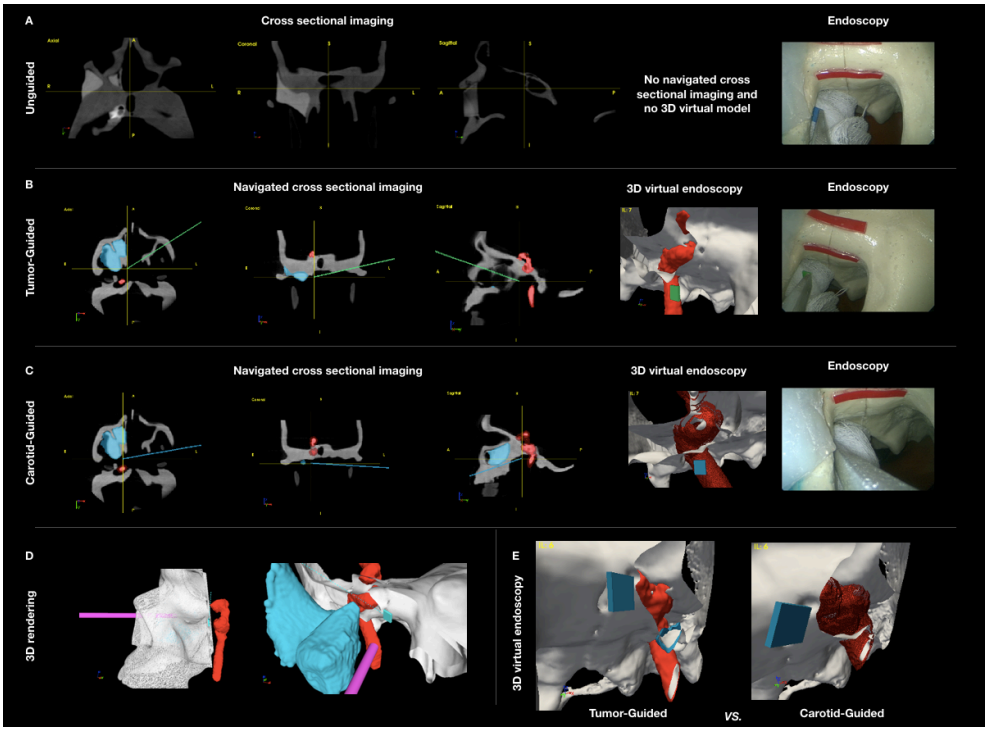


**Figure 3**. Panel showing the appearance of different settings of data acquisition: unguided simulations with cross sectional imaging pre-simulation analysis (**A**), tumor-guided (**B**), and carotid-guided (**C**) simulations with real time surgical navigation indicating the position of the instrument and posterior margin delineation. Pictures showing the appearance of the 3D rendering of the skull with the position of the scope and pointer (**D**); virtual margin delineation, simulating the cut of 3D objects (skull, tumor and carotid). Comparison of 3D virtual endoscopy appearance into the tumor-guided and carotid-guided settings (**E**).

***Navigation system***

CBCT images were displayed within an in-house navigation software package (GTx-Eyes), based on the open-source Image-Guided Surgery Toolkit.[34,35] Tumor and margin segmentations were superimposed on 3-planar views and separately as 3D surface renderings. Surgical tool tracking in this study was provided by a stereoscopic infrared camera (Polaris Spectra, NDI, Waterloo, Ontario). Image-to-tracker registration was obtained by paired-point matching of predrilled divots by means of a tracked pointer. A small 4-sphere reference tool (NDI, Waterloo, Ontario) was anchored to the skull throughout registration and simulations. A registration error of 1 mm or less was considered acceptable for the navigation experiments. A 4-sphere reference (Medtronic, Jacksonville, FL) was secured to each 3D printed tool (surgical pointer) and to a Storz® endoscope (Karl Storz Group. Tuttlingen, Germany), that was then calibrated using a custom calibration jig. Angled pointer navigation was implemented using software features for virtual planar tool clipping (*e.g.,* osteotome, saw) and colored accuracy indicators for distance, pitch, and roll developed previously for orthopedic oncology applications,[36] and subsequently applied to open head and neck procedures.[24,25,37] In this study, for transnasal simulations the 3D-rendering of the virtual endoscopic view could be freely rotated and the skull rendering clipped along the virtual cutting plane during the transnasal delineation of the PM (Figure 3).

***Surgical simulation***

Surgeons from the Department of Otolaryngology – Head and Neck Surgery of the University Health Network (Toronto, Ontario, Canada) and from the Unit of Otorhinolaryngology – Head and Neck Surgery of the University of Brescia (Brescia, Italy) were recruited for the simulations. Each surgeon received a brief explanation of the steps of the simulation and of the subsequent analysis methods. The surgical task was to choose among pointers with different angulations (0°, 30°, 45°, 60°, and 90°) and position the selected pointer under transnasal endoscopy guidance within the delineated areas (*i.e.*, superior and inferior part of the PM of resection) to provide a clear margin from the tumor posterior surface while avoiding intersection with the ipsilateral ICA. No physical cuts were performed to allow reuse of the models; rather, the pointer position and orientation were recorded when the surgeon gave vocal confirmation of his/her proposed delineation of the margin and the analysis was performed on the virtual trajectory. Surgeons were asked to define the superior and posterior part of the PM with 2 endoscopes (0° and 45°), first using only the surgical corridor of the ipsilateral nasal cavity and then through either a bilateral (*i.e.*, with the scope through one nostril and pointer through the other) or contralateral approach (i.e., with both scope and the pointer through the contralateral nostril). Surgeons were required to perform the PM delineation in 3 settings: (1) unguided; (2) tumor-guided; and (3) carotid-guided, as shown in Figure 3. In the unguided simulation, the surgeons could only view the cross-sectional images (*i.e.*, axial, sagittal, coronal) prior to start transnasal endoscopy, with no access to the real-time navigation system or the 3D tumor/margin renderings. In the tumor-guided simulation, virtual angled pointers were guided using real-time tool tracking and the 3D tumor and carotid segmentation (Figure 3). Finally, in the carotid-guided simulation, a 2-mm alert cloud surrounding the carotid was added to the tumor-

guided; in this setting a sonic alarm reproducing the arterial flow sound at Doppler examination was sounded when the trajectory of the PM definition was through the proximity alert zone,[38] and a beeping sonic alarm was activated when the trajectory of the PM definition was through the ICA (Figure 3).

To avoid recall bias, the phantoms were randomized for each surgeon and the sequence of the phantoms was arranged such that the guided and unguided simulations were never performed at close intervals. The rationale for this was based on the belief that guided simulations could have enhanced adequate pointer orientation in a subsequent unguided task.

***Virtual cutting plane analysis***

Analysis of cutting planes was performed by means of MATLAB software (MathWorks, Massachusetts). An area of 30 mm length along the longitudinal axis of the cut and 11 mm width (5.5 mm on both sides with respect to the longitudinal axis) was isolated from each plane starting from the pointer tip. The minimal distance with respect to the tumor and ICA surfaces was calculated for each point making up the isolated area and reproduced as a distribution of distances shown as a 30 × 11 (length x width) $mm^2$ color-scaled image (Figure 4). The cutting plane was deemed to be "intratumoral" when the cutting plane to tumor distance was ≤0 mm, and "adequate" when >0 mm. If the cutting plane was ≤0 mm to the ICA wall the ICA was considered "damaged", while a 0-2 mm margin to the ICA was deemed to be a "danger zone", and "adequate" distance was defined as >2mm. Each point of the isolated area was classified as follow: "red" (R) into the ICA; "orange 1" (O1), <2 mm from the ICA and into tumor; "orange 2" (O2), <2 mm from the ICA and <5 mm from tumor; "orange 3" (O3), <2 mm from the ICA and 5-10 mm from tumor; "orange 4" (O4), <2 mm from the ICA and >10 mm from tumor; "yellow 1" (Y1), >2 mm from the ICA and into tumor; "yellow 2" (Y2), >2 mm from the ICA and <5 mm from tumor; "green" (G), >2 mm from the ICA and 5-10 mm from the tumor; "blue" (B), >2 mm from the ICA and >10 mm from tumor. Each isolated area was described as a distribution among the above-mentioned categories.

***Surgeons' questionnaire***

At the end of the simulations each surgeon was asked to complete a validated questionnaire[38] (Table 1) to quantify opinions about the gain in terms of speed, accuracy, and self-confidence using tool-tracking and proximity alerts alongside the readiness for clinical translation of the technology.

***Statistical analysis***

Statistical analysis was run through XLSTAT® (Addinsoft®, New York). Simulations were grouped into three categories: unguided, tumor-guided, and carotid-guided. These 3 groups were compared in terms of the distance distributions through bilateral Kruskal-Wallis test and Steel-Dwass-Critchlow-Fligner post-hoc test. Rates of intratumoral and intra-ICA virtual cuts among the 3 groups of simulations were assessed with the Fisher exact test. Intraindividual differences in terms of percentage of adequate distance (G area) between

the tumor/carotid-guided and unguided groups of simulations were calculated and considered as the "gain" provided by 3D-SNVE. Level of significance was set at 0.05 for all statistical tests.

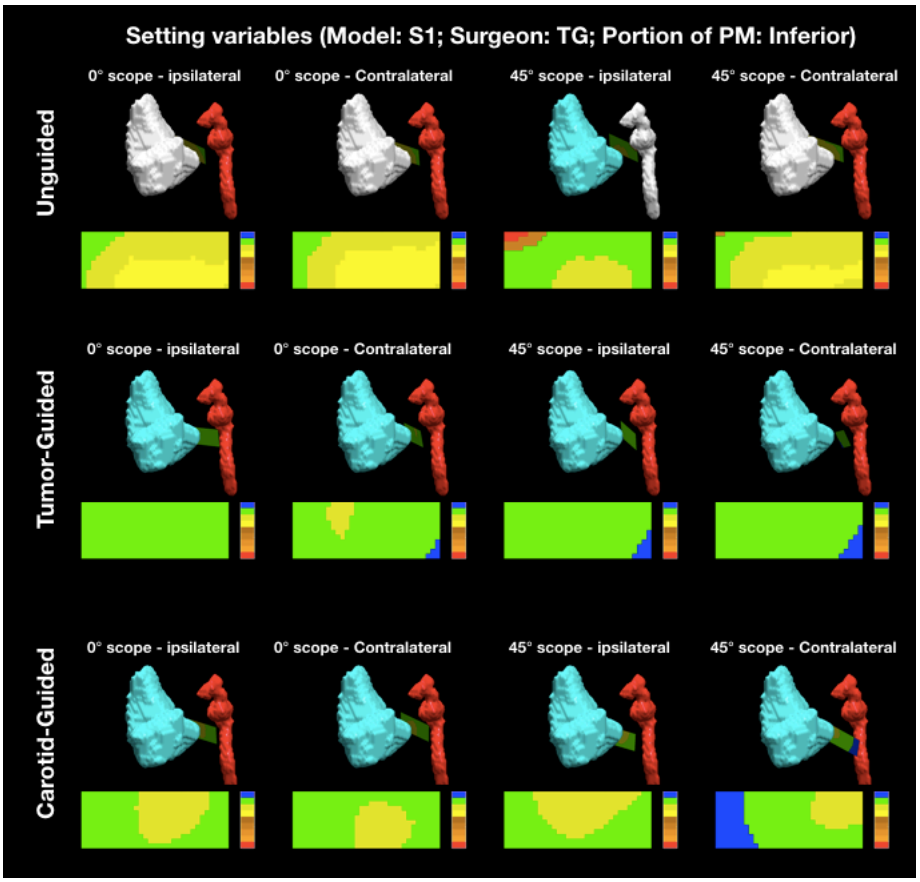


**Figure 4**. Example of the analysis of posterior margin delineation. Each point of the isolated area was classified as follow: "red" (R) into the internal carotid artery (ICA); "orange 1" (O1), <2 mm from ICA and into tumor; "orange 2" (O2), <2 mm from ICA and <5 mm from tumor; "orange 3" (O3), <2 mm from ICA and 5-10 mm from tumor; "orange 4" (O4), <2 mm from ICA and >10 mm from tumor; "yellow 1" (Y1), >2 mm from ICA and into tumor; "yellow 2" (Y2), >2 mm from ICA and <5 mm from tumor; "green" (G), >2 mm from ICA and 5-10 mm from the tumor; "blue" (B), >2 mm from ICA and >10 mm from tumor. Legend: PM, posterior margin.

| **Statement for questionnaire**[38] | **Median (interquartile range)*** |
|---|---|
| I felt faster to perform surgery when aided by the virtual view | 6.0 (6.0-6.8) |
| The system appeared to be sufficiently accurate for its intended use | 6.0 (6.0-6.0) |
| The dynamic tool tracking allowed me to quickly assess my proximity to critical structures without significantly interrupting dissection | 6.0 (6.0-6.8) |
| Proximity alerts increased my confidence during ablation close to critical structures | 6.0 (6.0-6.8) |
| The current technology is ready for clinical trial without significant changes | 5.5 (4.3-6.0) |
| *Based on seven-point Likert scale (7= strongly agree; 1=strongly disagree) | |

**Table 1.** Questionnaire answers and surgeons' responses.

| | Color code | Description | Unguided | Tumor-G | Carotid-G | P-value |
|---|---|---|---|---|---|---|
| % of cutting planes | **Red** | *Into carotid* | 6.7% | 0.9% | 1.0% | p<0.0001 |
| | **Orange 1** | *<2 mm carotid, into tumor* | 0.0% | 0.0% | 0.0% | NS |
| | **Orange 2** | *<2 mm carotid, <5 mm tumor* | 0.3% | 0.2% | 0.3% | NS |
| | **Orange 3** | *<2 mm carotid, 5-10 mm tumor* | 4.3% | 2.8% | 2.1% | p<0.0001 |
| | **Orange 4** | *<2 mm carotid, >10 mm tumor* | 1.6% | 0.2% | 0.4% | p<0.0001 |
| | **Yellow 1** | *>2 mm carotid, into tumor* | 3.6% | 0.4% | 0.2% | p<0.0001 |
| | **Yellow 2** | *>2 mm carotid, <5 mm tumor* | 19.1% | 23.8% | 23.5% | p=0.041 |
| | **Green** | *>2 mm carotid, 5-10 mm tumor* | 52.4% | 62.1% | 64.9% | p<0.0001 |
| | **Blue** | *>2 mm carotid, >10 mm tumor* | 12.1% | 9.5% | 7.5% | NS |

**Table 2**. Average percentage of points of the virtual margin delineation in each category of the "color code", according to the guidance setting. NS: not significant.

## Results

Eight head and neck surgeons with heterogeneous experience (ranging from 3 to 13 years of experience) in oncologic endoscopic resections participated to the study. Five surgeons completed head and neck fellowship training, while 3 were attending a residency training program at the time of simulations. Overall, 612 PM transnasal delineation were simulated, namely 204 per group (*i.e.,* unguided, tumor-guided, carotid-guided). Registration error was <1 mm in all simulations. Surgeons choose to use the 0°, 30°, 45°, 60°, and 90° pointers in 0 (0%), 61 (11%), 99 (18%), 246 (45%), 138 (25%) of transnasal simulations, respectively. Surgeons indicated that the surgical exposure was not adequate in 68 (11%) of simulations, of which 61 (90%) were through a transnasal ipsilateral approach, and no plane trajectories were recorded in these cases.

The virtual delineation of the PM of resection in maxillary tumor models transgressed the tumor in 47 (25.4%), 7 (4.0%), 4 (2.2%) of cases in the unguided, tumor-guided, and carotid-guided procedures, respectively (p<0.0001). The virtual margin delineation was more than 2 mm to the ICA in 80 (43.2%), 104 (59.4%) and 111 (60.3%) of cases in unguided, tumor-guided, and carotid-guided procedures, respectively (p<0.0001), and involved the ICA in 79 (42.7%), 30 (17.1%) and 25 (13.6%) of cases in unguided, tumor-guided, and carotid-guided procedures, respectively (p<0.0001).

Simulation tumor model S1 had a significantly lower rate of points falling into the carotid (at least one point into the carotid in 6% of simulations) and in the 2 mm carotid alert zone (at least one point into the alert zone in 7% of simulations), when compared to phantoms S2, S3, and S4 (32%, 30%, and 18% rate of intra-carotid simulations and 32%, 36%, and 35% rate of intra-alert zone simulations, respectively; p<0.0001 for both comparisons). The rate of clear margin (*i.e.*, margin not crossing the tumor) was not significantly different among the 4 phantoms (92%, 86%, 90%, 87% for S1, S2, S3, and S4, respectively; p=0.33).

The percentage of points falling within the tumor volume was significantly higher in the group of unguided simulations compared to the tumor- and carotid-guided (p<0.0001) (Table 2). In a bivariate analysis,

the guidance proved to be associated with a higher rate of clear margin ($p<0.0001$) and a lower rate of carotid damage ($p<0.0001$), independently from the increasing difficulty of the tumor-carotid model.

3D-SNVE significantly improved the rate of identification of an adequate plane of dissection while reducing the risk of carotid damage: the percentage of "red" points was significantly lower in the 2 guided groups with respect to the unguided group ($p<0.0001$) (Table 2) and the percentage of points with an adequate distance from the carotid and the tumor simultaneously (*i.e.*, "green" points) was significantly higher in the guided groups when compared to the unguided group ($p<0.0001$) (Table 2).

The gain of margin delineation provided by 3D-SNVE (considering both tumor- and carotid-guided settings) was on average 24.2% (ranging from 0.0% to 33.3%, when analyzing single-surgeon results) in terms of obtaining clear margins and 25.7% (ranging from 1.8% to 59.6%, when analyzing the single-surgeon results) in terms of avoiding carotid damage. The heterogeneity of training and experience resulted in a significant variability of the rate of intratumoral unguided cuts between surgeons (average value: 9.6%, range 0.0%-16.7%; $p=0.039$), but the gain in adequacy of margin delineation provided by 3D-SNVE was statistically independent of the operator ($p=0.202$).

***Surgeon preference***

All surgeons preferred using a bilateral trans-septal approach to have better vision and working volume in all models. Surgeons felt more self-confident using the 0° and the 45° scopes in 68% and 32% of unguided simulations and in 46% and 54% of guided simulations, respectively. When using 3D-SNVE, surgeons preferred the carotid-guided setting in 61% of simulations and the tumor-guided in 39%.

***Questionnaire score***

The seven-point Likert scale questionnaire statements and median (IQR) responses are shown in Table 1. No subject strongly disagreed (score 1–2) with any of the statements. Only one gave a negative response (score of 3) for question 1. One gave a negative response (score of 3) and 2 gave a neutral response (score of 4) for question 7. There was universal agreement (score 5–7) for all other questions, with uniform responses across the subjects.

**Discussion**

The present preclinical study demonstrates the beneficial role of 3D-SNVE in PM delineation and ICA preservation in ablative surgery for advanced maxillary tumors.

The frequency of "positive" margins decreased from 27% to 3% when the surgeon used navigation during the simulation, and the carotid damage decreased from 41% to 15%. Since margin control still represents a challenging goal in the surgical management of such cancers, implementation of 3D-SNVE into surgical practice is a promising strategy for the future. Furthermore, the possibility to add 3D rendering of critical structures on virtual views and cross-sectional imaging with associated sound alerts may increase the confidence of the surgeon during the procedure and help to avoid life-threatening complications.

While surgery combined with neoadjuvant and adjuvant radiation and chemotherapy has improved the overall outcomes of advanced sinonasal cancers, surgery still remains the principal modality of treatment.[39–41] Clear-margin resection has proven to significantly impact patient prognosis, and can be considered the most important surgeon-controllable variable.[13,42–45] Endoscopic surgery has been shown to improve the surgical precision and to reduce the morbidity of certain procedures. The benefits of guiding margin delineation in open maxillectomies through an endoscopic transnasal approach was demonstrated by Deganello *et al.*[13], who reported this technique as facilitating the detachment of the maxilla from the skull base and allowing for a more precise delineation of the posterior and medial margins of resection. This endoscopic technique was used to treat 79 advanced tumors involving the maxilla with a low rate of microscopic involvement of the PM (3.8%).[13] The authors classified posterior endoscopic resection in 3 types according to the anatomical structures progressively involved and found that even in the most complex scenario (*i.e.*, type 3 resection) the rate of free PM was remarkably high (87.5%).[13]

In previous clinical studies by Catanzaro *et al.*[26] and Tarsitano *et al.*[29], 3D navigation was helpful in achieving a significantly higher rate of clear deep margin when implemented to the standard procedure for advanced maxillary, oral, or orbital cancers (*i.e.*, ablation followed by mapping of the surgical bed with frozen-section biopsies). More recently, in studying maxillectomy surgery, Ricotta et al.[46] confirmed that the rate of overall positive margins was higher in the control group (10 patients) compared to a group of 18 patients operated on with SN.

A preclinical study by Ferrari *et al.*[24] was performed using a previous version of the same in-house navigation system employed here. That study evaluated cutting planes for osteotomies in open surgery of sinonasal advanced cancers and demonstrated a substantial benefit in delineation of the virtual osteotomies both for novel and experienced surgeons.

The present study adds to this previous work by testing the navigation system in a more complex setting, with critical anatomical structures close to the tumor. In addition to the complexity of the tumor-vessel model, the further development of real-time tool tracking with 3D virtual endoscopy for angled endoscopes allowed visual overlay of structures beyond the confines of the nasal wall and further allowed for clipping of the endoscopic 3D rendering along the angled pointer trajectory.

The surgical treatment of maxillary tumors requires accurate delineation of the posterior boundary of the resection in a very complex area with surrounding critical anatomical structures. The surgeon needs to base the ablation planning on a mental representation of the tumor and surrounding structures, relying upon specific anatomical landmarks identified throughout the dissection and this task becomes particularly challenging at the PM owing to poor visualization and maneuverability. Furthermore, cancers frequently have an irregular shape and have complex patterns of invasion into neighboring structures.[47] The use of 3D navigation provides the surgeon with a real-time direct visualization of the tumor and adjacent critical structures and facilitates positioning and orienting the margin with respect to the tumor and critical structures. The clinical translation of this navigation approach may help achieving a balance between adequacy of the oncological resection and

preservation of uninvolved surround anatomical structures. This benefit of the navigation has already been demonstrated in the field of pelvic tumor resection.[36]

In our preclinical study, a significant improvement in the virtual delineation of maxillectomy PM with high rates of complete and ICA-sparing virtual resection was demonstrated when 3D-SNVE was employed. The benefit of margin delineation guided by surgical navigation in terms of oncologic adequacy and critical structure preservation was remarkable (average gain of 24.2% in obtaining clear margins and 25.7% in avoiding carotid damage). Despite the heterogeneity of training and experience, which resulted in a significant variability of the rate of intratumoral unguided cuts ($p=0.039$), the gain in adequacy of margin delineation when relying on 3D-SNVE was statistically independent of the surgeon ($p=0.202$). This result suggests that surgical navigation could be beneficial both for expert and novice surgeons. The most reasonable explanation is that the 3D visualization of the tumor facilitates margin delineation, thus partially compensating for lack of experience in 3D mental representation of the tumor position and boundaries. In addition, with more extensive use of this technology, a learning curve with further improvement in surgical precision and time required can be expected, as already observed in other studies focusing on SN in the sinonasal area.[21]

Margins were not classified into either adequate or close for two main reasons: 1) the definition of a "negative", "close" or "positive" margin is not clear for sinonasal cancer resections, and 2) a complete resection with 5 mm or wider margin is hardly ever achievable in sinonasal cancers. In the present study we created phantoms with tumor models mimicking real cases with a very critical posterior extension, in which the minimal distance between the ICA and the tumor was 8.7 mm on average (median 8.2 mm, range 3.5-14.9 mm).

The preclinical nature of the present study represents its main limitation, as the results could be potentially biased by the "ideal" conditions of the laboratory setting. Therefore, the benefits conferred by 3D-SNVE should be interpreted cautiously. However, the preliminary clinical data published in the literature are in agreement with the conclusion of our experiment.[26,28,29,37,46] Translation of 3D-SNVE into clinical research should be the next step, in order to test the potential benefits on patient outcomes with application in live surgery and in the environment of an operating room. Another limitation was that an arbitrary area of 30 x 11 mm was chosen to simulate the endoscopic PM delineation; in real surgery, the margin shape would result more irregular and variably sized.

The authors acknowledge that repeating simulations with the same technology, even if with different guidance modalities, may have caused a "learning effect". Future studies will also investigate the benefits of navigation across a wider range of experience levels, including senior staff.

**Conclusions**

This preclinical study has demonstrated the substantial benefit of 3D-SNVE for PM definition in advanced maxillary tumors. This technology is expected to improve patient margins and potentially reducing critical structure injury, thus optimizing the oncological adequacy and overall safety of the resection simultaneously. Translation into the clinical setting, with a thoughtful analysis of oncological outcomes, is the proposed next step.

## References


1. Nicolai P, Castelnuovo P, Bolzoni Villaret A. Endoscopic resection of sinonasal malignancies. *Curr Oncol Rep*. 2011;13(2):138-144. doi:10.1007/s11912-011-0151-6
2. Hanna E, DeMonte F, Ibrahim S, Roberts D, Levine N, Kupferman M. Endoscopic resection of sinonasal cancers with and without craniotomy: oncologic results. *Arch Otolaryngol Head Neck Surg*. 2009;135(12):1219-1224. doi:10.1001/archoto.2009.173
3. Lund V, Howard DJ, Wei WI. Endoscopic resection of malignant tumors of the nose and sinuses. *Am J Rhinol*. 2007;21(1):89-94. doi:10.2500/ajr.2007.21.2957
4. Castelnuovo P, Battaglia P, Turri-Zanoni M, et al. Endoscopic endonasal surgery for malignancies of the anterior cranial base. *World Neurosurg*. 2014;82(6 Suppl):S22-31. doi:10.1016/j.wneu.2014.07.021
5. Moya-Plana A, Bresson D, Temam S, Kolb F, Janot F, Herman P. Development of minimally invasive surgery for sinonasal malignancy. *Eur Ann Otorhinolaryngol Head Neck Dis*. 2016;133(6):405-411. doi:10.1016/j.anorl.2016.06.001
6. Snyderman CH, Carrau RL, Kassam AB, et al. Endoscopic skull base surgery: principles of endonasal oncological surgery. *J Surg Oncol*. 2008;97(8):658-664. doi:10.1002/jso.21020
7. Lund VJ, Wei WI. Endoscopic surgery for malignant sinonasal tumours: an eighteen year experience. *Rhinology*. 2015;53(3):204-211. doi:10.4193/Rhin14.318
8. Nicolai P, Battaglia P, Bignami M, et al. Endoscopic surgery for malignant tumors of the sinonasal tract and adjacent skull base: a 10-year experience. *Am J Rhinol*. 2008;22(3):308-316. doi:10.2500/ajr.2008.22.3170
9. Villaret AB, Yakirevitch A, Bizzoni A, et al. Endoscopic transnasal craniectomy in the management of selected sinonasal malignancies. *Am J Rhinol Allergy*. 2010;24(1):60-65. doi:10.2500/ajra.2010.24.3397
10. Lund VJ, Stammberger H, Nicolai P, et al. European position paper on endoscopic management of tumours of the nose, paranasal sinuses and skull base. *Rhinol Suppl*. 2010;22:1-143.
11. Ferrari M, Bossi P, Mattavelli D, Ardighieri L, Nicolai P. Management of sinonasal adenocarcinomas with anterior skull base extension. *J Neurooncol*. Published online January 3, 2020. doi:10.1007/s11060-019-03385-8
12. Snyderman CH, Pant H, Carrau RL, Prevedello D, Gardner P, Kassam AB. What are the limits of endoscopic sinus surgery?: the expanded endonasal approach to the skull base. *Keio J Med*. 2009;58(3):152-160. doi:10.2302/kjm.58.152
13. Deganello A, Ferrari M, Paderno A, et al. Endoscopic-assisted maxillectomy: Operative technique and control of surgical margins. *Oral Oncol*. 2019;93:29-38. doi:10.1016/j.oraloncology.2019.04.002
14. Naunheim MR, Goyal N, Dedmon MM, et al. An Algorithm for Surgical Approach to the Anterior Skull Base. *J Neurol Surg Part B Skull Base*. 2016;77(4):364-370. doi:10.1055/s-0036-1580598
15. Balm AJM, Smeele LE, Lohuis PJFM. Optimizing exposure of the posterolateral maxillary and pterygoid region: The lower cheek flap. *Eur J Surg Oncol EJSO*. 2008;34(6):699-703. doi:10.1016/j.ejso.2007.08.009
16. Chatni SS, Sharan R, Patel D, Iyer S, Tiwari RM, Kuriakose MA. Transmandibular approach for excision of maxillary sinus tumors extending to pterygopalatine and infratemporal fossae. *Oral Oncol*. 2009;45(8):720-726. doi:10.1016/j.oraloncology.2008.11.005
17. Kreeft AM, Smeele LE, Rasch CRN, et al. Preoperative imaging and surgical margins in maxillectomy patients. *Head Neck*. 2012;34(11):1652-1656. doi:10.1002/hed.21987
18. Sun J, Shen Y, Weng Y-Q, Li J, Zhang Z-Y. Lateral Lip-Splitting Approach for Total and Subtotal Maxillectomy. *J Oral Maxillofac Surg*. 2009;67(6):1197-1205. doi:10.1016/j.joms.2008.06.078
19. McMahon JD, Crowther J, Taylor WM, et al. Anterolateral corridor approach to the infratemporal fossa and central skull base in maxillectomy: rationale and technical aspects. *Br J Oral Maxillofac Surg*. 2015;53(9):814-819. doi:10.1016/j.bjoms.2015.06.006
20. Citardi MJ, Yao W, Luong A. Next-Generation Surgical Navigation Systems in Sinus and Skull Base Surgery. *Otolaryngol Clin North Am*. 2017;50(3):617-632. doi:10.1016/j.otc.2017.01.012
21. Azarmehr I, Stokbro K, Bell RB, Thygesen T. Surgical Navigation: A Systematic Review of Indications, Treatments, and Outcomes in Oral and Maxillofacial Surgery. *J Oral Maxillofac Surg Off J Am Assoc Oral Maxillofac Surg*. 2017;75(9):1987-2005. doi:10.1016/j.joms.2017.01.004
22. Schramm A, Gellrich NC, Gutwald R, et al. Indications for computer-assisted treatment of cranio-maxillofacial tumors. *Comput Aided Surg Off J Int Soc Comput Aided Surg*. 2000;5(5):343-352. doi:10.1002/1097-0150(2000)5:5<343::AID-IGS4>3.0.CO;2-1
23. Schramm A, Suarez-Cunqueiro MM, Barth EL, et al. Computer-assisted navigation in craniomaxillofacial tumors. *J Craniofac Surg*. 2008;19(4):1067-1074. doi:10.1097/SCS.0b013e3181760fc0
24. Ferrari M, Daly MJ, Douglas CM, et al. Navigation-guided osteotomies improve margin delineation in tumors involving the sinonasal area: A preclinical study. *Oral Oncol*. 2019;99:104463. doi:10.1016/j.oraloncology.2019.104463
25. Bernstein JM, Daly MJ, Chan H, et al. Accuracy and reproducibility of virtual cutting guides and 3D-navigation for osteotomies of the mandible and maxilla. *PloS One*. 2017;12(3):e0173111. doi:10.1371/journal.pone.0173111
26. Catanzaro S, Copelli C, Manfuso A, et al. Intraoperative navigation in complex head and neck resections: indications and limits. *Int J Comput Assist Radiol Surg*. 2017;12(5):881-887. doi:10.1007/s11548-016-1486-0
27. Guo R, Guo YX, Feng Z, Guo CB. Application of a computer-aided navigation technique in surgery for recurrent malignant infratemporal fossa tumors. *J Craniofac Surg*. 2015;26(2):e126-132. doi:10.1097/SCS.0000000000001350

28. Feichtinger M, Pau M, Zemann W, Aigner RM, Kärcher H. Intraoperative control of resection margins in advanced head and neck cancer using a 3D-navigation system based on PET/CT image fusion. *J Cranio-Maxillo-fac Surg Off Publ Eur Assoc Cranio-Maxillo-fac Surg*. 2010;38(8):589-594. doi:10.1016/j.jcms.2010.02.004
29. Tarsitano A, Ricotta F, Baldino G, et al. Navigation-guided resection of maxillary tumours: The accuracy of computer-assisted surgery in terms of control of resection margins - A feasibility study. *J Cranio-Maxillo-fac Surg Off Publ Eur Assoc Cranio-Maxillo-fac Surg*. 2017;45(12):2109-2114. doi:10.1016/j.jcms.2017.09.023
30. Daly MJ, Siewerdsen JH, Moseley DJ, Jaffray DA, Irish JC. Intraoperative cone-beam CT for guidance of head and neck surgery: Assessment of dose and image quality using a C-arm prototype. *Med Phys*. 2006;33(10):3767-3780. doi:10.1118/1.2349687
31. Siewerdsen JH, Moseley DJ, Burch S, et al. Volume CT with a flat-panel detector on a mobile, isocentric C-arm: pre-clinical investigation in guidance of minimally invasive surgery. *Med Phys*. 2005;32(1):241-254. doi:10.1118/1.1836331
32. King E, Daly MJ, Chan H, et al. Intraoperative cone-beam CT for head and neck surgery: feasibility of clinical implementation using a prototype mobile C-arm. *Head Neck*. 2013;35(7):959-967. doi:10.1002/hed.23060
33. Jermyn M, Ghadyani H, Mastanduno MA, et al. Fast segmentation and high-quality three-dimensional volume mesh creation from medical images for diffuse optical tomography. *J Biomed Opt*. 2013;18(8):86007. doi:10.1117/1.JBO.18.8.086007
34. Enquobahrie A, Cheng P, Gary K, et al. The image-guided surgery toolkit IGSTK: an open source C++ software toolkit. *J Digit Imaging*. 2007;20 Suppl 1:21-33. doi:10.1007/s10278-007-9054-3
35. Daly MJ, Chan H, Nithiananthan S, et al. Clinical implementation of intraoperative cone-beam CT in head and neck surgery. In: Wong KH, Holmes III DR, eds. ; 2011:796426. doi:10.1117/12.878976
36. Sternheim A, Daly M, Qiu J, et al. Navigated pelvic osteotomy and tumor resection: a study assessing the accuracy and reproducibility of resection planes in Sawbones and cadavers. *J Bone Joint Surg Am*. 2015;97(1):40-46. doi:10.2106/JBJS.N.00276
37. Hasan W, Daly MJ, Chan HHL, Qiu J, Irish JC. Intraoperative cone-beam CT-guided osteotomy navigation in mandible and maxilla surgery. *The Laryngoscope*. 2020;130(5):1166-1172. doi:10.1002/lary.28082
38. Dixon BJ, Daly MJ, Chan H, Vescan A, Witterick IJ, Irish JC. Augmented real-time navigation with critical structure proximity alerts for endoscopic skull base surgery. *The Laryngoscope*. 2014;124(4):853-859. doi:10.1002/lary.24385
39. Castelnuovo P, Turri-Zanoni M, Battaglia P, Antognoni P, Bossi P, Locatelli D. Sinonasal Malignancies of Anterior Skull Base: Histology-driven Treatment Strategies. *Otolaryngol Clin North Am*. 2016;49(1):183-200. doi:10.1016/j.otc.2015.09.012
40. Ferrari M, Ioppi A, Schreiber A, et al. Malignant tumors of the maxillary sinus: Prognostic impact of neurovascular invasion in a series of 138 patients. *Oral Oncol*. 2020;106:104672. doi:10.1016/j.oraloncology.2020.104672
41. López F, Lund VJ, Suárez C, et al. The Impact of Histologic Phenotype in the Treatment of Sinonasal Cancer. *Adv Ther*. 2017;34(10):2181-2198. doi:10.1007/s12325-017-0605-9
42. Paulino AC, Marks JE, Bricker P, Melian E, Reddy SP, Emami B. Results of treatment of patients with maxillary sinus carcinoma. *Cancer*. 1998;83(3):457-465.
43. Nishio N, Fujimoto Y, Fujii M, et al. Craniofacial Resection for T4 Maxillary Sinus Carcinoma: Managing Cases with Involvement of the Skull Base. *Otolaryngol--Head Neck Surg Off J Am Acad Otolaryngol-Head Neck Surg*. 2015;153(2):231-238. doi:10.1177/0194599815586770
44. Ozsaran Z, Yalman D, Baltalarli B, Anacak Y, Esassolak M, Haydaroğlu A. Radiotherapy in maxillary sinus carcinomas: evaluation of 79 cases. *Rhinology*. 2003;41(1):44-48.
45. Bristol IJ, Ahamad A, Garden AS, et al. Postoperative radiotherapy for maxillary sinus cancer: long-term outcomes and toxicities of treatment. *Int J Radiat Oncol Biol Phys*. 2007;68(3):719-730. doi:10.1016/j.ijrobp.2007.01.032
46. Ricotta F, Cercenelli L, Battaglia S, et al. Navigation-guided resection of maxillary tumors: Can a new volumetric virtual planning method improve outcomes in terms of control of resection margins? *J Cranio-Maxillofac Surg*. 2018;46(12):2240-2247. doi:10.1016/j.jcms.2018.09.034
47. Ferrari M, Montalto N, Nicolai P (2021) Novel Approaches in Surgical Management: How to Assess Surgical Margins. In: Vermorken J.B., Budach V., Leemans C.R., Machiels JP., Nicolai P., O'Sullivan B. (eds) Critical Issues in Head and Neck Oncology. Springer, Cham. https://doi.org/10.1007/978-3-030-63234-2_7.

# Simulation of surgical navigation with three-dimensional rendering-aided ablations in the craniofacial area: a controlled, cadaver study

*Ferrari et al., Eur J Surg Oncol 2022; doi: 10.1016/j.ejso.2021.12.012*

**Introduction**

Despite the increasing availability of promising non-surgical strategies for the treatment of head and neck (HN) cancer, surgery still plays an essential role, often serving as the primary treatment. The adequacy of the surgical resection is the main controllable variable that is in the hands of the surgical team and is critical to maximize the chances to cure the patient. HN sites pose a special challenge to the surgeon, as the adequacy of resection for local tumor control must be balanced with the quality of life impact that taking surrounding tissue can have on patient function.[1]

At present, the margins for tumor resection are based on preoperative imaging interpretation, the surgeon's intraoperative assessment based on visualization of the tumor, palpation of local extent of disease, and the ability to build a 3-dimensional (3D) mental representation of the lesion with respect to neighboring anatomical landmarks. Finally, the definition of the adequacy of the resection requires a strong interdisciplinary relationship with the pathologist with the use of intraoperative frozen sections and gross specimen assessment. While this approach can provide acceptable results in terms of completeness of resection in many HN sites, there is an unmet need to increase the rate of negative margins, particularly in cancers invading the craniofacial area.[2–6] Owing to the complex 3D extent of many HN malignancies, several technical and technological refinements have been advocated to improve the quality of oncologic ablations.[1,5,7–11]

Margin involvement represents one of the main negative prognosticators in most HN cancers.[12] The presence of tumor cells at the margins of excised tissues significantly increases the probability of locoregional recurrence with decreased survival. Among strategies to enhance the surgeon's ability to appreciate intraoperative tumor extent, surgical navigation (SN) is particularly promising in view of its wide diffusion in operating theaters and relatively accessible use. Our group has already demonstrated a theoretical benefit of guiding ablations in the craniofacial district with SN in terms of margin delineation.[13] This observation was in line with preliminary reports[14–17] and a controlled non-randomized study[18] on SN-aided ablations in the HN. However, since clinical studies in the field were based on standard histopathological margin assessment, there is still no evidence on how SN affects margin status at a 3D level, which might be substantially different from standard, 2-dimensional margin evaluation in complex surgical specimens such as those resulting from maxillectomy surgery or craniofacial resection.[19]

The aim of the present study was twofold: first, to establish the 3D relationship between the outer surface of the surgical specimen and tumor surface and test the effect of guiding ablations on cadavers with SN; second, to develop and evaluate a cadaver tumor model to be used for research, educational, and training purposes, aimed at optimizing the use of SN to guide complex ablations in the HN.

## Materials and Methods

### *Tumor model preparation*

Seven cadaver heads (Medcure®, Portland, United States) were employed to create craniofacial tumor models in the Laboratory of Endoscopic Anatomy of the University of Brescia. A 4K-endoscopic camera with 0° telescope (Olympus®) was used to create transnasal, transoral, and/or transorbital corridors with minimal manipulation and removal of tissues (*i.e.*, through small mucosal/skin incision and bony window). Once the site of the tumor model was reached (*e.g.*, maxillary sinus), selected bone boundaries and adjacent tissues were removed to simulate tumor progression towards neighboring compartments. A bicomponent silicon (Xiameter RTV rubber base and catalyzer, Dow Corning®, Midland, Michigan, USA) stained with contrast agent (Ultravist 370 mg/mL, Bayer®, Leverkusen, Germany) and black ink was injected under endoscopic guidance into the created cavity. Gauzes and cottonoid-patties were used to prevent the silicon from flowing outside of the targeted space (Figure 1). Once the silicon hardened (in roughly 20 minutes), cadaver specimens were stored at -20°C. Two-to-4 tumor models were created for each cadaver; overall, 24 tumor models were prepared (8 maxillary, 2 nasoethmoidal, 5 frontal, 7 oral, and 2 orbital tumors).

Cadaver specimens underwent multidetector 128-slice CT scanner (Somatom Definition Flash, Siemens®, Forcheim, Germany) with 0.7-mm axial slices. CT scans were checked through a DICOM viewer (Horos®) to verify that the tumor models adequately simulated realistic scenarios of advanced HN cancers. All tumor models were classified as T4 according to the latest version (8$^{th}$) of the TNM classification. DICOM files were uploaded on Materialise® Mimics® and each tumor was separately segmented and exported as an .stl file (Figure 2).

### *Simulation of resection*

Simulation of tumor resections was performed by 7 otorhinolaryngologists – HN surgeons and 1 resident with heterogeneous experience (range of experience in HN surgical oncology: 0-23 years; interquartile range: 5-11 years). An optical navigation system (Polaris Vicra; NDI, Waterloo, Ontario, Canada) with in-house software (GTxEyesII - ApproachViewer; University of Toronto, Toronto, Ontario, Canada)[13,17,20–22] was employed and manual point-by-point registration using anatomical landmarks was repeated until achieving a target registration error of <1 mm within the area of interest (*i.e.*, an area of the skull including the tumor model to be resected).

The surgical team performing the simulation was composed of 3 surgeons (2 scrubbed surgeons performing the dissection, 1 surgeon using the navigation software and projecting its interface on a 55-in monitor placed in front of the operating table). Surgical teams were sorted so that surgeons had not participated in preparation of the tumor models. The .stl file of the tumor was uploaded alongside DICOM imaging files on the navigation software and the surgical team studied the extent of the tumor on the axial, coronal, and sagittal projections prior to starting the dissection. For each procedure, the main surgeon was indicated to follow the principles of oncologic HN surgery, thus performing a realistic and oncologically adequate ablation. The surgical team could employ the SN system as they felt appropriate throughout the procedure. They were equipped with a navigated pointer and could modify the opacity and threshold of cross-sectional and 3D-

rendered images as they preferred. They could also manipulate the clip function of the navigation software, which depicted a real-time virtual cut of the 3D-rendered image on the x-, y- or z-axis with respect to the pointer's end, as preferred (Figure 3). Fourteen tumor models underwent SN-guided ablation. Following ablation, the surgical team was allowed to examine the ablated specimen and navigate the surgical defect. Next, additional oriented resection could be performed to increase margin thickness if close or positive margins were suspected.

Each surgeon participating in the study was asked to perform at least one unguided ablation to be used as control. Ten unguided ablations were performed. In this case, the surgical team could analyze the cross-sectional imaging of the tumor model prior to or during the procedure. Neither 3D rendering of the tumor and skeleton nor SN were available during control resections. As for navigated resections, the surgical team could analyze the ablated specimen and perform additional oriented resection, if needed.

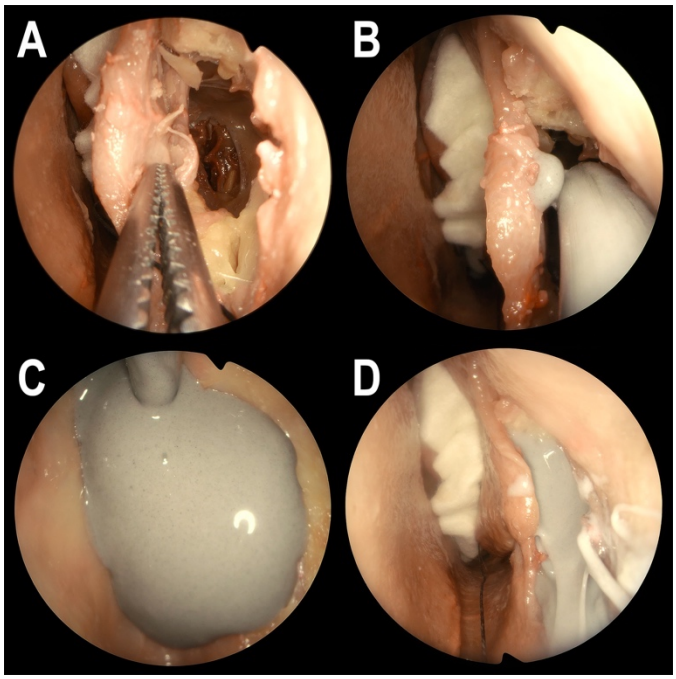


**Figure 1**. Endoscope-assisted preparation of a maxillary sinus cancer model. **A**. A prelacrimal recess approach to the left maxillary sinus is harvested and pterygopalatine and infratemporal fossa are accessed by partially removing the posterior maxillary wall, periosteum, and fat. **B, C**. Stained and contrasted bicomponent silicon is injected in the maxillary sinus, with paddies in the ostiomeatal preventing the silicon from outflowing into the nasal cavity. **D**. The prelacrimal window is closed.

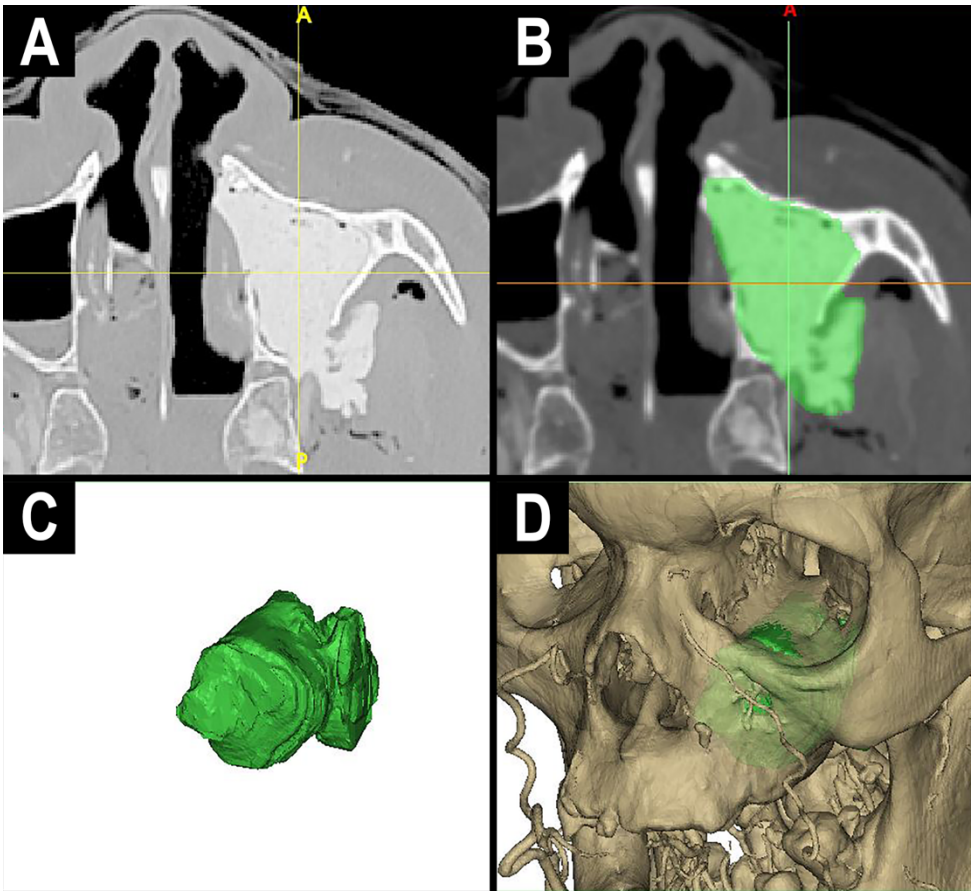


**Figure 2**. Radiologic appearance and segmentation of the tumor model. **A**. Appearance at computed tomography of the tumor model prepared in Figure 1. **B**. Slice-based manual segmentation of the tumor model. **C, D**. Three-dimensional rendering of the tumor model.

***Post-dissection analysis of surgical specimen***

In case of additional resections, the additional specimen was attached to the main surgical specimen using cyanoacrylate adhesive, as anatomically appropriate. Ablated specimens were stored at -20°C.

Surgical specimens were scanned with the aforesaid CT scanner and the DICOM files uploaded on Materialise® Mimics®. The entire specimen, tumor, and bony framework were segmented and uploaded on Materialise® 3-matic®. Part-comparison-analysis is a function of Materialise® 3-matic® that measures the minimum distance between each point composing the "entity" surface from the closest point making up the "target" surface. Signed part-comparison-analysis was used to analyze the 3D relationship between the outer surface of the ablated specimen (set as "entity" in the software) and the outer surface of the tumor (set as "target"). This result is hereafter referred to as "overall margin" (OM). In some models the tumors were in contact with air-filled cavities such as the oral, pharyngeal, and sinonasal cavities. This contact was not viewed as a margin and therefore this part of the tumor surface was excluded from the analysis (Figure 4). A sub-analysis of tumor surfaces that were not covered by bone was also performed: areas of the tumor surface without interposition of a bony structure between the tumor and the outer surface of the ablated specimen were manually marked and isolated to create a surface referred to as "bone-uncovered tumor surface". Signed part-comparison-analysis was repeated setting the bone-uncovered tumor surfaces as "entity" and the outer surface of the ablated specimen as "target". This result was referred to as "bone-uncovered margin" (BUM) (Figures 4-5). Distances were summarized as median, first quartile, third quartile, maximum, minimum, and root mean

square. Distribution of OM distances was clustered as follows: ≤0 mm – involved margin; >0 and ≤5 mm – close margin; >5 and ≤10 mm – adequate margin; >10 mm – excessive margin (Figure 3). The same cutoffs with inverted sign were used to cluster BUM distances.

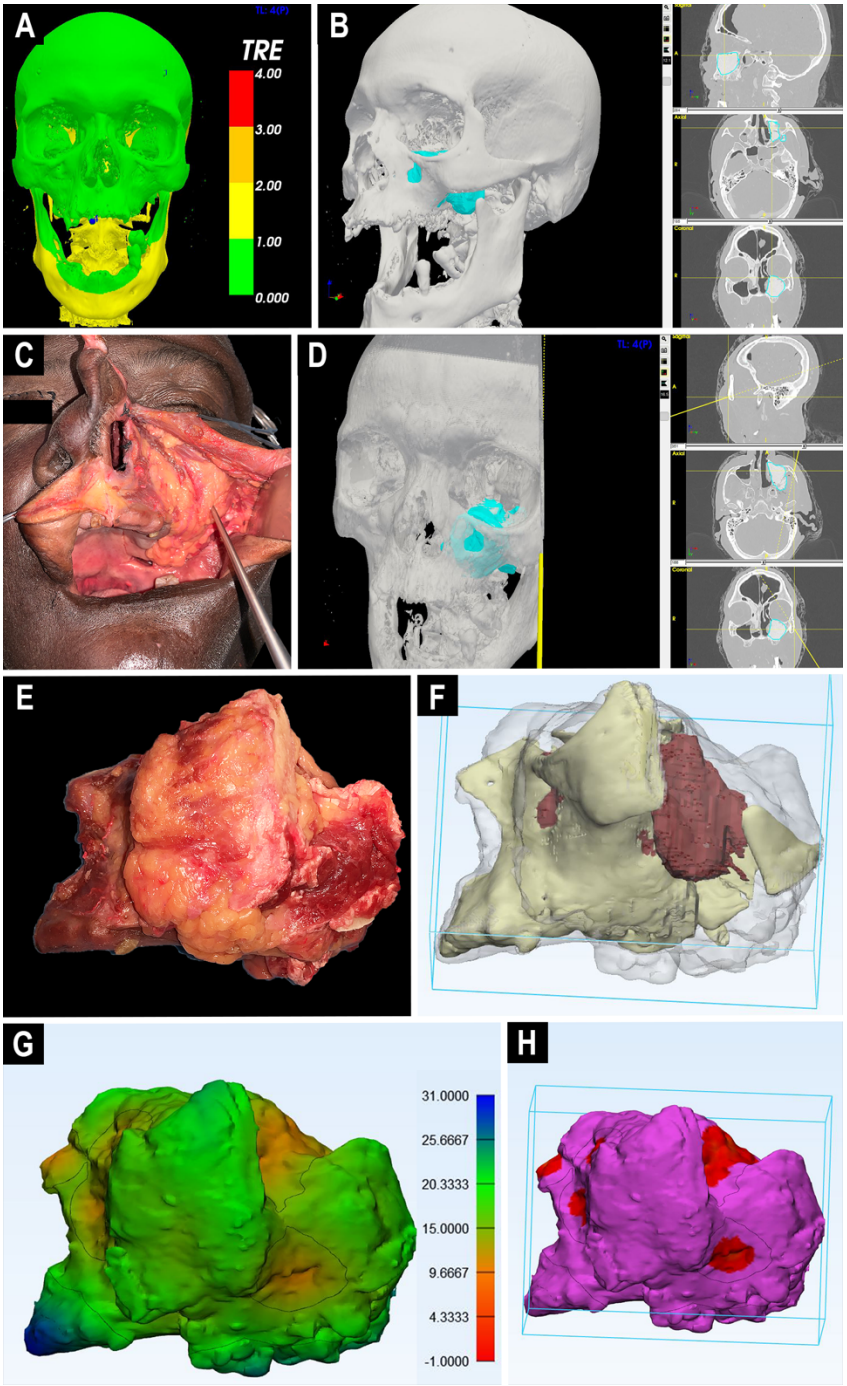


**Figure 3**. Main workflow of the preclinical experiment. **A**. The surgical navigation system is registered. The area where the targeted tumor model is located is checked for acceptable target registration error (TRE) (<1 mm) through a categorical color-code threshold scale. **B**. The extension of the targeted tumor model is analyzed through 3-dimensional rendering and cross-sectional projection. **C, D**. A navigation pointer was used to establish the adequate trajectory of cut around the lateral aspect of the tumor. **E**. Gross lateral-to-medial appearance of the ablated specimen. **F**. Three-dimensional rendering of specimen outer surface bony component, and tumor within the ablated tissue. This was obtained by manual and semi-automatic segmentation on computed tomography images of the resected specimen. **G**. Overall margin part-comparison-analysis rendered as a continuous color-code map. Distance between the outer specimen surface and the tumor is rendered through colors: blue areas are located at roughly 2.5-3 cm from the tumor surface, orange areas at 0.5-1 cm. **H**. Example of clustering of distances measured with part-comparison-analysis. Close distances (*i.e.*, between 0.5 and 1 cm) are highlighted in red.

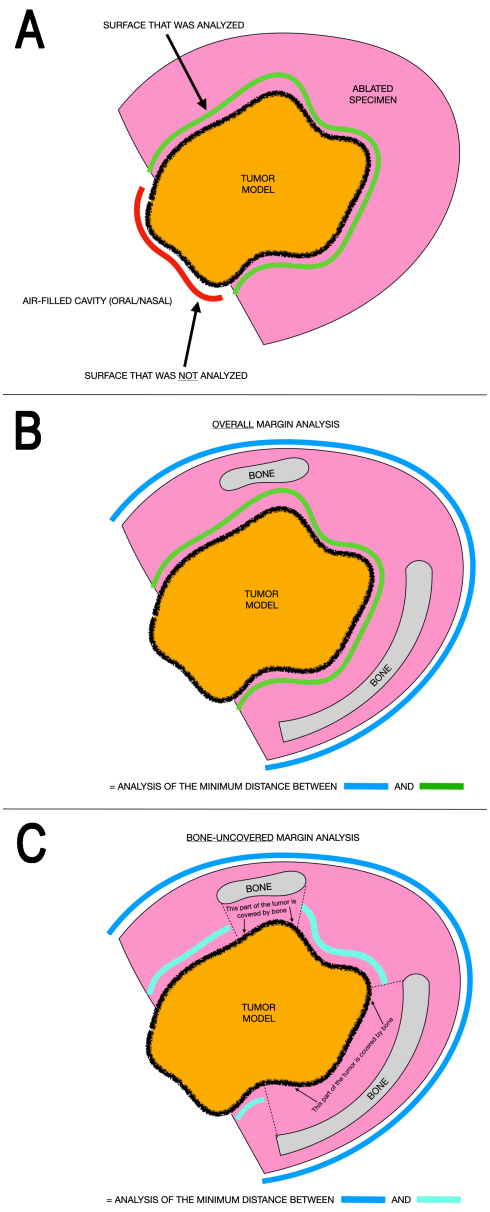


**Figure 4**. The schemes show which surfaces were considered in the part-comparison-analysis. **A**. Parts of the tumor that were initially in contact with air-filled cavity were excluded from margin analysis. **B**. Scheme illustrating the surfaces that were marked to run the overall margin part-comparison-analysis. **C**. Scheme illustrating the surfaces that were marked to run the bone-uncovered margin part-comparison-analysis.

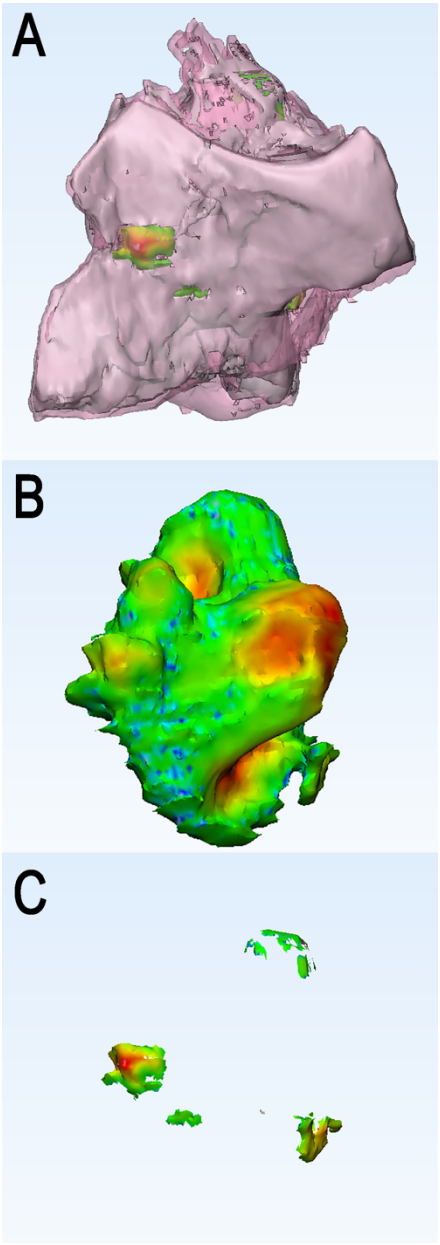


**Figure 5**. Bone-uncovered margin part-comparison-analysis. **A**. Three-dimensional rendering of the entire surgical specimen. Transparency of components allow appreciation of the outer surface (pink), bone (gray), and tumor (part-comparison-analysis color map). **B**. View of the entire tumor as it appears with part-comparison-analysis with the tumor as the entity and outer specimen surface as the target (not measured in the present study). **C**. Bone-uncovered areas of the tumor surface are isolated and part-comparison-analysis with them as the entity and outer specimen surface as the target is run.

***Statistical analysis***

Normality of data distribution was tested through the Shapiro-Wilk test, with a p-value <0.05 considered significant. SN-aided and control ablations were compared in terms of both distribution among the aforesaid OM and BUM distance clusters (*i.e.*, involved margin, close margin, adequate margin, and excessive margin) and presence or absence of margin involvement with Mann-Whitney and Fisher's exact tests, respectively.

***Task load assessment***

After completing the experiments, each surgeon was asked to fill the National Aeronautics and Space Administration (NASA) task load index (TLX)[23] module composed of a 15-pairwise comparison questionnaire and a 6-domain (mental demand, physical demand, temporal demand, performance, effort, frustration level) visual analogue scale (VAS) form. Domain-specific results were calculated as raw and weighted averages. Weighting of 6-domain results was performed based on a surgeon-specific domain hierarchy, which was calculated based on the results of the 15-pairwise comparison questionnaire. Mean of domain-specific average values was used to estimate the overall workload of the simulation.

***Model reliability assessment***

Two radiologists with HN expertise and 15-30-year experience (RM, MR) in sinonasal oncological imaging were asked to evaluate the CT of all tumor models and fill a VAS form to rate how realistic each model was in terms of: 1) shape, 2) local extension pattern, and 3) overall realistic rate.

Surgeons participating in the simulations were asked to rate through a VAS form how realistic the models were in terms of: 1) tumor consistency, 2) local extension pattern within soft tissues, 3) local extension pattern within bony structures, and 4) integrity of the model throughout the simulation.

**Results**

***Three-dimensional analysis of margin***

Additional ablations were performed in 4 cases, of which 2 (14.3%) in the SN-aided group and 2 (20.0%) in the control group (p>0.05). Median, first quartile, third quartile, maximum, minimum, and root mean square of OM and BUM part-comparisons-analyses are summarized in Table 1. When considering the full series of simulation, OM cluster distribution was as follows: involved (1.2%), close (28.8%), adequate (28.1%), and excessive (42.1%); BUM clustered as follows: involved (4.7%), close (68.0%), adequate (22.0%), and excessive (5.4%). Both OM and BUM cluster percentages were not normally distributed. Compared to the control group, SN-group had a significantly less represented cluster of involved OM (2.1% *vs* 0.5%, respectively; p=0.002) and involved BUM (9.4% *vs* 1.3%, respectively; p=0.024) (Figure 6). The SN-group showed a significantly more represented cluster of adequate BUM (29.3% *vs* 11.7%, respectively; p=0.045). The overall rate of margin involvement was 12/24 (50.0%) and was significantly lower in the SN-group compared to the control group of simulations (21.4% *vs* 90.0%, respectively; p=0.003).

| Margin analysis | Overall margin (mm)* | Bone-uncovered margin (mm)** |
|---|---|---|
| **Median** | 9.0 | -3.0 |
| **1st quartile** | 4.9 | -4.9 |
| **3rd quartile** | 13.9 | -1.6 |
| **Minimum** | -5.8 | -9.3 |
| **Maximum** | 30.3 | 0.5 |
| **Root mean square** | 11.8 | 3.9 |

**Table 1**. Average of median, first quartile, third quartile, minimum, maximum, and root mean square values of part-comparison-analyses of overall and bone-uncovered margin. *Values should be interpreted as the distance between the outer specimen surface and outer tumor surface (*i.e.*, a negative value means involved margin); **values should be interpreted as the distance between the outer tumor surface and outer specimen surface (*i.e.*, a positive value means involved margin).

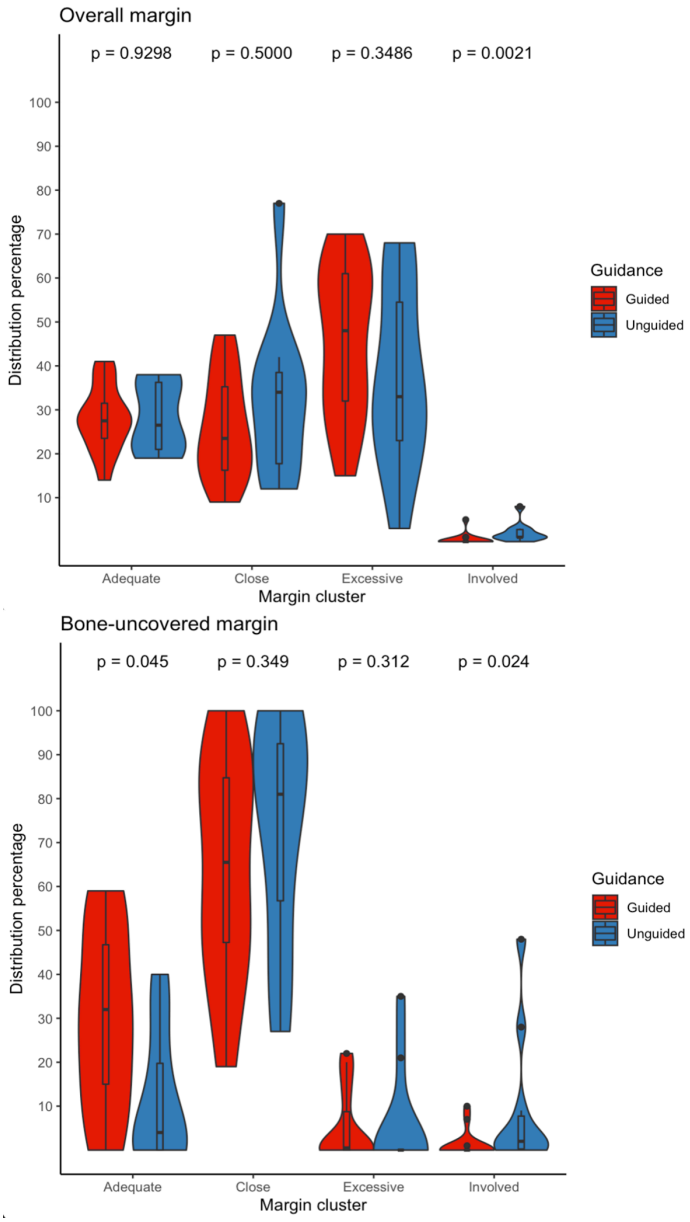


**Figure 4**. Violin plots comparing surgical navigation-guided versus unguided resections in terms of overall and bone-uncovered margin. P-values refer to Mann-Whitney tests.

***Task load assessment***

Overall raw and weighted NASA-TLX scores of the SN-aided ablation were 25.8 and 34.2, respectively. These values describe a medium-to-somewhat-high workload [24]. Average unweighted and weighted sub-scores were as follows: mental demand (42.9 and 165.0), physical demand (16.4 and 16.4), temporal demand (23.9 and 92.9), performance (21.4 and 96.4), effort (38.6 and 101.4), and frustration (12.1 and 40.7).

***Model reliability assessment***

Table 2 summarizes the results of surveys. Overall, the tumor models employed in this study were considered to be realistic from a radiologic standpoint (mean VAS overall realistic rate: 7.5/10, median 8/10). Local extension pattern was considered as good by radiologists (mean VAS: 7.6/10, median 8/10) and sufficient by surgeons, with extension towards bony structures being less reliably rendered than that towards soft tissues (mean VAS: 6.9 *vs* 5.5, median 7 *vs* 5.5, respectively).

| **Query** | **Mean (range)** | **Median** |
|---|---|---|
| R1 – How realistic was tumor shape? | 7.3/10 (3-9) | 8/10 |
| R2 – How realistic was local extension pattern? | 7.4/10 (3-9) | 8/10 |
| R3 – What was the overall realistic rate of the model? | 7.5/10 (3-9) | 8/10 |
| S1 – How realistic was the tumor model consistency? | 7.6/10 (3-9) | 8/10 |
| S2 – How realistic was local extension pattern within soft tissues? | 6.9/10 (5-9) | 7/10 |
| S3 – How realistic was local extension pattern within bone? | 5.5/10 (2-9) | 5.5/10 |
| S4 – How was the model capable of maintaining integrity during the simulation? | 8.9/10 (8-10) | 9/10 |

**Table 2**. Mean, range, and median values of replies by radiologists (R, n=2) and surgeons (S, n=8) to whom the questionnaire was administered.

**Discussion**

SN has been most commonly employed to assess adequacy of reconstruction, particularly after trauma surgery, and minimize the risk of complications.[25–27] Moreover, SN has been hypothesized to provide therapeutic advantages by enhancing the precision of oncologic treatment, with benefits ranging from improved margin control[10,11,14–16,18] to 3D mapping of critical extensions and involved margins aimed at tailoring the radiotherapy planning.[28]

The present study assessed the effect of SN on 3D delineation of margin in cadaveric HN cancer models. Different from the standard classification of a surgical ablation, which is labelled as either complete or with involved margins, the part-comparison-analysis adopted herein also provided a quantitative measure of the 3D relationship between the tumor and specimen outer surfaces. In a previous study by our group, the beneficial role of real-time 3D SN in terms of margin delineation on tumor models embedded in artificial skulls was demonstrated. With 381 simulated cuts in the craniofacial area, it was observed that SN decreases the rate of intratumoral cuts from 18.1% to 0.0% in unguided and guided osteotomies, respectively.[13] Despite

raising interesting results, this experiment was based on non-realistic, simplified models and, consequently, some substantial differences were found with respect to the present study.

First, the overall rate of margin involvement was remarkably higher in this preclinical experiment (50.0% *vs* 6.0%, accounting the overall number of simulated cuts),[13] and more reliably mirrors the rate of margin involvement in very advanced cancers of the HN.[29–32] Second, the decrease in positive margins provided using SN was even more pronounced in this experiment (90.0% *vs* 21.4%) compared to our previous observations on simulated cuts (18.1% *vs* 0.0%).[13] Third, cluster distributions of OM were less promising compared to virtual cuts at 3D analysis,[13] where there was more evident gain in adequate, excessive, and close margin distribution with the addition of SN (Figure 6). Two main factors could have determined these discrepancies:[13] 1) ablations in the craniofacial area rely on several osteotomies and dissection maneuvres of soft tissues all around the tumor, each associated with a cumulative chance of margin involvement; 2) performing a realistic procedure led the surgical team to spare critical structures that were ignored in virtual simulations. Moreover, aiming to compensate for post-resection shrinkage of tissues (which was deemed to be due to division of soft tissues, even if cautery and chemical fixation were omitted),[33,34] the threshold to classify adequate *versus* excessive margin was reduced from 15 mm (as defined in our previous analysis)[13] to 10 mm, which might have partially contributed to the discrepancy with our previous results.

Among paradigms guiding margin delineation in HN oncologic surgery, the "barrier approach" assumes that grossly uninvolved fascial, muscular or bony structures serve as healthy margin irrespective of their thickness.[35] Based on this principle, a sub-analysis of the margin uncovered by intact bony structures was performed, assuming that portions of the tumor that were covered by normal bone were adequately removed. Interestingly, BUM analysis showed that SN significantly increased the percentage of adequate distant margins, while reducing that of involved points on the specimen surface (Figure 6). Ricotta *et al*. observed a similar positive trend in involvement of soft tissue margins when using SN: out of 287 pathologically evaluated margins in 28 patients, they registered a 12%-decrease in deep margin involvement when performing either a "reference point resection" or a "volumetric resection" compared to standard resections.[18] Similarly, an 8% average decrease in the rate of points falling within the "involved" BUM cluster was observed in this study. Additionally, an 18%-gain in adequate BUM was found. The fact that SN was more beneficial for BUM than for OM is of special interest. The hypothesis to explain this observation is that HN surgeons mostly rely upon the bony framework to get oriented throughout a craniofacial ablation. Thus, bone-uncovered protrusions within soft tissues might be less accurately rendered in the surgeons' mental representation of the tumor and dissection margins could be accordingly mis-delineated.

The other innovative aspect of the present study lies in the creation and evaluation of gross craniofacial tumor models for HN surgery research. Other groups have used injectable material[36–39] or balloon-based[40,41] models to simulate skull base, cheek, and lung tumors in cadavers. 3D printing technology is another emerging approach to create training models that ease access to educational activities compared to cadaver dissection.[42–44] Consistency, contrast at computed tomography, and integrity throughout the ablation are the main strengths of the model used in this study. Indeed, most parameters employed to evaluate it showed satisfactory outcomes

from both radiologic and surgical perspectives (Table 2), suggesting that the model is sufficiently realistic. However, extension into the bony structures was less-than-optimally rendered (average VAS = 5.5/10) and future research will be oriented towards optimization of this aspect. Another major limitation of our model is the impossibility to recreate a surrogate for microscopic tumor spread, which is often encountered in clinical practice and is usually linked to suboptimal resections with focally involved margins.

Nevertheless, in view of their similarity to real tumors of the craniofacial area, the tumor models described herein could be useful not only for research purposes, but also for educational and training activities. In this regard, it is worth highlighting that SN-ablation required a medium-to-somewhat-high workload according to the results of the NASA-TLX survey. Mental demand, effort, temporal demand, and performance were the main determinants of the workload. All of these issues suggest that adequate training could ease, speed up, and improve SN-aided surgery in the craniofacial area. With this in mind, the continued development and optimization of a realistic tumor model is paramount to enhance surgical training.

## Conclusions

A promising HN cancer model was developed and evaluated. This model demonstrated a high degree of realism based on radiologic and surgical evaluation, but the model was suboptimal in simulating bony invasion and did not mimic microscopic tumor spread. This model could be utilized for research, educational, and training activities. While some differences in the magnitude of SN-effect were observed with respect to our previous study,[13] the controlled experiments on SN-aided ablations confirmed that SN effectively reduces margin involvement, especially by improving margin delineation in bone-uncovered aspects of the tumor.

Performing SN-aided ablation resulted in a medium-to-somewhat-high workload. The NASA-TLX questionnaire items displaying the highest values suggest that training of HN surgeons could decrease SN-related workload.

The result of this and other studies from our research group has prompted us to organize a prospective controlled trial on the employment of SN in ablations of the craniofacial area, aimed at verifying the clinical and oncologic utility of this surgical method.

## References


1. Ferrari M, Montalto N, Nicolai P. Novel Approaches in Surgical Management: How to Assess Surgical Margins. In: *Critical Issues in Head and Neck Oncology*. Springer, Cham; 2021:95-110. doi:10.1007/978-3-030-63234-2_7
2. Ravasz LA, Slootweg PJ, Hordijk GJ, Smit F, van der Tweel I. The status of the resection margin as a prognostic factor in the treatment of head and neck carcinoma. *J Cranio-Maxillofacial Surg*. 1991;19(7):314-318. doi:10.1016/S1010-5182(05)80339-7
3. McMahon J, O'Brien CJ, Pathak I, et al. Influence of condition of surgical margins on local recurrence and disease-specific survival in oral and oropharyngeal cancer. *Br J Oral Maxillofac Surg*. 2003;41(4):224-231. doi:10.1016/S0266-4356(03)00119-0
4. Woolgar JA, Triantafyllou A. A histopathological appraisal of surgical margins in oral and oropharyngeal cancer resection specimens. *Oral Oncol*. 2005;41(10):1034-1043. doi:10.1016/j.oraloncology.2005.06.008
5. Deganello A, Ferrari M, Paderno A, et al. Endoscopic-assisted maxillectomy: Operative technique and control of surgical margins. *Oral Oncol*. 2019;93. doi:10.1016/j.oraloncology.2019.04.002
6. Pierik AS, Leemans CR, Brakenhoff RH. Resection margins in head and neck cancer surgery: An update of residual disease and field cancerization. *Cancers (Basel)*. 2021;13(11):1-16. doi:10.3390/cancers13112635
7. Balm AJM, Smeele LE, Lohuis PJFM. Optimizing exposure of the posterolateral maxillary and pterygoid region: The lower cheek flap. *Eur J Surg Oncol*. 2008;34(6):699-703. doi:10.1016/j.ejso.2007.08.009

8. Kreeft AM, Smeele LE, Rasch CRN, et al. Preoperative imaging and surgical margins in maxillectomy patients. *Head Neck*. 2012;34(11):1652-1656. doi:10.1002/hed.21987
9. McMahon JD, Crowther J, Taylor WM, et al. Anterolateral corridor approach to the infratemporal fossa and central skull base in maxillectomy: Rationale and technical aspects. *Br J Oral Maxillofac Surg*. 2015;53(9):814-819. doi:10.1016/j.bjoms.2015.06.006
10. Taboni S, Ferrari M, Daly MJ, et al. Navigation-Guided Transnasal Endoscopic Delineation of the Posterior Margin for Maxillary Sinus Cancers : A Preclinical Study. 2021;11(November):1-10. doi:10.3389/fonc.2021.747227
11. Sahovaler A, Chan HHL, Gualtieri T, et al. Augmented Reality and Intraoperative Navigation in Sinonasal Malignancies: A Preclinical Study. *Front Oncol*. 2021;11(November):1-10. doi:10.3389/fonc.2021.723509
12. Baddour HM, Magliocca KR, Chen AY. The importance of margins in head and neck cancer. *J Surg Oncol*. 2016;113(3):248-255. doi:10.1002/jso.24134
13. Ferrari M, Daly MJ, Douglas CM, et al. Navigation-guided osteotomies improve margin delineation in tumors involving the sinonasal area: A preclinical study. *Oral Oncol*. 2019;99. doi:10.1016/j.oraloncology.2019.104463
14. Catanzaro S, Copelli C, Manfuso A, et al. Intraoperative navigation in complex head and neck resections: indications and limits. *Int J Comput Assist Radiol Surg*. 2017;12(5):881-887. doi:10.1007/s11548-016-1486-0
15. Tarsitano A, Ricotta F, Baldino G, et al. Navigation-guided resection of maxillary tumours: The accuracy of computer-assisted surgery in terms of control of resection margins – A feasibility study. *J Cranio-Maxillofacial Surg*. 2017;45(12):2109-2114. doi:10.1016/j.jcms.2017.09.023
16. Feichtinger M, Pau M, Zemann W, Aigner RM, Kärcher H. Intraoperative control of resection margins in advanced head and neck cancer using a 3D-navigation system based on PET/CT image fusion. *J Cranio-Maxillofacial Surg*. 2010;38(8):589-594. doi:10.1016/j.jcms.2010.02.004
17. Hasan W, Daly MJ, Chan HHL, Qiu J, Irish JC. Intraoperative cone-beam CT-guided osteotomy navigation in mandible and maxilla surgery. *Laryngoscope*. 2020;130(5):1166-1172. doi:10.1002/lary.28082
18. Ricotta F, Cercenelli L, Battaglia S, et al. Navigation-guided resection of maxillary tumors: Can a new volumetric virtual planning method improve outcomes in terms of control of resection margins? *J Cranio-Maxillofacial Surg*. 2018;46(12):2240-2247. doi:10.1016/j.jcms.2018.09.034
19. Kulkarni SA, Kulkarni K, Schacht D, et al. ASO Visual Abstract: High-Resolution Full 3D Specimen Imaging for Lumpectomy Margin Assessment in Breast Cancer. *Ann Surg Oncol*. 2021. doi:10.1245/s10434-021-10610-0
20. Lee CY, Chan H, Ujiie H, et al. Novel Thoracoscopic Navigation System With Augmented Real-Time Image Guidance for Chest Wall Tumors. *Ann Thorac Surg*. 2018;106(5):1468-1475. doi:10.1016/j.athoracsur.2018.06.062
21. Chan HHL, Haerle SK, Daly MJ, et al. An integrated augmented reality surgical navigation platform using multi-modality imaging for guidance. *PLoS One*. 2021;16(4 April):1-14. doi:10.1371/journal.pone.0250558
22. Daly MJ, Chan H, Nithiananthan S, et al. Clinical implementation of intraoperative cone-beam CT in head and neck surgery. In: *Progress in Biomedical Optics and Imaging. Proceedings of SPIE; 201*. Vol 7964. ; 2011:796426. doi:10.1117/12.878976
23. Hart SG, Staveland LE. Development of NASA-TLX (Task Load Index): Results of Empirical and Theoretical Research. *Adv Psychol*. 1988;52(C):139-183. doi:10.1016/S0166-4115(08)62386-9
24. Prabaswari AD, Basumerda C, Utomo BW. The Mental Workload Analysis of Staff in Study Program of Private Educational Organization. *IOP Conf Ser Mater Sci Eng*. 2019;528(1). doi:10.1088/1757-899X/528/1/012018
25. Austin RE, Antonyshyn OM. Current applications of 3-D intraoperative navigation in craniomaxillofacial surgery: A retrospective clinical review. *Ann Plast Surg*. 2012;69(3):271-278. doi:10.1097/SAP.0b013e31822a3ec3
26. Bell RB. Computer Planning and Intraoperative Navigation in Cranio-Maxillofacial Surgery. *Oral Maxillofac Surg Clin North Am*. 2010;22(1):135-156. doi:10.1016/j.coms.2009.10.010
27. Azarmehr I, Stokbro K, Bell RB, Thygesen T. Surgical Navigation: A Systematic Review of Indications, Treatments, and Outcomes in Oral and Maxillofacial Surgery. *J Oral Maxillofac Surg*. 2017;75(9):1987-2005. doi:10.1016/j.joms.2017.01.004
28. Essig H, Rana M, Meyer A, et al. Virtual 3D tumor marking-exact intraoperative coordinate mapping improve post-operative radiotherapy. *Radiat Oncol*. 2011;6(1):159. doi:10.1186/1748-717X-6-159
29. Ferrari M, Ioppi A, Schreiber A, et al. Malignant tumors of the maxillary sinus: Prognostic impact of neurovascular invasion in a series of 138 patients. *Oral Oncol*. 2020;106. doi:10.1016/j.oraloncology.2020.104672
30. Torabi SJ, Spock T, Cardoso B, et al. Margins in Sinonasal Squamous Cell Carcinoma: Predictors, Outcomes, and the Endoscopic Approach. *Laryngoscope*. 2020;130(6):E388-E396. doi:10.1002/lary.28315
31. Lombardi D, Ferrari M, Paderno A, et al. Selection of the surgical approach for lesions with parapharyngeal space involvement: A single-center experience on 153 cases. *Oral Oncol*. 2020;109(June):104872. doi:10.1016/j.oraloncology.2020.104872
32. Baddour HM, Ochsner MC, Patel MR, et al. Surgical Resection is Justifiable for Oral T4b Squamous Cell Cancers With Masticator Space Invasion. *Laryngoscope*. 2021;131(2):E466-E472. doi:10.1002/lary.28725
33. Mistry RC, Qureshi SS, Kumaran C. Post-resection mucosal margin shrinkage in oral cancer: Quantification and significance. *J Surg Oncol*. 2005;91(2):131-133. doi:10.1002/jso.20285
34. Umstattd LA, Mills JC, Critchlow WA, Renner GJ, Zitsch RP. Shrinkage in oral squamous cell carcinoma: An analysis of tumor and margin measurements in vivo, post-resection, and post-formalin fixation. *Am J Otolaryngol - Head Neck Med Surg*. 2017;38(6):660-662. doi:10.1016/j.amjoto.2017.08.011

35. Upile T, Fisher C, Jerjes W, et al. The uncertainty of the surgical margin in the treatment of head and neck cancer. *Oral Oncol*. 2007;43(4):321-326. doi:10.1016/j.oraloncology.2006.08.002
36. Dell' Aversana Orabona G, Romano A, Bonavolontà P, et al. Tumor model for surgical simulation to assess a minimally invasive endoscopic approach for midcheek mass removal. *Surg Oncol*. 2017;26(3):286-289. doi:10.1016/j.suronc.2017.05.005
37. Gragnaniello C, Nader R, Van Doormaal T, et al. Skull base tumor model. *J Neurosurg*. 2010;113(5):1106-1111. doi:10.3171/2010.3.JNS09513
38. Gragnaniello C, Gagliardi F, Chau AMT, et al. Intracranial Injectable Tumor Model: Technical Advancements. *J Neurol Surgery, Part B Skull Base*. 2014;75(5):301-308. doi:10.1055/s-0034-1368148
39. Székely R, Suhai FI, Karlinger K, et al. Human Cadaveric Artificial Lung Tumor-Mimic Training Model. *Pathol Oncol Res*. 2021;27:630459. doi:10.3389/pore.2021.630459
40. Bozkurt B, Belykh E, Yağmurlu K, et al. A morphometric and analytical cadaver dissection study of a tumor-simulation balloon model. *J Clin Neurosci*. 2018;49:76-82. doi:10.1016/j.jocn.2017.12.005
41. Oyama K, Prevedello DM, Ditzel Filho LFS, et al. Anatomic comparison of the endonasal and transpetrosal approaches for interpeduncular fossa access. *Neurosurg Focus*. 2014;37(4). doi:10.3171/2014.7.FOCUS14329
42. Chan HHL, Siewerdsen JH, Vescan A, Daly MJ, Prisman E, Irish JC. 3D rapid prototyping for otolaryngology-head and neck surgery: Applications in image-guidance, surgical simulation and patient-specific modeling. *PLoS One*. 2015;10(9):1-18. doi:10.1371/journal.pone.0136370
43. Hoetzenecker K, Chan HHL, Frommlet F, et al. 3D Models in the Diagnosis of Subglottic Airway Stenosis. *Ann Thorac Surg*. 2019;107(6):1860-1865. doi:10.1016/j.athoracsur.2019.01.045
44. Nicolosi F, Pessina F, Gelmi CAE, et al. New neuroanatomy learning paradigms for the next generation of trainees: A novel literature-based 3D methodology. *Clin Neurol Neurosurg*. 2021;210(May):106948. doi:10.1016/j.clineuro.2021.106948

# Pilot clinical implementation of surgical navigation with three-dimensional rendering during open and endoscopic oncologic ablations in the craniofacial area: feasibility analysis

*Unpublished data*

## Introduction

Despite the increasing availability of promising non-surgical strategies, surgery still represents an essential step in the treatment of patients affected by head and neck cancer, often serving as upfront modality. Presence of tumor cells at the margins of the excised tissues significantly increases the probability of loco-regional recurrence and decreases survival. This fact is of utmost importance when considering that a radical resection with negative margins should theoretically be achieved in most patients undergoing surgery, provided that the surgical indication was correct. However, a considerable proportion of oncologic ablations in the head and neck is still characterized by margins involvement.[1-4] In some unfavorable cases, the subtle diffusion of the tumor (submucosal, subperiosteal, perineural, intraosseous) lies beneath clinical and radiological detection accuracy.[5] This hampers the possibility to correctly estimate the real extension of the tumor, with a consequent misjudgment that jeopardizes the chances of obtaining a sound resection. Overall, head and neck surgeons face the major unmet need to intraoperatively rely on technologies that augment the ability to see the tumor within the complexity of surrounding tissues and structures.

Surgical navigation (SN) is regularly used to avoid complications in some subspecialties of otorhinolaryngology – head and neck surgery. Its employment to optimize margin delineation and control in oncologic ablations have been reported in few publications.[6-14] This technology has been tested either through non-rigorous, exploratory methodology or limitedly to preclinical setting, nor were they exploited comprehensively in terms of tumor visualization and margin status evaluation. The novelty of the present project consists of measuring the actual accuracy and benefit of SN with 3-dimensional rendering in margin control through a stepwise translation towards the clinical setting.

## Materials and Methods

An electromagnetic SN system (StealthStation S8 Surgical Navigation System; Medtronic®, Dublin, Ireland) has been used between March and June 2021 in the operating room of Section of Otorhinolaryngology – Head and Neck Surgery of the University of Padua – "Azienda Ospedale Università di Padova". Fourteen patients requiring open and endoscopic procedures for craniomaxillofacial skeleton-involving tumors preoperatively diagnosed as a malignancy of the head and neck or skull base were considered eligible to the study (Figure 1). In these patients, the resection was aided by the electromagnetic SN system.

A pair-matched 1:1 cohort was identified from the series of patients operated on by the same surgical team, in the same operating theater, within a timeframe of 3 years (2020-2022), with no aidance of SN. Pair-matching was performed by a physician external to the project, who was instructed to prioritize the following variables to identify controls: histology, primary vs recurrent presentation, clinical and pathological TNM categories, epicenter and topographic extension of the tumor, and adjuvant therapy. Outcome-related information were blinded during controls selection. For each of the aforesaid variables, symmetry rate was

calculated as the number of controls sharing the same characteristic with the respective cases over the total number of controls.

The following outcomes were evaluated to assess the feasibility of permanent (*i.e.*, non-experimental) translation of SN with 3-dimensional rendering as aidance to achieve margin control during oncologic ablations in the head and neck: set-up timing, spatial error after set-up, preoperative patient preparation time, surgery duration, loss of spatial accuracy during surgery, and implementation-related adverse events.

**Figure 1 (following page)**. Examples of surgical navigation with 3-dimensional rendering-aided margin delineation to open and endoscopic surgical procedures. **A, B**. Open intraoperative view and cross-sectional with 3-dimensional rendering view in a case of advanced, recurrent squamous cell carcinoma of the nasal vestibule. Bone-fixed reference. **C-E**. Field preparation with skin margin delineation (C), 3-dimensional rendering showing initial (green) and post-chemotherapy (red) volume of the tumor (D), and bone margin delineation in the left maxilla (E) in a patient affected by undifferentiated pleomorphic sarcoma of the cheek. Skin-fixed reference. **F-I**. Preoperative T2-weighted magnetic resonance imaging (F, H), and intraoperative navigation of the surgical bed after endoscopic ablation (G, I) in 2 cases of sinonasal chondrosarcoma.

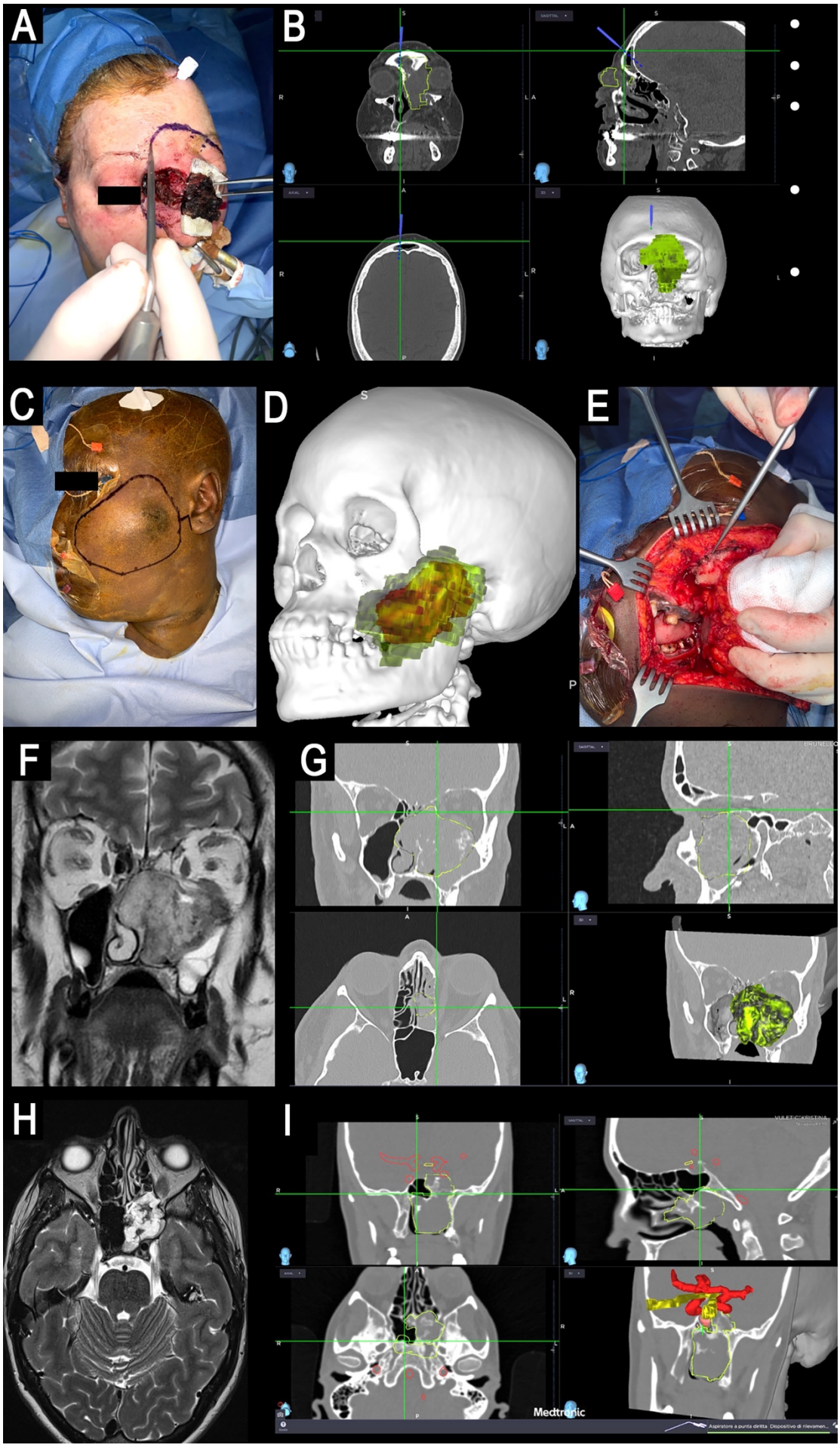
A
B
C
D
E
F
G
H
I
Medtronic

**Results**

Fourteen patients affected by a very advanced tumor of the craniofacial area (*i.e.*, T4a or T4b, when applicable) were recruited in this pilot study during the inclusion period (March-June 2021), out of which 9 underwent an endoscopic resection and 5 an open, possibly endoscopic-assisted, procedure. The SN system was set in less than 10 minutes in all cases and a spatial error <1 mm was achieved in all cases. In 2 (14.3%) cases of long and complex procedures, accuracy was lost after several hours of surgery and repeated patient's head repositioning. However, the ablative phase was already completed, and this loss of accuracy did not affect the margin delineation. After these 2 events, a bone-fixed reference (Figure 1A) was used instead of a skin-fixed reference (Figure 1B) when long and complex procedures were expected, and loss of accuracy was no longer observed. No implementation-related adverse events were registered.

The time for patient preparation prior to surgery was not statistically different when comparing the study and control cohort (1.4 h vs 1.3 h, respectively; Mann-Whitney test p=0.824; Figure 2). Similarly, duration of surgery was not significantly different in the 2 groups (8.4 h vs 6.9 h, respectively; Mann-Whitney test p=0.299; Figure 3).

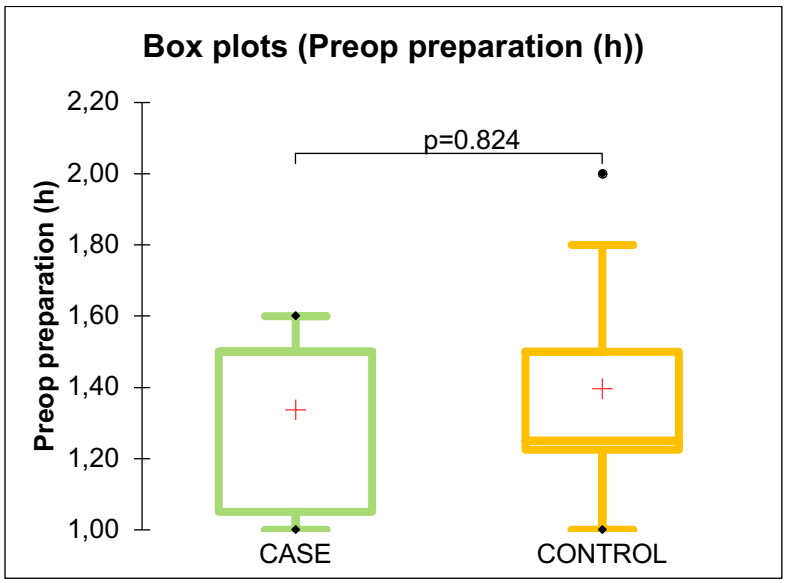


**Figure 2**. Box plots showing the preoperative preparation timing in the study (case) and control cohorts. No significant difference was observed.

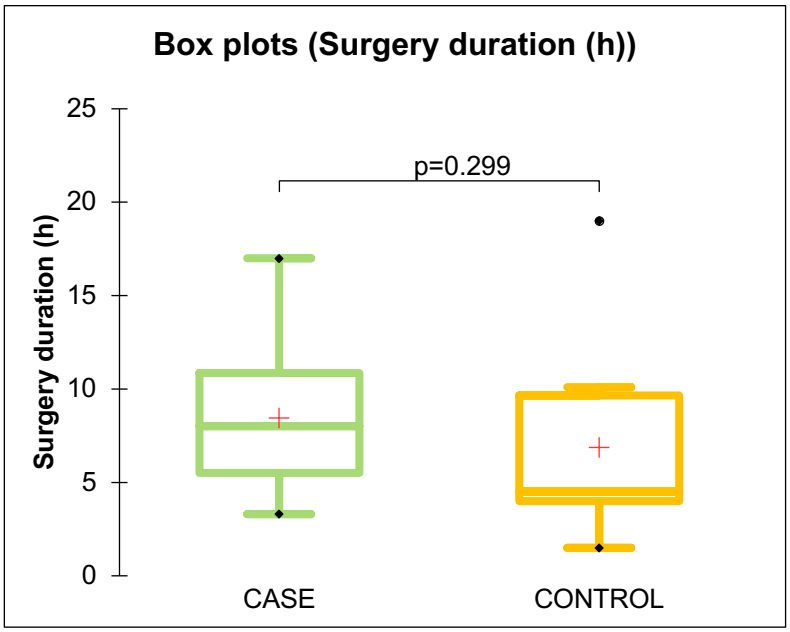


**Figure 3**. Box plots showing the total operation duration in the study (case) and control cohorts. No significant difference was observed.

## Conclusions

Implementation of SN with 3-dimensional rendering in the standard procedure to resect very advanced cancers of the head and neck is feasible. Set-up time (<10 minutes) was negligible in comparison to preoperative patient preparation time, which was not significantly affected using SN. Operating time was higher in the cohort of patients treated with SN-aided surgery, though with no statistical significance. This finding is in keeping with the preclinical evidence that using SN implies a moderate slowdown of surgery.[15]

## References

1. Ravasz LA, Slootweg PJ, Hordijk GJ, Smit F, van der Tweel I. The status of the resection margin as a prognostic factor in the treatment of head and neck carcinoma. J Craniomaxillofac Surg 1991; 19:314-318.
2. McMahon J, O'Brien CJ, Pathak Iet al. Influence of condition of surgical margins on local recurrence and disease-specific survival in oral and oropharyngeal cancer. Br J Oral Maxillofac Surg 2003; 41:224-231.
3. Woolgar JA, Triantafyllou A. A histopathological appraisal of surgical margins in oral and oropharyngeal cancer resection specimens. Oral Oncol 2005; 41:1034-1043.
4. Deganello A, Ferrari M, Paderno Aet al. Endoscopic-assisted maxillectomy: Operative technique and control of surgical margins. Oral Oncol 2019; 93:29-38.
5. Ferrari M, Montalto N, Nicolai P. Novel Approaches in Surgical Management: How to Assess Surgical Margins. In: Critical Issues in Head and Neck Oncology. Springer, Cham; 2021:95-110. doi:10.1007/978-3-030-63234-2_7
6. To EW, Yuen EH, Tsang WMet al. The use of stereotactic navigation guidance in minimally invasive transnasal nasopharyngectomy: a comparison with the conventional open transfacial approach. Br J Radiol 2002; 75:345-350.
7. Azarmehr I, Stokbro K, Bell RB, Thygesen T. Surgical Navigation: A Systematic Review of Indications, Treatments, and Outcomes in Oral and Maxillofacial Surgery. J Oral Maxillofac Surg 2017; 75:1987-2005.
8. Austin RE, Antonyshyn OM. Current applications of 3-d intraoperative navigation in craniomaxillofacial surgery: a retrospective clinical review. Ann Plast Surg 2012; 69:271-278.
9. Schramm A, Suarez-Cunqueiro MM, Barth ELet al. Computer-assisted navigation in craniomaxillofacial tumors. J Craniofac Surg 2008; 19:1067-1074.
10. Bell RB. Computer planning and intraoperative navigation in cranio-maxillofacial surgery. Oral Maxillofac Surg Clin North Am 2010; 22:135-156.
11. Guo R, Guo YX, Feng Z, Guo CB. Application of a computer-aided navigation technique in surgery for recurrent malignant infratemporal fossa tumors. J Craniofac Surg 2015; 26:e126-132.
12. Feichtinger M, Pau M, Zemann W, Aigner RM, Karcher H. Intraoperative control of resection margins in advanced head and neck cancer using a 3D-navigation system based on PET/CT image fusion. J Craniomaxillofac Surg 2010; 38:589-594.

13. Tarsitano A, Ricotta F, Baldino Get al. Navigation-guided resection of maxillary tumours: The accuracy of computer-assisted surgery in terms of control of resection margins - A feasibility study. J Craniomaxillofac Surg 2017; 45:2109-2114.
14. Catanzaro S, Copelli C, Manfuso Aet al. Intraoperative navigation in complex head and neck resections: indications and limits. Int J Comput Assist Radiol Surg 2017; 12:881-887.
15. Ferrari M, Daly MJ, Douglas CM, et al. Navigation-guided osteotomies improve margin delineation in tumors involving the sinonasal area: A preclinical study. *Oral Oncol*. 2019;99.

# Pilot clinical implementation of surgical navigation with three-dimensional rendering during open and endoscopic oncologic ablations in the craniofacial area: oncologic outcomes analysis

*Unpublished data*

## Introduction

This study assessed the oncologic outcomes of patients included in the pilot series with pair-matched controls reported in the previous chapter.

## Materials and methods

Three patients were excluded as definitive pathology showed a benign lesion as opposed to the preoperative diagnosis (chordoma → infrasellar Rathke's cleft cyst; pituitary lesion with uncertain malignant potential → pituitary adenoma; axial lesion with uncertain malignant potential → osteoid osteoma). Thus, in the present study, the case and control cohorts were made up by 11 patients each.

The following oncologic outcomes were assessed to verify whether implementation of surgical navigation (SN) confers benefits compared to the standard of care: rate of gross total resection (evaluated through early postoperative imaging, pre-radiotherapy imaging or first follow-up imaging on a case-by-case basis), microscopic margin status, overall survival, recurrence-free survival, and local recurrence-free survival.

## Results

Gross total resection was established with early postoperative imaging (n=4), pre-radiotherapy imaging (n=4), or follow-up imaging (n=3) in the study cohort. In the control cohort, the same methods were employed in 5, 5, and 1 case. Gross total resection was achieved in all patients of the study cohort and in 10/11 (90.9%) patients of the control cohort (Fisher's exact test p=1.000). In this patient, the residue was suspected intraoperatively and ascertained with early postoperative imaging. The patient underwent early redo surgery with macroscopically complete resection and microscopic margin involvement. Microscopic residual disease (inferred based on margin status at definitive pathology) was found in 2 (18.2%) and 8 (72.7%) patients in the study and control cohorts, respectively (Fisher's exact test p=0.030) (Figure 1).

Mean follow-up duration was 16.4 and 15.9 months in the study and control cohorts, respectively (Mann-Whitney test p=1.000). One-year was the only timepoint at which a comparison was feasible (the longest follow-up duration in the study group was 19 months). One-year overall survival was 100% and 80.0% in the study and control cohorts, respectively (log-rank test p=0.967). One-year recurrence-free survival was 90.9% and 70.7%, respectively (log-rank test p=0.210). One-year local recurrence-free survival was 100% and 90.9%, respectively (log-rank test p=0.317).

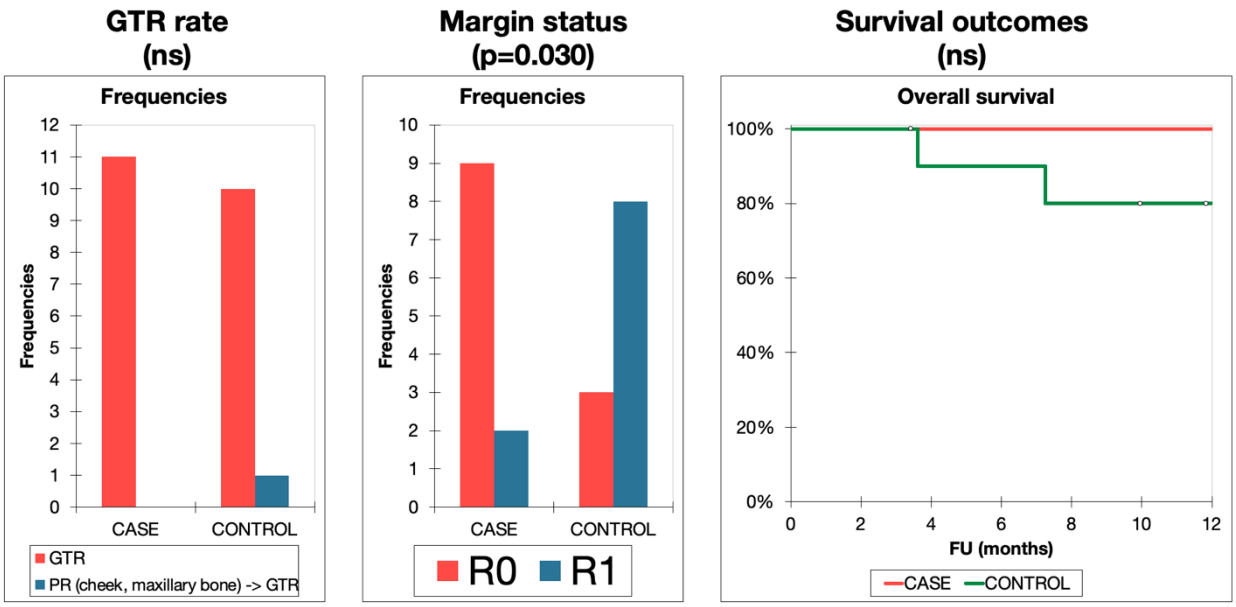


**Figure 1**. Histogram plots and Kaplan-Meier curves showing gross total resection (GTR) rate, margin status, and overall survival of cases and pair-matched controls, respectively. FU, follow-up; PR, partial resection; R0, complete resection with no microscopic residual disease (based on margin status); R1, macroscopically complete resection with suspect for microscopic residual disease (based on margin status).

## Conclusions

Overall, the use of SN with 3-dimensional rendering surgical navigation was associated with a decreased rate of microscopic residual disease. This is due to the more precise margin delineation, as demonstrated in the preclinical studies reported previously in this thesis. Despite local control estimate was higher in the cases cohort as compared with the controls cohort, no significant benefits in terms of prognosis could be demonstrated in the very short term. Possible explanations include the effect size, sample size, and follow-up duration. Despite these exploratory results are promising, longer follow-up and larger series are needed to draw firm conclusions on the actual benefits of SN implementation from a prognostic standpoint. However, if one considers altogether the absence of relevant harms, costs, and risks alongside with the evidence of improved margin status ensuing from more precise ablations, implementation of SN with 3-dimensional rendering into the standard of surgical care for very advanced cancers of the craniofacial area appears as a logical step forward.

# Development and use of a hybrid platform including pico projector-based augmented reality and surgical navigation with three-dimensional rendering to improve the margin status of oncological ablations in the head and neck

## Hybrid platform including pico projector-based augmented reality and surgical navigation with three-dimensional rendering: development and test on preclinical animal models

*Chan et al., PloS One 2021; doi: 10.1371/journal.pone.0250558*

**Introduction**

Imaging-based surgical navigation (SN) systems are routinely used to guide surgical procedures in anatomically complex areas such as the head and neck.[1] Previous studies have demonstrated that the use of SN can improve efficiency and safety in these challenging areas.[2] The added value of SN is twofold: firstly, it facilitates the identification of critical anatomical structures to avoid unnecessary complications; and furthermore, it helps to delineate tumor boundaries during oncologic ablations with the intent to improve adequacy of margins.[3–5]

Currently, research is focused on augmented reality (AR) methods such as video-computed tomography (CT) augmentation[6,7] and intraoperative imaging[8] to further improve the usefulness of SN. Optical "see-through" techniques, such as video-CT, consist of generating virtual anatomical structures from cross-sectional images (*e.g.*, CT or magnetic resonance imaging [MRI]) that are overlaid on the endoscopic image.[9] Literatures reveal that augmented reality in medical research had been very active in past decade.[10] However, majority of proposed approaches are AR system independently operate and not integrate into surgical navigation system. Nowadays, the surgical navigation system has been routinely used in the interventional procedure. The integration of SN with AR would synergistically improve the performance of technology-based guidance. In fact, an integrated AR-SN system would provide a precise, real-time topographical localization of the surgical field by means of intuitive visual enhancement.

Following this line of research, the Guided Therapeutics (GTx) group (TECHNA Institute, University Health Network, Toronto, Ontario, Canada) has developed a handheld AR device integrated into a SN system, which is capable of surgical site augmentation using both medical images and computer-generated virtual images. Briefly, this augmentation is achieved by using a tracked pico-projector which superimposes pre-contoured structures (*i.e.*, the volume occupied by the tumour, or critical neural and vascular structures) onto the surgical field. The aim of this was to assess the feasibility of this novel imaging system (AR-SN integrated) through pre-clinical mice models.

## Materials and methods

### *System architecture*

The prototype AR-SN system consists of pico-projector (L1 v2, AAXA Technology Inc., Santa Ana, California, United States), an infrared (IR) real-time optical tracking system (Polaris Spectra, NDI, Waterloo, Ontario, Canada), a universal serial bus (USB) 2.0M pixels generic camera, and a laptop computer. The pico-projector employed in the prototype is light (170g) and physically small (54mm x 170mm x 21mm).

The enclosure of the AR device is fabricated with acrylic and designed to encase the pico-projector, the IR reference marker mount, and the USB camera. The signal transmission of pico-projector is via High-Definition Multimedia Interface (HDMI) connector. Data processing is performed using a laptop computer (M4500, Precision laptop, Dell, Round Rock, Texas). Figure 1 illustrates the spatial relationship and interaction between individual components in the augmented reality surgical navigation platform. A SN platform, named "GTxEyes" (in-house development) was used in combination with the prototype as it allows for image display, fusion, and overlay of multiple imaging modalities including standard CT, cone beam CT, MRI, single photon emission CT (SPECT), positron emission tomography (PET), and video-endoscopy. The GTxEyes platform[11] was developed using open-source, cross-platform libraries included IGSTK,[12] ITK,[13] and VTK.[14]

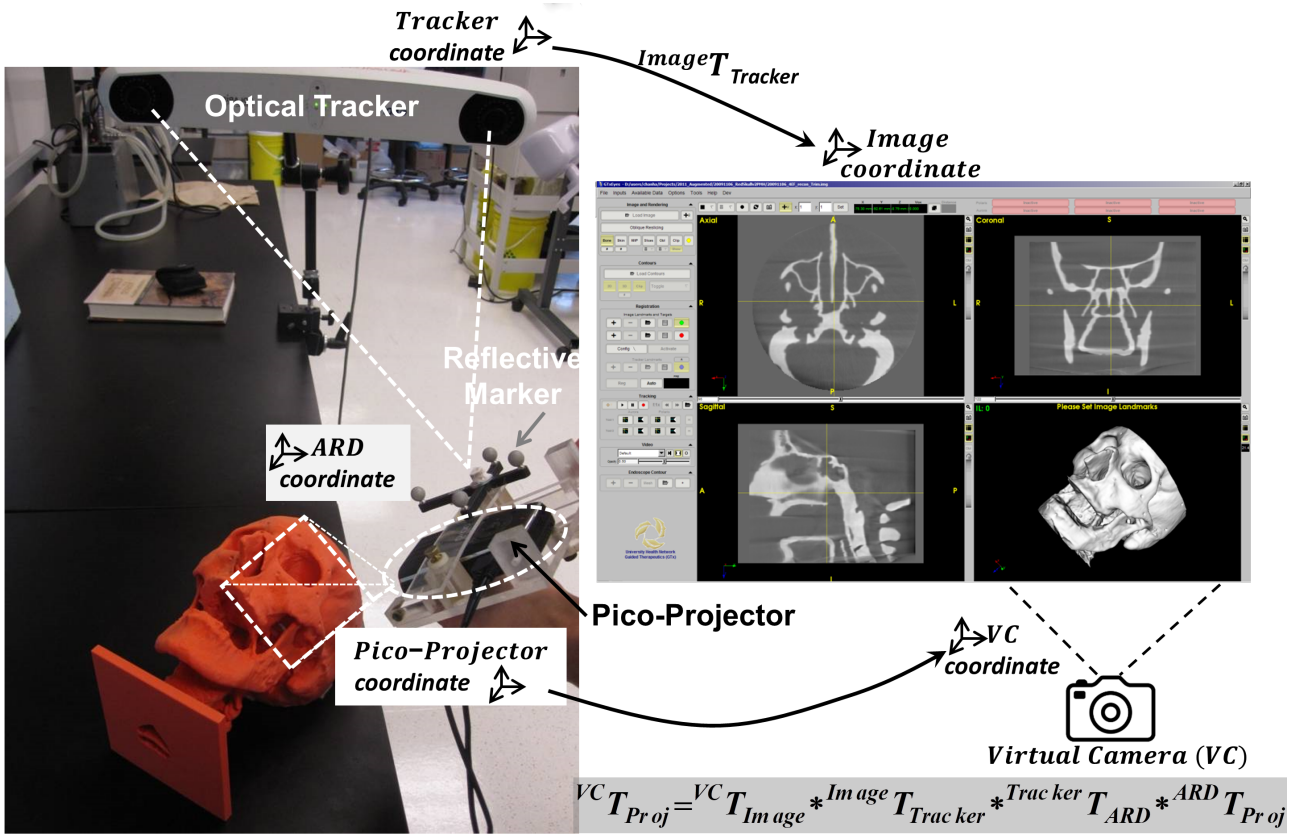


**Figure 1**. Prototype augment reality surgical navigation platform consists of optical tracking system and tracked pico-projector.

Surgical plans including the target lesion, ablation margins, critical structures, and safety margin (*i.e.*, voxel contouring of structures to be spared during ablation) were created preoperatively using ITK-SNAP[15] and built on the SN system. Real-time tracking detects the location of the surgical instruments in 3D space,

thus guiding the surgeon throughout the ablation and can alert the surgeon when the navigated instrumentation enters a pre-determined safety margin volume.[16] The AR-SN platform supports fully automatic bony and soft tissue digital segmentation based on voxel intensity threshold value (*e.g.*, Hounsfield Unit for CT imaging) and all surgical plans can be represented by either 3D surface or volume rendering and overlaid onto the surgical field with adjustable opacity. The AR-SN platform allows the surgeon to scroll through image slices projected on the operative field with a tracked pointer and to accordingly decide the depth of images through which to augment the surgical view.

***Image overlay and system operation***

The AR-SN system was registered into a single coordinate system by pairing correspondent landmarks using fiducial markers identifiable in both the image and subject. Once registration was completed, the AR-SN platform could track multiple surgical instruments simultaneously, as described in a previous study.[17,18]

To facilitate real-time tracking of the AR device in 3D space, an optical sensor attachment was mounted to the enclosure of the pico-projector. Pre-operative calibration consecutively performs to define the spatial relationship between the sensor and the center of the pico-projector, which elaborates by a transformation matrix stored in the AR-SN platform. Additionally, calibration allows tracking of the spatial position of the projector and synchronization of a virtual camera in the AR-SN platform. This calibration procedure ensures the pico-projector correctly illuminates the surgical field providing a reliable image of the pre-contoured structures (*i.e.*, those delineated in the surgical plans). By virtue of the real-time tracking, the pico-projector can be repositioned during the surgical procedure according to intraoperative requirements without compromising projection accuracy. Moreover, the integrated AR-SN can project multiple virtual objects and render multimodality fused imaging. Contours from external software such as ITK-SNAP[15] and 3D slicer[18,19] can also be imported into the AR-SN platform for sophisticated delineation of anatomical structures.

***Preclinical animal studies***

The integrated AR-SN system was evaluated on four preclinical mice models. All animal studies were performed in the animal care resource facility at the Princess Margaret Cancer Research Centre in accordance with protocols approved by the animal care committee at University Health Network. Four independent studies were performed to evaluate system performance and to investigate multimodality imaging in intraoperative AR-SN-based guidance. The first two studies investigated PET/CT for AR image guidance, whereas the third and fourth studies investigated PET/MRI and SPECT/CT, respectively.

In the first study, $^{64}$Cu isotope (10–13 MBq per mouse) was administered to a healthy, immunocompetent CD-1 mouse (Charles River, Wilmington, Massachusetts, United States) intravenously via a lateral tail vein one hour before micro-PET imaging (Focus 220, Siemens, Malvern, Pennsylvania, United States). A whole-body image acquisition time took 15 minutes per mouse, the image resolution was 0.146 x 0.146 x 0.796 mm$^3$. CT images were acquired after PET-imaging using a micro-CT scanner (Locus Ultra, GE

Healthcare, Pittsburgh, Pennsylvania, United States) with imaging parameters set at 80 kVp and 50 mA. During CT scanning, multiple 3D printed polycarbonate fiducial markers were introduced to surround the mouse bed to facilitate the subsequent AR-SN system registration. The resulting image volume was 366 x 196 x 680 voxels (366 x 196 matrix with 680 slice images), with isotropic voxel size of 0.154 $mm^3$. PET/CT images were then co-registered using Inveon Research Workplace (IRW) software (Siemens Healthcare, Malvern, Pennsylvania, United States). CT images were downsampled to 0.3 $mm^3$ isotopic voxel size to minimize computational intensity.

In the second study, 5 million BT474-M3 cells (HER2-overexpressing breast carcinoma) suspended in 100μL PBS were injected subcutaneously into the right mammary fat pad of athymic female CD-1 nude mouse. The animal was then monitored bi-weekly for tumour growth. Once the tumor reached a size of ~400-500 $mm^3$, the animal underwent the PET/CT as previously described. The tumour was preoperatively contoured based on available imaging using ITK-SNAP,[15] and subsequently imported into the AR-SN platform.

The third study investigated PET/MRI AR image guidance: a female CD-1 nude mouse was inoculated with 5 million MDA-MB-231 breast cancer cells through a subcutaneous injection in the bilateral upper mammary fat pads (100μL on each side). The mouse was then monitored as previously described. Once tumours reached a size of approximately 200-250$mm^3$, liposomes loaded with 64Cu were administrated intravenously 24 hours prior to imaging at a dose of 10–13 MBq/mouse and 20 μmol phospholipid/kg.[20] The mouse then underwent micro-PET imaging with a longer acquisition time of 60 minutes. Whole thorax-abdomen MRI was then performed using a 7T micro-MRI scanner (M2, Aspect Imaging, Shoham, Israel). The fusion of the MR and PET data sets was registered using IRW software with a rigid body algorithm based on normalized mutual information.

The fourth study experimented SPECT/CT image modality for AR image guidance. A female athymic CD-1 nude mouse were injected 10 million 231-H2N cells (human breast cancer cells) into the left thigh. The mouse was monitored as previously described until the tumour reached a volume of 125 $mm^3$. The mouse was then injected intravenously with 37 MBq of 111In-Fab fragments of anti-HEGF (human epidermal growth factor) antibody via lateral tail vein injection 48 hours prior to imaging.[21] SPECT/CT imaging (Bioscan, Washington DC, Washington, United States), was performed with dual-modality machine. Photons were accepted from the 10% windows centered on indium two photo-peaks at 171 and 245 keV. The SPECT projections were acquired in a 256 x 256 x 16 matrix for 85 minutes. Voxel size was isotropic (0.3 $mm^3$). Images were reconstructed using an ordered-subset expectation maximization algorithm (9 iterations).[22] Cone-beam CT images were acquired (180 projections, 45 kVp) immediately before the micro-SPECT images. Eight 3D printed markers were attached around the scan bed for tracking registration. Co-registration of SPECT and CT images was performed using pertinent software (InvivoScope, Bioscan Inc, Washington DC, Washington, United States).

Upon completion of all multimodality imaging studies, mice were euthanized using an overdose of 5% inhaled isoflurane and their body position was rigidly maintained in the scan bed. For each experiment,

the AR device was mounted on an articulating arm located at approximately 250–350 mm above the supine mouse.

***AR-SN system accuracy measurement***

The accuracy of the AR-SN system was quantitatively evaluated by overlaying the projection image on a checkerboard phantom with known dimensions. The phantom was composed of 25 rectangular grids (10 x 10 $mm^2$ each) with central divots (5 rows and 5 columns). The distance between the central divots was 20mm. The acrylic phantom was fabricated by a high precision computer numerical control (CNC) machine. The guidance images for the phantom navigation were acquired with a prototype cone-beam CT C-arm.[23] CT images were 256 x 256 x 192 voxels by volume with an isotopic voxel size of 0.78 $mm^3$. The accuracy of the AR-SN system was evaluated by comparing landmark localization on the phantom with and without the use of AR guidance. The central divot of each grid was localized manually using the tracked pointer three separate times per grid. The represented location of the divot was calculated from the mean location of the tracked pointer over the three measurements. These localization exercises were conducted over a range of distances between the phantom and AR projector including 200, 300, and 400 mm. The uncertainty of the projected location was calculated as follows: $(x_i,y_i,z_i)_{real}$ represents as "real" location of the divot center acquired manually without AR image guidance and $(x_i,y_i,z_i)_{virtual}$ represents as "virtual" location of the divot generated from the AR projection image, the estimation of error is the distance between the "real" and "virtual" location of the central divot such that $Err = ||(x_i,y_i,z_i)_{real} - (x_i,y_i,z_i)_{virtual}||$.

**Results**

***Preclinical animal study***

*First and second study: AR-SN with PET/CT*. In both the first and second studies, the AR-SN system provided reliable augmentation of 3D virtual skeleton (in gray) and a semiopaque coronal slice of PET image. Figure 2 demonstrates the experiment setup and AR projection images indicate skeleton and uptake of isotope from PET image in the liver and bladder.

In the second study, the right mammary fat pad tumour was delineated with ITK-SNAP[15] and imported to the AR-SN system in addition to the PET/CT images. The content of AR projection images (Figure 3A) included fusion with semi-opaque coronal slices of both CT (in gray) and PET (in hot colour scale) images. Additionally, a surface rendering of 3D bone structures (in gray) was also projected on the surgical field. The 3D virtual tumour on the right mammary fat pad (Figure 3A, in green) distinctively highlighted the tumour location relative to the other anatomy on PET/CT slice. Figure 3B demonstrates the virtual image created through projection of a PET/CT coronal slice onto the mouse body, with the virtual tumour seen in green and the mouse skeleton seen in gray. The surgical dissection of the mouse (Figure 3C) demonstrated that the anatomical tumor location matched the location identified by the augmented image overlay on the mouse body (Figure 3D). This confirmed the correlation of the virtual tumor projection and the anatomical findings at the time of surgery and demonstrated the precision of the AR instrument in physical space.

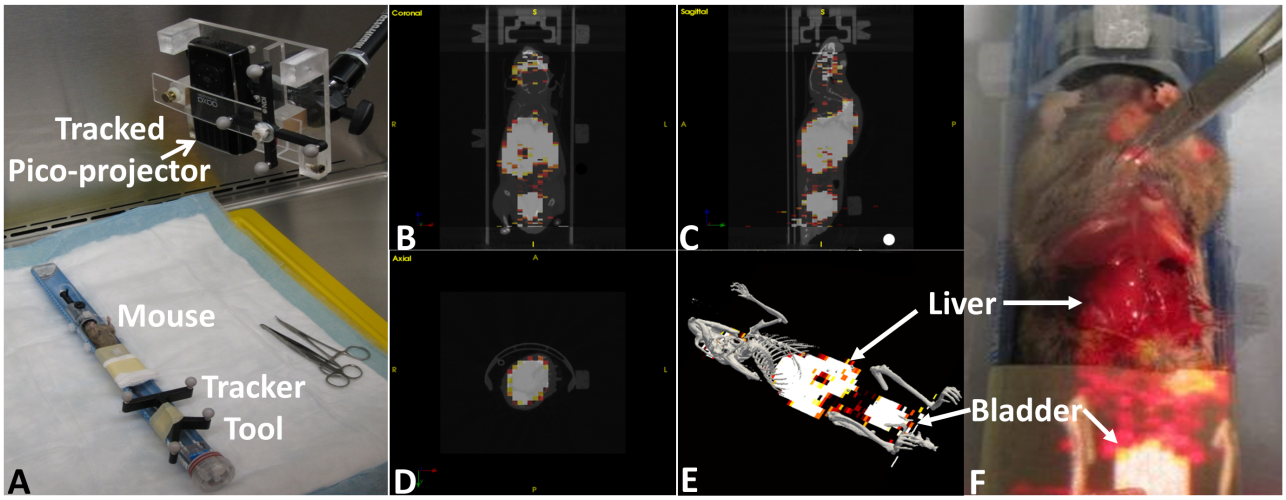


**Figure 2**. Augmented reality guided procedure with immunocompetent CD-1 healthy mouse model using PET/CT image. **A**. experimental setup. **B-D**. cross-sectional view of coronal, sagittal and axial imaging slices respectively. **E**. virtual image containing 3D skeleton (gray) and coronal slice of PET image. **F**. showing the image projection on the abdominal surface of dissected mouse indicate the accumulated isotope in the liver and bladder.

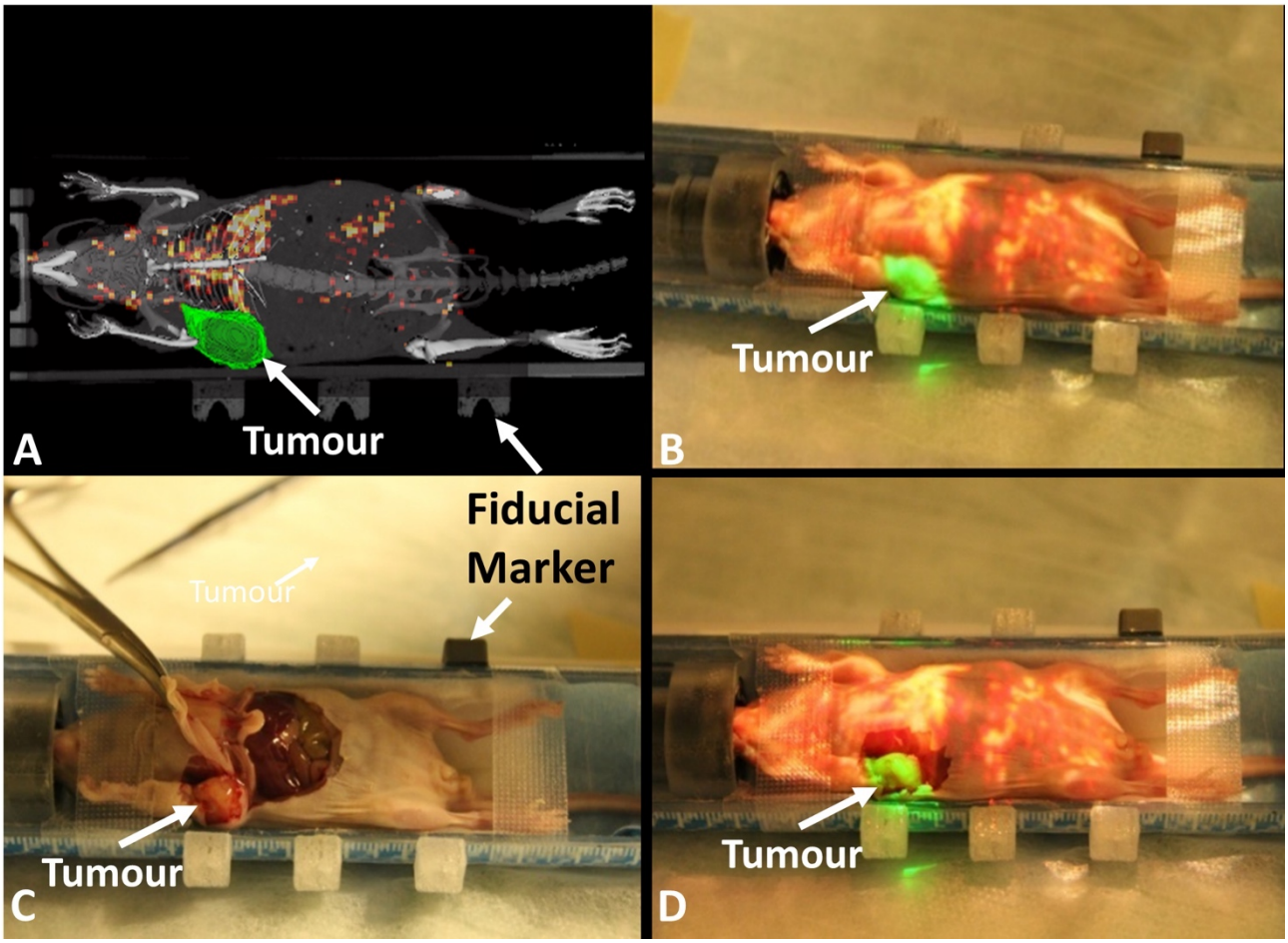


**Figure 3**. Augmented reality guided procedure with the breast carcinoma xenograft model. **A**. projection image includes semi-opaque fused micro-CT and PET images with contour of tumor in green and skeleton of mouse in gray. **B**. projection image overlaid on top of the mouse indicates the tumor location (green) and highlights isotope uptake in the liver. **C**. mouse dissection demonstrating the tumor location. **D**. mouse dissection with the overlaid projection image demonstrating the correct anatomical localization of the virtual contoured tumor on the mammary fat pad tumour.

*Third study: AR-SN with PET/MRI*. The registered PET/MRI was imported into the AR-SN system. The content of the augmented reality projection image included a fused PET/MRI coronal slice (Figure 4). The projected PET image displayed increased signal intensity signifying $^{64}$Cu-isotope uptake by the bilateral fat-pad tumour which was precisely overlaid onto the anatomical location of the tumours. The projection image also highlighted the high-level lung uptake of the $^{64}$Cu-radioisotope (Figure 4).

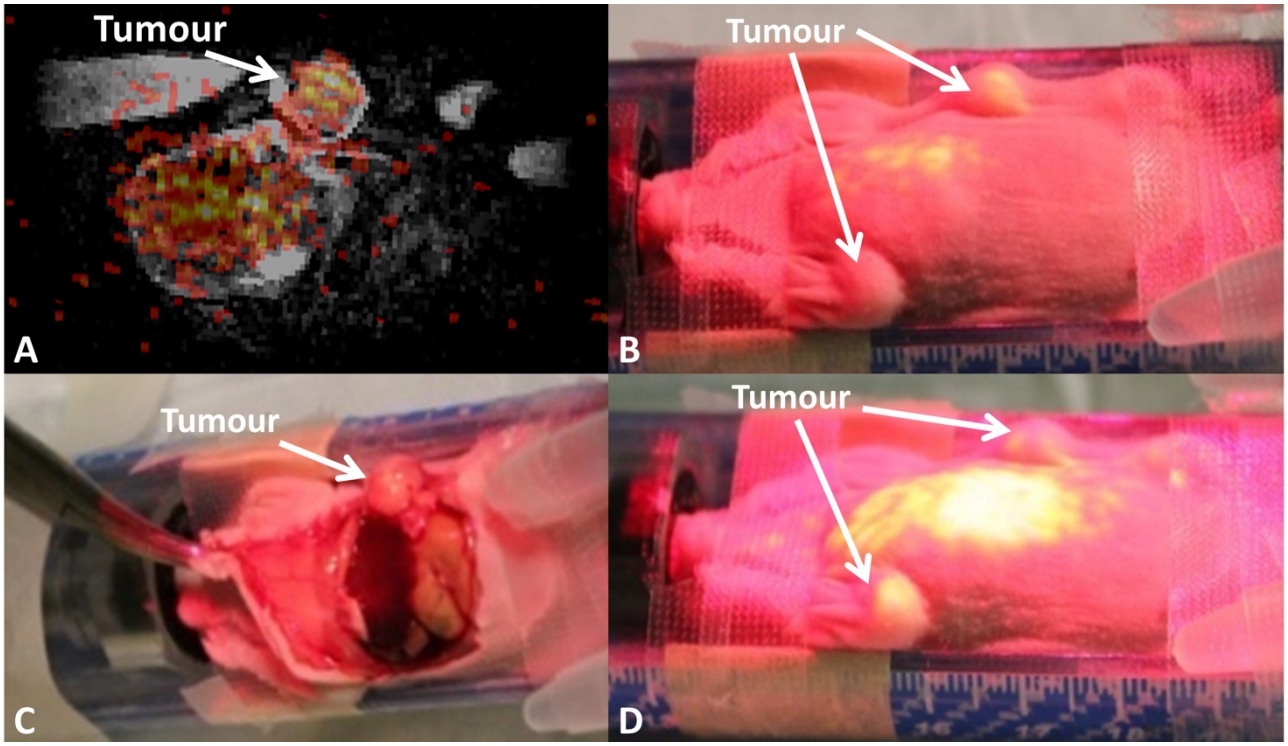


**Figure 4**. Augmented reality guided procedure with the breast carcinoma xenograft model demonstrating breast tumors in the left and right mammary fat pads. **A**. A registered PET/MRI image coronal slice for AR guide procedure. **B**. The AR PET image projected on the mouse's body surface highlights the tumor location. **C**. The dissected mouse reveals the tumor location on the right in the same location. **D**. AR projection on the mouse demonstrates the tumor location on the left side and the $^{64}$Cu isotope uptake in the lungs and liver.

*Fourth study: AR-SN with SPECT/CT*. SPECT/CT DICOM data was imported to the AR-SN navigation platform and fiducial markers were used to register the images with the AR platform. The content of the AR projection image included a semi-opaque fused SPECT (in rainbow) and CT (in gray) Coronal slice (Figure 5B). The axial slice and sagittal slice of the same mouse is showing in Figures 5A and 5C, respectively. In addition, the surface rendering of the full mouse skeleton (Figure 5D) created using bone segmentation was virtually projected in purple. Figure 5E also highlights the high-level isotope uptake in the liver.

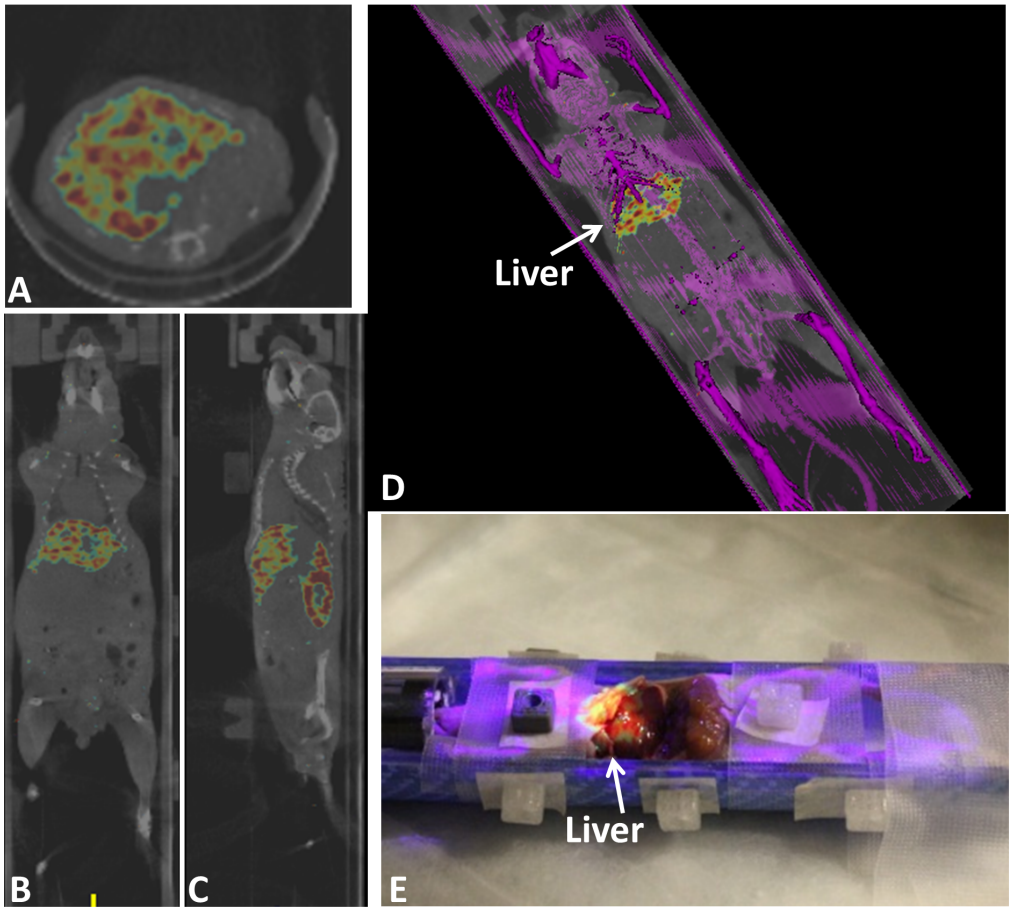


**Figure 5**. Augmented reality guided procedure with the tumor bearing athymic CD-1 nude mouse using registered SPECT/CT image. **A-C**. Axial, coronal and sagittal images of fused SPECT/CT images respectively. SPECT signal is seen in rainbow and CT in gray. **D**. An augmented reality projection image showing surface rendering of bone in purple combined with SPECT/CT coronal slice. **E**. Mouse dissection mouse demonstrating augmented reality projection SPECT-CT images overlaid on the mouse body also highlighting isotope uptake by the liver.

### *AR-SN system accuracy measurement*

The accuracy measurement proceeds with determining the divots 3D location with and without AR guidance in a range of projection distance from 200 mm to 400 mm. The fiducial registration error (FRE) with 4 divots is 0.45 mm. After tracker-image registration, a tracked pointer is used to localize the central of divot per described in the method section. Fiducial localization error (FLE) represented by root-mean-square (RMS) reveal the discrepancy between real divot and virtual divot location. At 200 mm, 300 mm and 400 mm projection distance, the RMS of measured divots is 0.42 ± 0.25 mm, 0.53 ± 0.31 mm, and 0.7 ± 0.37 mm, respectively. The overall system RMS across various projection distances was 0.55 ± 0.33 mm. Figure 6A illustrates the checkerboard phantom partially augmented by the projection image of 3D virtual checkerboard generated from CBCT. The projection demonstrated remarkable spatial accuracy and correlation between the physical location of the phantom central divots and the projected AR image (Figure 6B). The FLE for each projection distance is summarized in Figure 6C. The AR system performed best at projection distance of 200 mm and progressively worsened increasing the distance to 300 and 400 mm (Figure 6C).

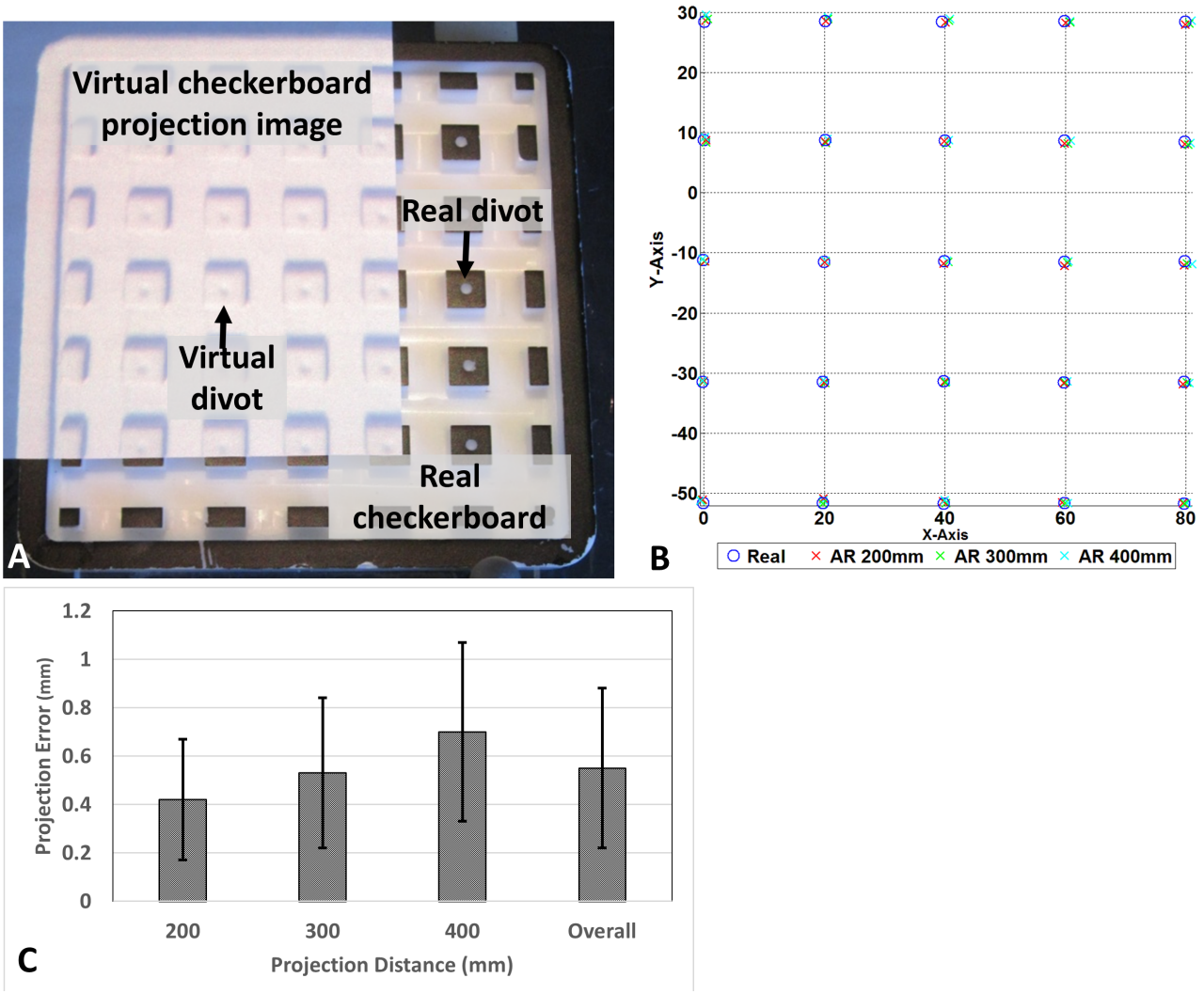


**Figure 6**. Accuracy estimation of augmented reality navigation system. **A**. CBCT generated virtual checkerboard overlaid on a real checkerboard. **B**. Graphical representation of localization for each divot from various projection distances. **C**. Projection error at varies projection distance.

## Discussion

This study demonstrates the feasibility and accuracy of our novel AR-SN system prototype. This system is composed of AR device fully integrated with a real-time SN system and is capable of providing target anatomical localization with an accuracy of 0.55 mm. Our implementation of AR technology is distinct from existing approaches that are published in the literatures where most of the existing projection-based AR device operates separately from the navigation system and incapable to track surgical instruments.[24–26] Firstly, our AR system is fully migrated to surgical navigation system. Secondly, our AR system use of surgical tracking device which provides real-time localization therefore displacement of AR device does not require re-registration.

The rationale behind this novel system is that the projection of virtual images on the surgical field can provide a useful visual guide to localize the extent of tumour intraoperatively and to alert surgeons to the presence of critical structures including vasculature or nerves that may not be readily visible. The principle of the surgical safety alert is discussed in our published manuscript regarding skull base surgery.[6,16] In developing

this AR-SN system we hope to provide a tool to aid in challenging surgical ablations at high risk of incomplete resection and major complications due to complex anatomy.

Several AR devices have previously been reported in the surgical literature. The majority of these devices have been designed as head-mounted display (HMD), as first described in 1969 by Land and Sutherland in collaboration with the Department of Defence.[27] In 1994, advances in static and dynamic registration of an optical see-through HMD were reported.[28] Since then, optical see-through AR has been successfully implemented in a number of non-medical applications as well as more recent medical applications in the field of neurosurgery and head and neck surgery.[29–31] However, HMD have several drawbacks including the indirect view of the surgical field and extra equipment that crosses the surgeon's sightline and/or restricts head movement due to device wiring. The add-on weight of HMD on the surgeon head could potentially reduce strength and concentration with prolonging usage of HMD during the course of surgery.

To address these limitations, scientists proposed using image overlay systems, which provide an alternative approach to enhance surgical visualization. Weiss *et al*. developed an inexpensive image overlay system composed of an LCD monitor and a half-silvered mirror mounted on an MRI scanner, which could be adapted to various angles and procedures.[32] With this method, the surgical field is augmented by superimposing the images from the translucent mirror on to the operative field. However, with this system the operator is required to be stationary, and the procedure must by accomplished close to the MRI scanner which may not be clinically practical. Baum et al. recently improved the versatility of this system by miniaturizing the monitor with a tablet device capable of operating independently from the scanner.[33]

The next logical step forward for surgical AR is directly projecting the desired visual information onto the operative field. However, few papers have reported the application of this concept in the field of head and neck surgery.[31,34,35] Our preliminary results demonstrate that our AR-SN system can reliably and accurately augment visualization intraoperatively on both phantoms and animal models, while overcoming some disadvantages of existing systems.

Our system was created using light equipment that can be easily adapted to the operative setting without any interference with the surgeons' sightline and working space. The capability of visually enhancing the position of both the tumour and critical structures on the anatomical planes could allow for both accurate tumour delineation and the prevention of major complications. Moreover, our preclinical analysis demonstrated how the prototype could be adapted to several potential imaging sources (*i.e.*, PET/CT, PET/MRI, SPECT/CT). This aspect is critically important as it provides the surgeon with a visual image based on radiologic and nuclear medicine semiotics (*i.e.*, contrast agent uptake, inflammation- vs neoplastic-induced changes) and enables seamless incorporation of patient-specific medical information into an image-guided procedure. Meanwhile, the multi-image modality guidance can be very helpful in surgical navigation system with AR capability.

The checkerboard phantom study provided a quantitative proof of system accuracy, with over 225 points being localized with minimal error at various projection distances ($0.55 \pm 0.33$ mm). This sub-millimeter accuracy is consistent with navigation system requirements and comparable to reported literature.[36] Our

prototype system is based on a low-cost video camera that serves as a sensor for the pico-projector calibration. This calibrated camera could be additionally used as a video see-through AR device to stream surgical video to the navigation platform. This potential to combine video into the pico-projector system could further enhance the functionality of our platform as a dual AR device.

There are a wide range of potential clinical applications for this type of AR-SN system. This technology may be beneficial for a broad spectrum of surgical procedures requiring sophisticated surgical planning, precise resection, and sparing of critical structures (*e.g.*, spine surgery, chest wall surgery, orthopedic oncological surgery, and head and neck surgery). In the field of head and neck oncology, this technology could be applied to guide complex resections especially in areas where the bony framework substantially limits the motion of soft tissues during the surgical procedure. Furthermore, this technology could help identify small volume mass such as intraparenchymal lesions. The added clinical value of this AR-SN system is currently under investigation at the hybrid preclinical/clinical Guided Therapeutics Operating Room (GTxOR–TECHNA Institute, University Health Network, Toronto, Ontario, Canada) at our institution.

Our study does have some limitations that we hope to overcome during future technology development. Firstly, our data is based on a preclinical study with a limited number of animals. Consequently, the highly controlled operative environment of animal models may not accurately reflect the clinical setting. Meanwhile, several publications had already demonstrated the value of AR technology in clinical setting.[37] Secondly, the surgical site and anatomical structures in the pre-clinical studies are relatively motionless. This led us to assume that this system would be applicable only to areas where soft tissue morphological changes are limited by the bony framework (*i.e.*, the maxillofacial skeleton and surrounding spaces). In fact, our system does not currently have the capacity to account for tissue deformation induced by cauterization, manipulation, and resection. Therefore, procedures involving mainly soft tissues areas that are prone to significant deformation (*i.e.*, lung) may not benefit from this AR-SN system. Finally, image distortion due to projection on non-planar surfaces is a further limitation of projection-based AR techniques. Despite these potential limitations, we are currently in the process of translating this technology to patient studies in key surgical applications such as head and neck and orthopedic oncology to evaluate system performance under clinical conditions.

**Conclusions**

We have reported the development of a novel, integrated AR-SN system. This proof-of-concept study demonstrated the feasibility of our AR-SN system for multi-modality image-guided surgery in a preclinical setting. The accuracy demonstrated from the phantom study was within acceptable uncertainty. Our AR-system was found to be highly precise and capable of sub-millimeter accuracy, which is in keeping with existing commercially available SN systems. These preliminary results represent a promising framework for future technology development and possible clinical translation.

## References


1. Keschner D, Lee J (2010) Use of surgical navigation during endoscopic skull base surgery. Operative Techniques in Otolaryngology-Head and Neck Surgery 21: 44-50.
2. Eliashar R, Sichel JY, Gross M, Hocwald E, Dano I, et al. (2003) Image guided navigation system-a new technology for complex endoscopic endonasal surgery. Postgrad Med J 79: 686–690. PMID: 14707243
3. Feichtinger M, Pau M, Zemann W, Aigner RM, Karcher H (2010) Intraoperative control of resection margins in advanced head and neck cancer using a 3D-navigation system based on PET/CT image fusion. J Craniomaxillofac Surg 38: 589–594. https://doi.org/10.1016/j.jcms.2010.02.004 PMID: 20381368
4. Catanzaro S, Copelli C, Manfuso A, Tewfik K, Pederneschi N, et al. (2017) Intraoperative navigation in complex head and neck resections: indications and limits. Int J Comput Assist Radiol Surg 12: 881–887. https://doi.org/10.1007/s11548-016-1486-0 PMID: 27659282
5. Tarsitano A, Ricotta F, Baldino G, Badiali G, Pizzigallo A, et al. (2017) Navigation-guided resection of maxillary tumours: The accuracy of computer-assisted surgery in terms of control of resection margins—A feasibility study. J Craniomaxillofac Surg 45: 2109–2114. https://doi.org/10.1016/j.jcms.2017.09.023 PMID: 29092758
6. Haerle SK, Daly MJ, Chan H, Vescan A, Witterick I, et al. (2015) Localized intraoperative virtual endoscopy (LIVE) for surgical guidance in 16 skull base patients. Otolaryngol Head Neck Surg 152: 165–171. https://doi.org/10.1177/0194599814557469 PMID: 25385806
7. Lee CY, Chan H, Ujiie H, Fujino K, Kinoshita T, et al. (2018) Novel Thoracoscopic Navigation System With Augmented Real-Time Image Guidance for Chest Wall Tumors. Ann Thorac Surg 106: 1468–1475. https://doi.org/10.1016/j.athoracsur.2018.06.062 PMID: 30120940
8. Siewerdsen JH, Daly MJ, Chan H, Nithiananthan S, Hamming N, et al. (2009) High-performance intraoperative cone-beam CT on a mobile C-arm: an integrated system for guidance of head and neck surgery. Proc SPIE 7261: 72610J.
9. Rolland JP, Fuchs H (2000) Optical Versus Video See-Through Head-Mounted Displays in Medical Visualization. Presence: Teleoperators and Virtual Environments 9: 287–309.
10. Ayoub A, Pulijala Y (2019) The application of virtual reality and augmented reality in Oral & Maxillofacial Surgery. BMC Oral Health 19: 238. https://doi.org/10.1186/s12903-019-0937-8 PMID: 31703708
11. Daly MJ, Chan H, Nithiananthan S, Qiu J, Barker E, et al. (2011) Clinical implementation of intraoperative cone-beam CT in head and neck surgery. Medical Imaging 2011: Visualization, Image-Guided Procedures, and Modeling 7964: 796426–796428.
12. Enquobahrie A, Cheng P, Gary K, Ibanez L, Gobbi D, et al. (2007) The Image-Guided Surgery Toolkit IGSTK: An Open Source C++ Software Toolkit. Journal of Digital Imaging 20: 21–33. https://doi.org/10.1007/s10278-007-9054-3 PMID: 17703338
13. Ibanez L, Schroeder W, Ng L, Cates J The ITK software guide.
14. Schroeder W, Martin K, Lorensen B The Visualization Toolkit: An Object Oriented Approach to 3D Graphics. Kitware Inc., 2004. ISBN 1-930934-19-X.
15. Yushkevich PA, Piven J, Hazlett HC, Smith RG, Ho S, et al. (2006) User-guided 3D active contour segmentation of anatomical structures: significantly improved efficiency and reliability. Neuroimage 31:1116–1128. https://doi.org/10.1016/j.neuroimage.2006.01.015 PMID: 16545965
16. Dixon BJ, Daly MJ, Chan H, Vescan A, Witterick IJ, et al. (2014) Augmented real-time navigation with critical structure proximity alerts for endoscopic skull base surgery. Laryngoscope 124: 853–859. https://doi.org/10.1002/lary.24385 PMID: 24122916
17. Erovic BM, Daly MJ, Chan HH, James AL, Papsin BC, et al. (2013) Evaluation of intraoperative cone beam computed tomography and optical drill tracking in temporal bone surgery. Laryngoscope 123:2823–2828. https://doi.org/10.1002/lary.24130 PMID: 23918182
18. Sternheim A, Daly M, Qiu J, Weersink R, Chan H, et al. (2015) Navigated pelvic osteotomy and tumor resection: a study assessing the accuracy and reproducibility of resection planes in Sawbones and cadavers. J Bone Joint Surg Am 97: 40–46. https://doi.org/10.2106/JBJS.N.00276 PMID: 25568393
19. Fedorov A, Beichel R, Kalpathy-Cramer J, Finet J, Fillion-Robin JC, et al. (2012) 3D Slicer as an image computing platform for the Quantitative Imaging Network. Magn Reson Imaging 30: 1323–1341. https://doi.org/10.1016/j.mri.2012.05.001 PMID: 22770690
20. Lee H, Zheng J, Gaddy D, Orcutt KD, Leonard S, et al. (2015) A gradient-loadable (64)Cu-chelator for quantifying tumor deposition kinetics of nanoliposomal therapeutics by positron emission tomography. Nanomedicine 11: 155–165. https://doi.org/10.1016/j.nano.2014.08.011 PMID: 25200610
21. Chan C, Scollard DA, McLarty K, Smith S, Reilly RM (2011) A comparison of $^{111}$In- or $^{64}$Cu-DOTAtrastuzumab Fab fragments for imaging subcutaneous HER2-positive tumor xenografts in athymic mice using microSPECT/CT or microPET/CT. EJNMMI Res 1: 15. https://doi.org/10.1186/2191-219X-1-15 PMID: 22214307
22. Hudson HM, Larkin RS (1994) Accelerated image reconstruction using ordered subsets of projection data. Medical Imaging, IEEE Transactions on 13: 601–609. https://doi.org/10.1109/42.363108 PMID: 18218538

23. Chan Y, Siewerdsen JH, Rafferty MA, Moseley DJ, Jaffray DA, et al. (2008) Cone-beam computed tomography on a mobile C-arm: novel intraoperative imaging technology for guidance of head and neck surgery. J Otolaryngol Head Neck Surg 37: 81–90. PMID: 18479633
24. Besharati Tabrizi L, MahvashM (2015) Augmented reality-guided neurosurgery: accuracy and intraoperative application of an image projection technique. J Neurosurg 123: 206–211. https://doi.org/10.3171/2014.9.JNS141001 PMID: 25748303
25. Marmulla R, Hoppe H, Muhling J, Eggers G (2005) An augmented reality system for image-guided surgery. Int J Oral Maxillofac Surg 34: 594–596. https://doi.org/10.1016/j.ijom.2005.05.004 PMID: 16053885
26. Qu M, Hou Y, Xu Y, Shen C, Zhu M, et al. (2015) Precise positioning of an intraoral distractor using augmented reality in patients with hemifacial microsomia. J Craniomaxillofac Surg 43: 106–112. https://doi.org/10.1016/j.jcms.2014.10.019 PMID: 25465484
27. Land RI, Sutherland IE (1969) Real-time, color, stereo, computer displays. Appl Opt 8: 721–723. https://doi.org/10.1364/AO.8.000721 PMID: 20072296
28. Azuma R, Bishop G (1994) Improving static and dynamic registration in an optical see-through HMD. Proceedings of the 21st annual conference on Computer graphics and interactive techniques: ACM. pp.197–204.
29. Bajura M, Neumann U. Dynamic registration correction in augmented-reality systems; 1995 11–15 Mar 1995. pp. 189–196.
30. Khamene A, Wacker F, Vogt S, Azar F, Wendt M, et al. (2003) An Augmented Reality system for MRI-guided needle biopsies. Stud Health Technol Inform 94: 151–157. PMID: 15455881
31. Wong K, Yee HM, Xavier BA, Grillone GA (2018) Applications of Augmented Reality in Otolaryngology: A Systematic Review. Otolaryngol Head Neck Surg 159: 956–967. https://doi.org/10.1177/0194599818796476 PMID: 30126323
32. Weiss CR, Marker DR, Fischer GS, Fichtinger G, Machado AJ, et al. (2011) Augmented reality visualization using Image-Overlay for MR-guided interventions: system description, feasibility, and initial evaluation in a spine phantom. AJR Am J Roentgenol 196: W305–307. https://doi.org/10.2214/AJR.10.5038 PMID: 21343479
33. Baum Z, Ungi T, Lasso A, Fichtinger G (2017) Usability of a real-time tracked augmented reality display system in musculoskeletal injections: SPIE.
34. Chand M, Keller DS, Devoto L, McGurkM (2018) Furthering Precision in Sentinel Node Navigational Surgery for Oral Cancer: a Novel Triple Targeting System. J Fluoresc 28: 483–486. https://doi.org/10.1007/s10895-018-2211-x PMID: 29359237
35. Marmulla Rd, Hoppe H, Mu¨ hling J, Hassfeld S (2005) New Augmented Reality Concepts for Craniofacial Surgical Procedures. Plastic and Reconstructive Surgery 115: 1124–1128. https://doi.org/10.1097/01.prs.0000156215.06282.76 PMID: 15793455
36. Gavaghan KA, Peterhans M, Oliveira-Santos T, Weber S (2011) A portable image overlay projection device for computer-aided open liver surgery. IEEE Trans Biomed Eng 58: 1855–1864. https://doi.org/10.1109/TBME.2011.2126572 PMID: 21411401
37. Eckert M, Volmerg JS, Friedrich CM (2019) Augmented Reality in Medicine: Systematic and Bibliographic Review. JMIR Mhealth Uhealth 7: e10967. https://doi.org/10.2196/10967 PMID: 31025950

Use of the hybrid platform to improve the margin delineation in oncological ablations of the craniofacial area: a preclinical study on phantom-based tumor models

*Sahovaler et al., Front Oncol 2021; doi: 10.3389/fonc.2021.723509*

**Introduction**

The complex anatomy and close proximity of critical structures in the sinonasal region represent a major challenge for surgeons when treating advanced tumors in this location, and incomplete resections are not uncommon, both in open and endoscopic approaches.[1,2] Intraoperative navigation (IN) has been proposed as a potential strategy to improve surgical margins.[3] IN enables co-registration of computed tomography (CT) and/or magnetic resonance imaging (MRI) studies with surgical instruments. As a result, real-time feedback of instrument location is provided in order to help the surgeon during the operation.

Our group has recently published an advanced IN system for open sinonasal approaches during the resection of locally aggressive cancers.[4] This technology not only allows the surgeon to locate a registered instrument or pointer tool in two-dimensions, but also introduces planar cutting tool capabilities along with three-dimensional (3D) volume rendering. Therefore, the surgeon can anticipate the direction of the cutting instrument in 3D planes with respect to the tumor and improve accuracy of margin delineation. Still, one key drawback of all IN systems is that the information is displayed outside the surgical field, and therefore surgeons are forced to switch their gaze between the actual procedure and the navigation monitor, which can impact safety and efficiency.

Augmented reality (AR) uses visual inputs to enhance the user's natural vision, and therefore can integrate navigation information onto the surgical field.[5] This feature can potentially address the gaze toggling drawback of IN, and at the same time provide valuable information to the surgeon, for example facilitating tumor localization and delineation. Reports of AR in Otolaryngology- Head and Neck Surgery are scarce, and most of them come from endoscopic sinus surgery,[6] transoral robotic surgery,[7] and otology[8,9]. Nevertheless, open sinonasal procedures also represent an adequate indication for AR. The rigid structure of the sinonasal region facilitates the co-registration processes required for AR, and the high rates of incomplete resections in advanced sinonasal tumors could be improved with the use of this technology.

The objective of this study was to report the first use of a novel AR system in open sinonasal tumor resections in preclinical models, and to compare an AR approach with an advanced IN navigation system.

**Materials and Methods**

***Tumor models***

Two artificial skulls (Sawbones®) and a mouldable material (Play-Doh®) mixed with acrylic glue were employed to build 4 locally advanced sinonasal tumor models (Figure 1A). Tumor surfaces were disguised with tape. Five different areas to be osteotomized were delineated: palatal osteotomy (Pa), fronto-maxillary junction (FMJ), latero-inferior orbital rim (LIOR), zygomatic arch (Zy) and pterygomaxillary junction (PMJ) (Figure 1B).

***Image acquisition and tumor contouring***

Cone-beam computed tomography (CBCT) scans acquired 3D images of the skull models.[9] Tumors showed higher x-ray attenuation than the artificial bone (Figure 1C). Tumour contouring was performed semi-automatically.[10] First, a global threshold was applied to provide a quick, coarse segmentation, and then manual refinement was used to smooth the segmentation (Figure 1D).

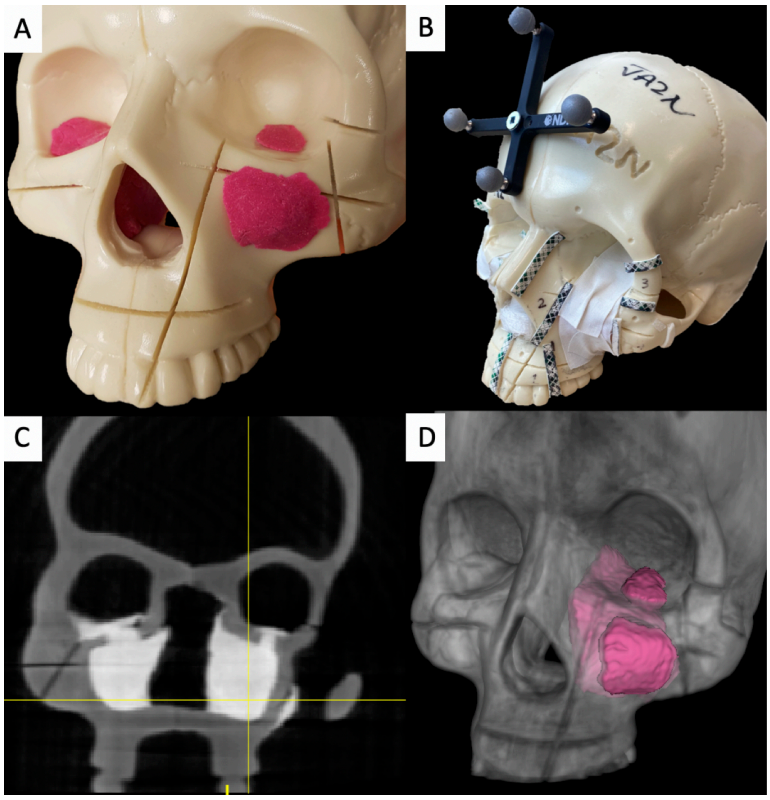


**Figure 1**. Tumor models, image acquisition and tumor contouring. **A**. Artificial skulls with mouldable material simulating advanced sinonasal tumors. **B**. Final tumor model, with the tumors covered with white tape. The areas to be osteotomized are delineated with visible tape and marked with numbers. A 4-sphere reference tool drilled to the skull to co-register the intraoperative navigation. **C**. Higher attenuation of the artificial tumor models in the CBCT images. **D**. 3D contouring of the left tumor.

***Advanced Intraoperative Navigation system***

An in-house navigation software package, GTx-Eyes, processed and displayed the CBCT images.[11] This software has been proven useful in a breadth of surgical oncology subspecialties[12–15] and the technical aspects are described elsewhere.[16] Tumor and margin segmentations were superimposed on tri-planar views and also shown as 3D surface renderings (Figure 2A). Tool tracking was achieved by a stereoscopic infrared camera. Image-to-tracker registration was obtained by paired-point matching of pre-drilled divots in the skull by means of a tracked pointer. A 4-sphere reference tool was drilled to the skull. A fiducial registration error of ≤1mm was deemed acceptable. A 3-sphere reference was attached to an osteotome, and calibrated. This advanced IN system allows visualization of the entire trajectory of the cutting instrument with respect to the tumor in 3D views (Figures 2).

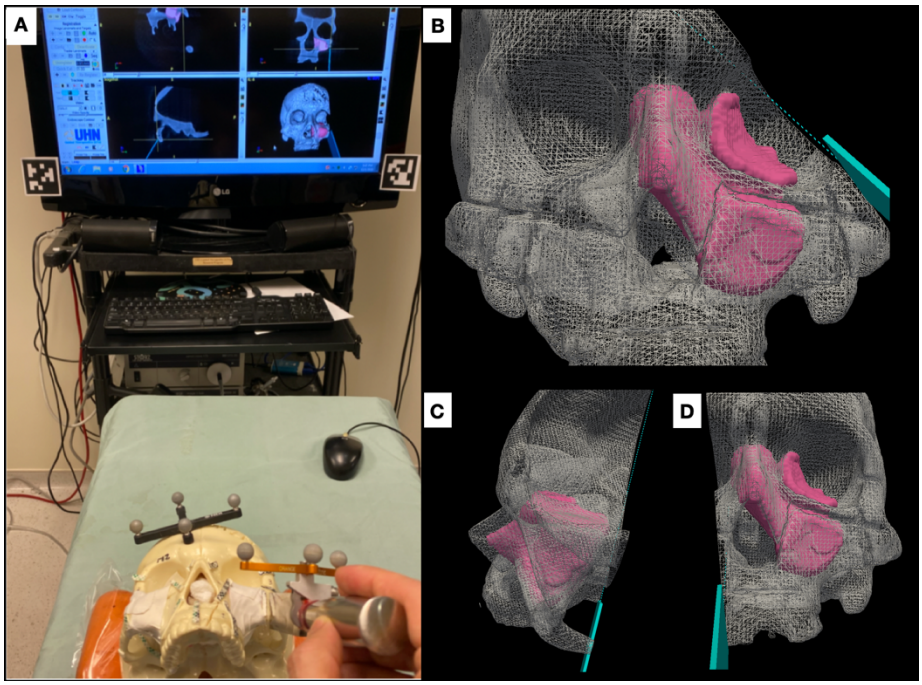


**Figure 2**. Advanced intraoperative navigation system. **A**. Setup of the system, depicting the 3-planar cutting views and the 3D rendering of the tumor on the screen. The skull and the cutting instrument (in this case an osteotome) are referenced to be tracked and co-registered. **B-D**. The system allows users to visualize cutting trajectories of the instrument with respect to the tumor during simulation of latero-inferior orbital rim (B), pterygomaxillary junction (C), and palate (D) osteotomies.

### *Augmented Reality system*

The AR system was composed of a portable high-definition projector (PicoPro, Celluon Inc, Federal Way, WA), a stereoscopic infrared camera (Polaris Spectra, NDI, Waterloo, Ontario, Canada), a USB 2.0M pixel generic camera (ICAN Webcam 2MP, China), and a laptop computer (M4500, Precision laptop, Dell, Round Rock, Texas). A custom-made 3D printed case was fabricated to anchor a 4-sphere reference tool and contain the other elements of the AR system (Figure 3). The technical details of this system including the kinematic transformation, reference system, and conventional image-to-tracker registration method have also been described elsewhere.[17]

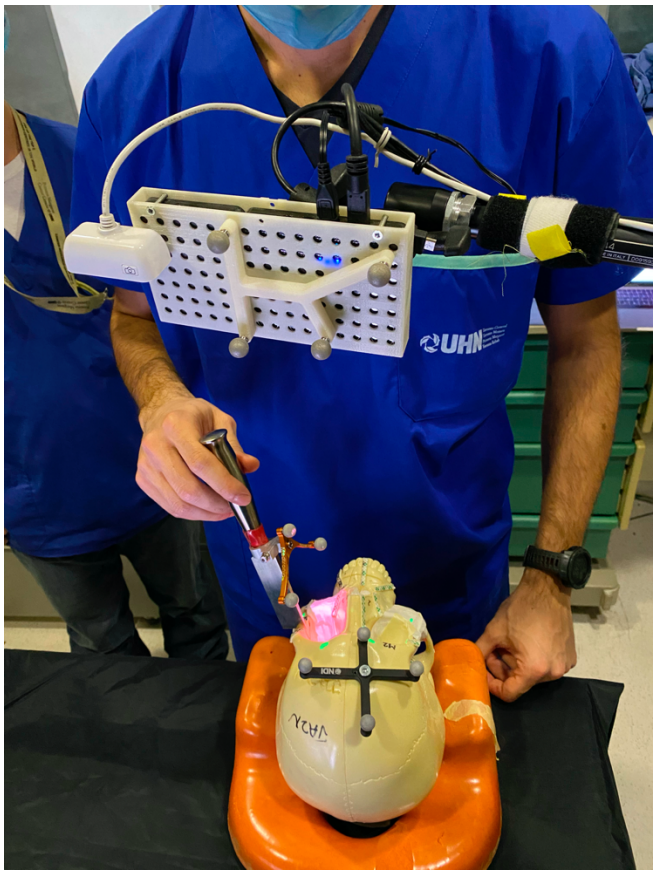


**Figure 3**. Augmented reality system mounted and projecting the tumor position onto the surgical field. The hybrid platform includes also surgical navigation with 3-dimensional rendering.

The AR system was registered into a single coordinate system by pairing correspondent landmarks using fiducial markers identifiable in both the images and projection surface (Figure 4). GTx-Eyes provided the 3D surface rendering of the tumors, which were projected by the AR system onto the skulls. The virtual tumor is delineated with CBCT imaging through ITK-SNAP software (ref below). The optical sensor mounted to the projector case facilitated real-time tracking of the AR device, to allow the projector and/or skull to be repositioned during tasks without compromising projection accuracy, with a registration error <1 mm. This approach facilitated identification of the tumors and in consequence guided the virtual cuts of the participants.

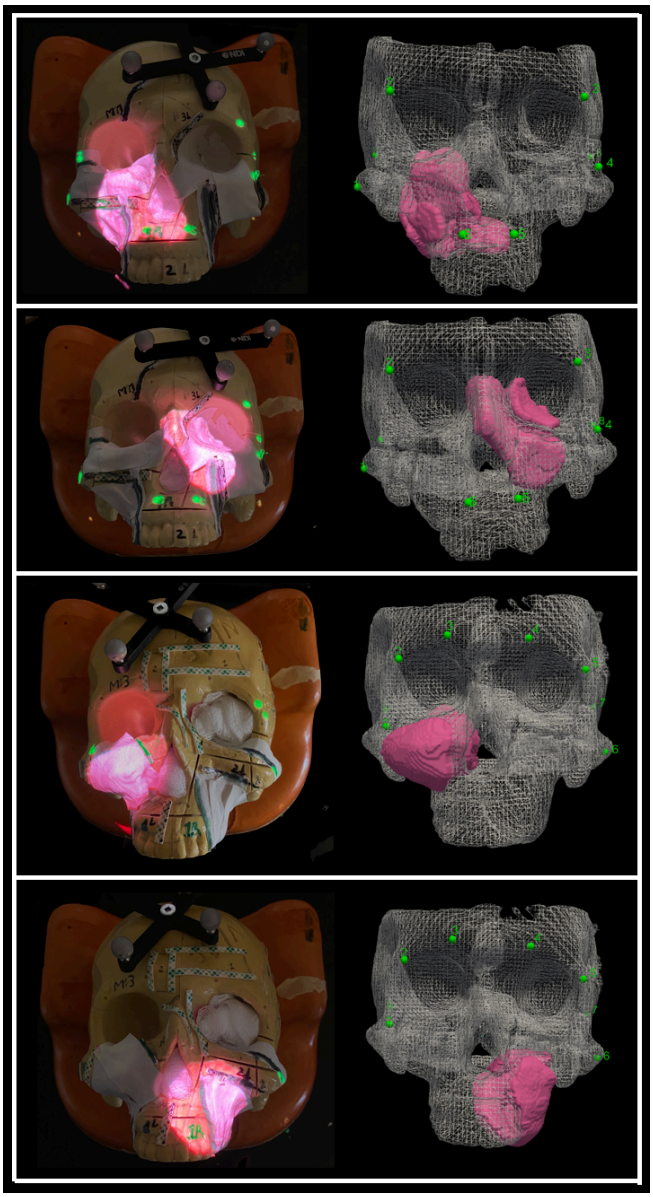

**Figure 4**. Projection of the four sinonasal tumors using augmented reality, which enables tumor localization. The alignment points are depicted as well as the 3D reconstruction of the tumors. Pictures were taken without light for demonstration purposes, but good visualization is obtained with light as well.

### *Gaze-tracking system*

A wearable gaze-tracker headset was developed to continuously monitor and locate the user's gaze (e.g., surgical field vs. navigation monitor) during surgical tasks. This headset was used solely for gaze-tracking and did not project any information. The eye-tracker (Pupil Labs, Berlin, Germany) consists of two cameras; one trained on the eye and the other, a 'world camera', recording the individual's field of view. A series of computer vision algorithms are applied to the input from the eye camera to reliably detect the pupil throughout the eye's range of motion. A calibration step provides a triangulating mapping function between the pupil and world cameras, which enables the user's gaze to be precisely tracked (Figure 5).

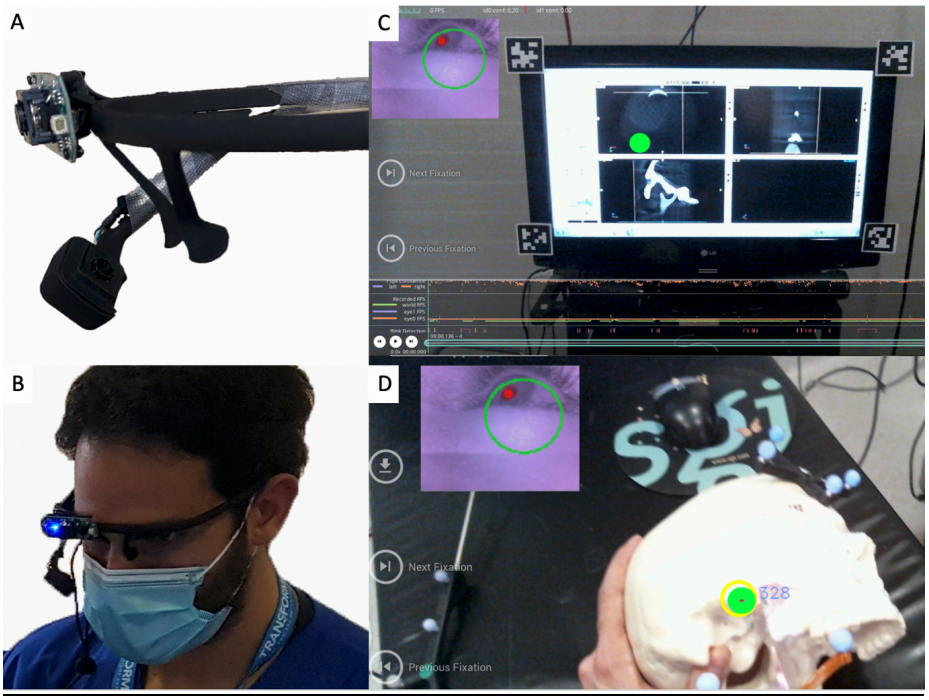


**Figure 5**. Gaze tracking system. **A**. Gaze tracking system with the two cameras which allow it to visualize the pupils and also, the participants' view. **B**. The device placed on one of the participants. **C-D**. The 'world camera' showing the participants' view, which could be either on the screen (C) or on the surgical field (D). The green dot indicates the exact position of the gaze. A small picture-in-picture screen (upper left) shows the position of the pupil.

### *Simulations*

Five head and neck fellowship trained surgeons with 3 to 5 years of experience in oncologic ablations from the Department of Otolaryngology–Head and Neck Surgery of the University Health Network participated in the simulations.

Surgeons were instructed to position the osteotome between the delineated areas of the different osteotomy sites in a sequential order (Pa-FMJ-LIOR-Zy-PMJ) and to provide a 1cm margin from the tumor along the plane trajectory. Instead of cutting the skulls, virtual cuts were performed in order to allow the reutilization of the models. This involved recording the osteotome position and orientation in the navigation software after the surgeon placed the osteotome in a certain direction and provided confirmation of obtaining the proposed cut. The analysis was performed on the virtual cutting trajectory after all the simulations were completed.

Four procedures were performed: 1) Unguided using axial, sagittal, coronal images, 2) AR-guided, 3) IN-guided, and 4) AR-IN-guided. This last group was possible as both systems are contained in the same platform software and can be used simultaneously. Analysis of cutting planes was performed using MATLAB software. An area of 4 cm x 2 cm (1 cm on both sides with respect to the longitudinal axis) along the longitudinal axis of the cut was isolated from each plane. The minimal distance with respect to the tumor surface was calculated for each point making up the isolated area and reproduced as a distribution of distances shown as a 4 x 2 $cm^2$ color scaled image. Distance from the tumor surface was classified as “intratumoral” when ≤ 0 mm, “close” when > 0mm and ≤ 5 mm, “adequate” when > 5 mm and ≤ 15mm, and “excessive”

when > 15 mm. The percentages of points at intratumoral, close, adequate, and excessive distances were calculated for each simulation plane.

The gaze-tracking system was calibrated to each participant, and it was used in all the simulations. The eye tracking data was analyzed to identify each time point the participant switched their gaze between the navigation monitor and the surgical field. The metric reported is the % of total study time spent looking at the navigation monitor.

Finally, a NASA Task Load Index (NASA-TLX) questionnaire which measures the workload of a task was completed by the participants to evaluate the different approaches.[18] This questionnaire is widely used and validated, and rates the perceived workload to assess a task, system or other aspects of performance.[19–21] It has been employed to assess the workload of new technologies during surgical procedures.[22] The total workload is divided into six subjective subscales, which assess mental, physical and temporal demand, performance, effort and frustration. Scores range between very low to very high.

### *Statistical analysis*

Statistical analysis was run through XLSTAT® (Addinsoft®, New York). Simulations were grouped in four categories: unguided, AR, IN and AR+IN. Rates of intratumoral virtual cuts was the main outcome and was assessed with the Fisher exact test. Multivariable analysis adjusting for surgeon and tumor was performed through logistic regression analysis. The groups were also compared in terms of percentage of intratumoral, close, adequate, and excessive distances from the tumor, and duration of the simulations through the bilateral Kruskal-Wallis test and Steel-Dwass-Critchlow-Fligner post-hoc test. The Kruskal-Wallis test was also employed to analyze the gaze-tracking outcomes and the NASA-TLX scores. Level of significance was set at 0.05 for all statistical tests.

## Results

### *Intratumoral Cuts*

A total of 335 cuts were simulated. Intratumoral cuts were observed in 20.7%, 9.4%, 1.2% and 0% of the unguided, AR, IN and AR+IN simulations respectively ($p<0.0001$). Univariate analysis comparing different procedures with AR showed that this technology improved margins with respect to unguided simulations. The advanced IN approach reduced the intratumoral cut rates compared with AR, and the combination of AR and IN did not significantly decrease the intratumoral cut rate compared with IN alone ($p=0.51$). These differences were also seen in a multivariate model adjusted for tumor and surgeon.

### *Distribution of points forming simulation planes*

The percentage of points forming the simulation planes were also registered. We observed that only the advanced IN system and the combined approach significantly decreased the percentage of intratumoral ($p<0.0001$) and close margin points ($p=0.008$) compared with the unguided resections (Table 1).

| Outcome | Unguided | AR | IN | AR+IN | p-value (Kruskal-Wallis test) |
|---|---|---|---|---|---|
| Intratumoral points (mean [IQR]) | 3.0% [0.0-0.0%]$^{A}$ | 1.4% [0.0-0.0%]$^{A}$ | 0.0% [0.0-0.0%]$^{B}$ | 0.0% [0.0-0.0%]$^{B}$ | ***<0.0001*** |
| Close points (mean [IQR]) | 11.7% [0.0-22.9%]$^{A}$ | 7.6% [0.0-13.7%]$^{A,B}$ | 3.7% [0.0-4.6%]$^{B}$ | 3.8% [0.0-3.0%]$^{B}$ | ***0.008*** |
| Excessive points (mean [IQR]) | 29.1% [3.5-42-2%]$^{A}$ | 28.9% [7.7-46.8%]$^{A}$ | 30.9% [5.9-48.5%]$^{A}$ | 29.2% [8.5-44.3%]$^{A}$ | 0.865 |
| Adequate points (mean [IQR]) | 56.2% [42.3-72.0%]$^{A}$ | 62.1% [39.6-83.2%]$^{A,B}$ | 65.4% [51.5-85.7%]$^{A,B}$ | 67.0% [49.6-87.7%]$^{B}$ | ***0.021*** |

**Table 1**. Distribution of points forming simulation planes. $^{A,B}$Groups significantly different based on Steel-Dwass-Critchlow-Filgner post-hoc test. AR, augmented reality; IN, intraoperative navigation; IQR, interquartile range.

### *Duration of simulations and gaze tracking results*

Mean total duration of the simulation was 215 seconds for unguided procedures and 117, 134 and 120 seconds in the AR, IN and AR+IN respectively. Participants required significantly more time to perform the unguided simulations compared to the AR and IN guided ones (p=0.004). There were no differences between the AR, IN and AR+IN guided procedures. The percentage of time looking at the screen during the procedures was 55.5% for the unguided approaches and 0%, 78.5% and 61.8% in AR, IN and AR + IN, respectively (p<0.001). Adding the AR technology to the combined approach significantly reduced the screen-time compared with the advanced IN procedures alone (Table 2).

| Outcome | Unguided | AR | IN | AR+IN | p-value (Kruskal Wallis test) |
|---|---|---|---|---|---|
| Total duration (mean [IQR]) | 215.8" [154.7-263.8"]$^{A}$ | 117.4" [83.4-145.0"]$^{B}$ | 134.7" [83.7"-170"]$^{B}$ | 120.9" [81.8-145.0"]$^{B}$ | ***0.0004*** |
| Screen time (mean [IQR]) | 55.5% [51.3-59.0%]$^{A}$ | 0.0% [0.0-0.0%]$^{B}$ | 78.5% [72.6-83.9%]$^{C}$ | 61.8% [53.4-70.0%]$^{A}$ | ***<0.0001*** |

**Table 2**: Total duration and screen time during the simulations. $^{A,B,C}$Groups significantly different based on Steel-Dwass-Critchlow-Filgner post-hoc test. AR, augmented reality; IN, intraoperative navigation; IQR, interquartile range.

### *NASA-TLX Scores*

We found no differences in scores between the unguided and the AR procedures, and both of them exhibited high degree of mental demand, effort and frustration. Combining AR to IN showed a significant improvement on the previous scores (Figure 6, Table 3).

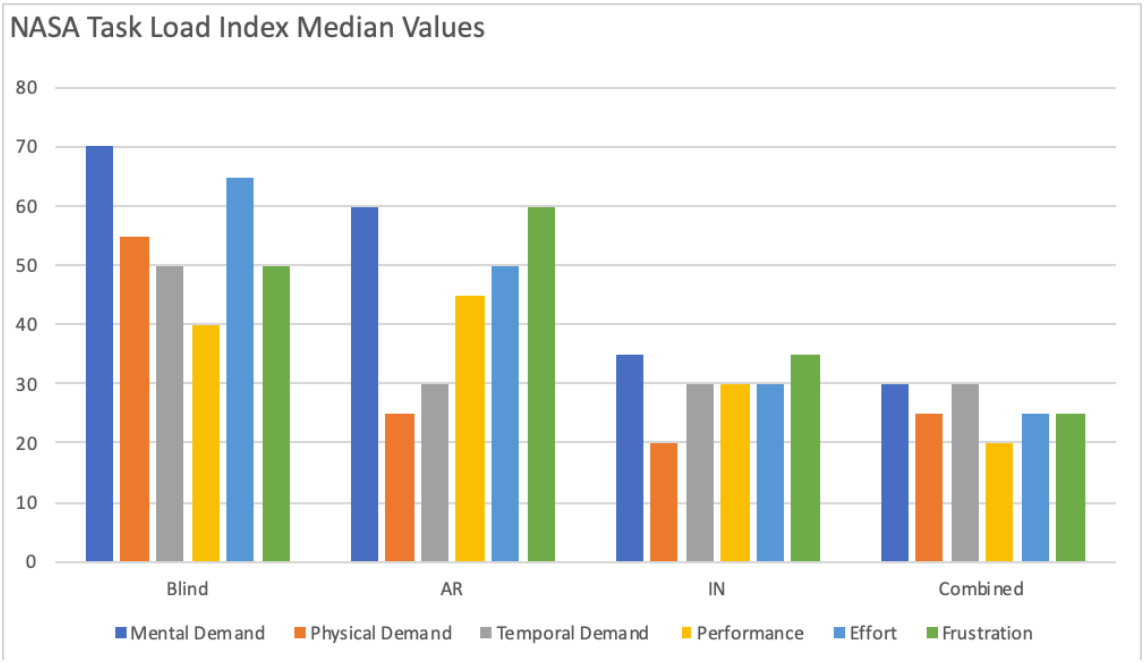


**Figure 6.** NASA-TLX median values.

| Outcome | Unguided | AR | IN | AR+IN | p-value (Kruskal-Wallis test) |
|---|---|---|---|---|---|
| Mental demand (median) | 70[A] | 60[A,B] | 35[B] | 30[B] | ***0.002*** |
| Physical demand (median) | 55[A] | 25[A] | 20[A] | 25[A] | 0.474 |
| Temporal demand (median) | 50[A] | 30[A] | 30[A] | 30[A] | 0.516 |
| Performance (median) | 40[A] | 45[A] | 30[A,B] | 20[B] | ***0.006*** |
| Effort (median) | 65[A] | 50[A] | 30[B] | 25[B] | ***0.002*** |
| Frustration (median) | 50[A] | 60[A] | 35[A,B] | 25[B] | ***0.010*** |

**Table 3**. NASA-TLX scores analysis. [A,B]Groups significantly differed based on Steel-Dwass-Critchlow-Filgner post-hoc test. AR, augmented reality; IN, intraoperative navigation; IQR, interquartile range.

## Discussion

In this study we observed that both advanced IN and AR technologies improved margin delineation compared with unguided procedures. Advanced IN was better for margin delineation than AR but required gaze toggling between the surgical field and the navigation monitor, whereas AR allowed the surgeon to focus only on the surgical field. The combination of both technologies partially improved the flaws on margins and staring outside the surgical field of the AR and IN techniques, respectively. The integration of AR and IN also improved Mental Demand, Performance, Effort and Frustration domains in the NASA-TLX questionnaires.

Margin control is among the most important prognostic factors and the only surgeon-controlled variable in head and neck cancer and efforts have been centered around obtaining clear margins after tumor resections. Nevertheless, positive surgical margins represent a major issue, even in the hand of experienced surgeons. In a report from the largest tertiary referral head and neck cancer center in the Netherlands, 39% out of 69 resections of advanced maxillary tumours (>T3) were incomplete, being posterior and superior margins the most commonly involved.[23] In a bi-institutional study from the Cleveland Clinic and the UC San

Francisco,[24] 24% out of 75 post-maxillectomy patients had positive margins in definitive pathology. Positive margins were associated with a two-fold increase of risk of death, and in multivariate analysis after controlling for age, nodal stage and surgical treatment, margins were independently associated with survival.[25] Moreover, it has been reported that intraoperative frozen sections (which are probably the only intraoperative resource to evaluate adequacy of the resection) have only 40% sensitivity in open sinonasal approaches.[26]

Currently, IN is employed in many centers in endoscopic sinonasal procedures.[27–29] By point-tracking an instrument and locating it on two-dimensions in tri-planar views, IN has shown an increase in accuracy and a reduction in operative time, impacting favorably in surgical outcomes and complications. Utilization of IN in open procedures to resect malignant tumors has been less reported, but promising results were obtained in margin status in small cohorts.[3,30,31] Our group has recently published a preclinical experience utilizing the same advanced IN system used in the present study, to assist in open sinonasal approaches.[4] The main novelty is that our advanced IN system allows surgeons not only to track the desired instrument, but also to visualize the entire cutting trajectory of a tracked cutting tool in 3D. In our previous experience using this technology, eight head and neck surgeons performed 381 simulated osteotomies for the resection of 7 tumor models. The use of 3D navigation for margin delineation significantly improved control of margins: unguided cuts had 18.1% intratumoral cuts compared to 0% intratumoral cuts with 3D navigation ($p<0.0001$). Furthermore, a clinical study using this advanced IN system for mandibulectomies demonstrated a <1.5mm accuracy between the planned cuts and the actual bone resection in the post-resection imaging.[15] One of the main criticisms to the system by the surgeons in this report was the multitasking challenge between the surgical field and the IN monitor, which can ultimately impact not only in efficiency but also on patient safety as the surgeon has to look away from the surgical field.

AR enhances the surgeons' vision rather than replacing it: CT, PET-CT or MRI scans can be visualized in 3D and in real time, granting 'X-ray vision' to the physician.[32,33] It has recently gained interest by computer assisted surgery researchers as it integrates the imaging information onto the surgical field. This has the potential to overcome the main drawback of the IN technology, which stems from the frequent switching of focus from the navigation screens to the surgical field and the translation of 2D imaging data to a 3D anatomical structure.[33] Despite there are reports of for AR application in the field of Otolaryngology-Head and Neck Surgery, the majority describe the use of AR using wearable computers (Microsoft HoloLens®, Microsoft Corporation, Redmond) and other head-mounted displays (HMD), which might be cumbersome especially in long procedures, and preclude the use of loupes/headlights. There are literature reports about HMD limitations including heaviness of the devices, breeches in patient privacy/information, battery life, potential lag time secondary to preoperative image processing, and the potential of signal interferences of wireless internet or Bluetooth connections that may cause intermittent data transmission of image.[34] Moreover, most reports of HMD rely solely on the operator visual alignment between the projected images and the anatomical area of interest[35] without any co-registration steps between the projecting surface and the AR system, which can lead to errors. Lastly, there are descriptions of the use of AR in the operating room but they are merely descriptive and not aimed to improve a surgical task,[36] or for educational purposes only.[37]

Our study reports several innovations. Tracking the AR projector as well as the projection surface with reflecting markers allowed us to be able to reposition the skull models and the projector without losing accuracy,[17,38] and this is something which was not described previously in head and neck surgery. This is paramount in computer assisted surgery as it allows precise projection even when movement occurs, as in real-time situations in the operating room. Another key aspect of our approach is the use of an external projector, which avoids the need for heavy wearable headsets. As a clarification, the headsets used in our study were for gaze-tracking only. The sinonasal/skull base region rigidity represents an excellent indication for AR as the deformation of tissue is minimal and co-registration is facilitated. Deformation has to be taken into consideration during soft-tissue resections as it is not possible to adjust the projections during AR.[7,39] By tracking the gaze of the participants, we were able to quantitatively measure the percentage of time that the surgeons had to look away from the surgical field. As our results suggest, there is significant improvement when AR is employed alone or in combination with IN, addressing the main disadvantages of IN utility. Our AR system shares the same software platform as the advanced IN system, and both approaches can be used at concurrently, allowing to evaluate the combination of both. Finally, there is a lack of user evaluation analysis with AR, so we utilized a validated questionnaire to investigate the differences between approaches.

Despite being significantly superior to unguided simulations in terms of intratumoral cut rates, there is room for improvement of our AR system. The advanced IN technology performed better than the AR in terms of intratumoral cut rates, as well as intratumoral and close distribution of points forming the simulation planes. This might be explained by the challenge in finding the correct angle between the projector and the projecting surface. We observed that if the angle differed greatly from 90 degrees, the image can be distorted and therefore lead to inaccuracies in surgical guidance to the operator. For example, when performing the PMJ cuts, by turning the skull 180 degrees, there were cases that the alignment was lost which might have impacted on the positive margin cuts. Another important limitation is that the sense of depth can be lost in the projections and the image can be interpreted in 2D on the surface rather than in 3D, especially with changes in ambient light. One last limitation of image projection is the parallax issue.[40] This phenomenon occurs when there is a 3D space non-alignment between the viewer and the projection perspectives. Our system minimizes this issue by adjusting the perspective of the pico-projector close to the surgeon's sight. In addition, the AR system is fully integrated into our intraoperative navigation system with real-time tracking technology, therefore the relocation/movement/displacement of the projector will not affect projection accuracy, with no need of further re-calibration and registration procedure. These limitations were also reflected on the NASA-TLX scores, where mental demand, effort and frustration rates for AR were higher than for IN, and similar to those of unguided approaches. Participants commented on the fact that when the adequate angle of projection was lost, they had difficulties interpreting the information from the AR system, which negatively impacted in the aforementioned domains of the NASA-TLX questionnaire. A plausible way of improving these flaws, and in consequence improving the margin delineation, is to project the cutting trajectory using AR. Similar to the advanced IN capabilities, the AR could further incorporate the intended cut trajectories on the surgical field, in addition to its projection of the tumor for localization. We also acknowledge the limitations of using

preclinical models which may not perfectly replicate the conditions of the operating room. Lastly, another limitation is the non-randomization of the simulated cuts. This was done in order to prevent that participants retained memory of the guided views if seen prior to the unguided cuts. Still, the fact that the sequence unguided-AR-IN-AR+IN was followed by all surgeons, could have resulted in some degree of learning effect by the participants towards the end of the tasks.

**Conclusions**

We reported the use of AR for open sinonasal approaches, and improved margin delineation compared with unguided techniques. The advanced IN performed better in terms of margin delineation, but the AR improved the gaze-toggling drawback of IN. Further research within our group is currently underway before translating our experience to the clinical practice.

**References**


1. Deganello A, Ferrari M, Paderno A, et al. Endoscopic-assisted maxillectomy: Operative technique and control of surgical margins. *Oral Oncol*. 2019;93:29-38. doi:10.1016/j.oraloncology.2019.04.002
2. Nishio N, Fujimoto Y, Fujii M, et al. Craniofacial Resection for T4 Maxillary Sinus Carcinoma. *Otolaryngol Neck Surg*. 2015;153(2):231-238. doi:10.1177/0194599815586770
3. Catanzaro S, Copelli C, Manfuso A, et al. Intraoperative navigation in complex head and neck resections: indications and limits. *Int J Comput Assist Radiol Surg*. 2017;12(5):881-887. doi:10.1007/s11548-016-1486-0
4. Ferrari M, Daly MJ, Douglas CM, et al. Navigation-guided osteotomies improve margin delineation in tumors involving the sinonasal area: A preclinical study. *Oral Oncol*. 2019;99:104463. doi:10.1016/j.oraloncology.2019.104463
5. Moawad GN, Elkhalil J, Klebanoff JS, Rahman S, Habib N, Alkatout I. Augmented Realities, Artificial Intelligence, and Machine Learning: Clinical Implications and How Technology Is Shaping the Future of Medicine. *J Clin Med*. 2020;9(12):3811. doi:10.3390/jcm9123811
6. Khanwalkar AR, Welch KC. Updates in techniques for improved visualization in sinus surgery. *Curr Opin Otolaryngol Head Neck Surg*. 2021;29(1):9-20. doi:10.1097/MOO.0000000000000693
7. Liu WP, Richmon JD, Sorger JM, Azizian M, Taylor RH. Augmented reality and cone beam CT guidance for transoral robotic surgery. *J Robot Surg*. 2015;9(3):223-233. doi:10.1007/s11701-015-0520-5
8. Creighton FX, Unberath M, Song T, Zhao Z, Armand M, Carey J. Early Feasibility Studies of Augmented Reality Navigation for Lateral Skull Base Surgery. *Otol Neurotol*. 2020;41(7):883-888. doi:10.1097/MAO.0000000000002724
9. King E, Daly MJ, Chan H, et al. Intraoperative cone-beam CT for head and neck surgery: Feasibility of clinical implementation using a prototype mobile C-arm. *Head Neck*. 2013;35(7):959-967. doi:10.1002/hed.23060
10. Jermyn M, Ghadyani H, Mastanduno MA, et al. Fast segmentation and high-quality three-dimensional volume mesh creation from medical images for diffuse optical tomography. *J Biomed Opt*. 2013;18(8):086007. doi:10.1117/1.JBO.18.8.086007
11. Daly MJ, Chan H, Nithiananthan S, et al. Clinical implementation of intraoperative cone-beam CT in head and neck surgery. In: Wong KH, Holmes III DR, eds. ; 2011:796426. doi:10.1117/12.878976
12. Dixon BJ, Chan H, Daly MJ, et al. Three-dimensional virtual navigation versus conventional image guidance: A randomized controlled trial. *Laryngoscope*. 2016;126(7):1510-1515. doi:10.1002/lary.25882
13. Sternheim A, Daly M, Qiu J, et al. Navigated pelvic osteotomy and tumor resection: a study assessing the accuracy and reproducibility of resection planes in Sawbones and cadavers. *J Bone Joint Surg Am*. 2015;97(1):40-46. doi:10.2106/JBJS.N.00276
14. Lee CY, Chan H, Ujiie H, et al. Novel Thoracoscopic Navigation System With Augmented Real-Time Image Guidance for Chest Wall Tumors. *Ann Thorac Surg*. 2018;106(5):1468-1475. doi:10.1016/j.athoracsur.2018.06.062
15. Hasan W, Daly MJ, Chan HHL, Qiu J, Irish JC. Intraoperative cone-beam CT-guided osteotomy navigation in mandible and maxilla surgery. *Laryngoscope*. 2020;130(5):1166-1172. doi:10.1002/lary.28082
16. Daly MJ, Siewerdsen JH, Moseley DJ, Jaffray DA, Irish JC. Intraoperative cone-beam CT for guidance of head and neck surgery: Assessment of dose and image quality using a C-arm prototype. *Med Phys*. 2006;33(10):3767-3780. doi:10.1118/1.2349687
17. Chan HHL, Haerle SK, Daly MJ, et al. An integrated augmented reality surgical navigation platform using multi-modality imaging for guidance. Máthé D, ed. *PLoS One*. 2021;16(4):e0250558. doi:10.1371/journal.pone.0250558
18. Hancock, Peter A.; Meshkati N. Development of NASA-TLX (Task Load Index): Results of Empirical and Theoretical Research. *Adv Psychol*.:139–183. doi:10.1016/S0166-4115(08)62386-9

19. Rainieri G, Fraboni F, Russo G, et al. Visual Scanning Techniques and Mental Workload of Helicopter Pilots During Simulated Flight. *Aerosp Med Hum Perform*. 2021;92(1):11-19. doi:10.3357/AMHP.5681.2021
20. Lebet RM, Hasbani NR, Sisko MT, et al. Nurses' Perceptions of Workload Burden in Pediatric Critical Care. *Am J Crit Care*. 2021;30(1):27-35. doi:10.4037/ajcc2021725
21. Devos H, Gustafson K, Ahmadnezhad P, et al. Psychometric Properties of NASA-TLX and Index of Cognitive Activity as Measures of Cognitive Workload in Older Adults. *Brain Sci*. 2020;10(12):994. doi:10.3390/brainsci10120994
22. Lowndes BR, Forsyth KL, Blocker RC, et al. NASA-TLX Assessment of Surgeon Workload Variation Across Specialties. *Ann Surg*. 2020;271(4):686-692. doi:10.1097/SLA.0000000000003058
23. Kreeft AM, Smeele LE, Rasch CRN, et al. Preoperative imaging and surgical margins in maxillectomy patients. *Head Neck*. 2012;34(11):1652-1656. doi:10.1002/hed.21987
24. Likhterov I, Fritz MA, El-Sayed IH, Rahul S, Rayess HM, Knott PD. Locoregional recurrence following maxillectomy: implications for microvascular reconstruction. *Laryngoscope*. 2017;127(11):2534-2538. doi:10.1002/lary.26620
25. Mücke T, Loeffelbein DJ, Hohlweg-Majert B, Kesting MR, Wolff KD, Hölzle F. Reconstruction of the maxilla and midface - Surgical management, outcome, and prognostic factors. *Oral Oncol*. 2009;45(12):1073-1078. doi:10.1016/j.oraloncology.2009.10.003
26. Murphy J, Isaiah A, Wolf JS, Lubek JE. The influence of intraoperative frozen section analysis in patients with total or extended maxillectomy. *Oral Surg Oral Med Oral Pathol Oral Radiol*. 2016;121(1):17-21. doi:10.1016/j.oooo.2015.07.014
27. Leong J-L, Batra PS, Citardi MJ. CT-MR Image Fusion for the Management of Skull Base Lesions. *Otolaryngol Neck Surg*. 2006;134(5):868-876. doi:10.1016/j.otohns.2005.11.015
28. Kacker A, Tabaee A, Anand V. Computer-Assisted Surgical Navigation in Revision Endoscopic Sinus Surgery. *Otolaryngol Clin North Am*. 2005;38(3):473-482. doi:10.1016/j.otc.2004.10.021
29. Vicaut E, Bertrand B, Betton J-L, et al. Use of a navigation system in endonasal surgery: Impact on surgical strategy and surgeon satisfaction. A prospective multicenter study. *Eur Ann Otorhinolaryngol Head Neck Dis*. 2019;136(6):461-464. doi:10.1016/j.anorl.2019.08.002
30. Tarsitano A, Ricotta F, Baldino G, et al. Navigation-guided resection of maxillary tumours: The accuracy of computer-assisted surgery in terms of control of resection margins – A feasibility study. *J Cranio-Maxillofacial Surg*. 2017;45(12):2109-2114. doi:10.1016/j.jcms.2017.09.023
31. Feichtinger M, Pau M, Zemann W, Aigner RM, Kärcher H. Intraoperative control of resection margins in advanced head and neck cancer using a 3D-navigation system based on PET/CT image fusion. *J Cranio-Maxillofacial Surg*. 2010;38(8):589-594. doi:10.1016/j.jcms.2010.02.004
32. Chen X, Xu L, Wang Y, et al. Development of a surgical navigation system based on augmented reality using an optical see-through head-mounted display. *J Biomed Inform*. 2015;55:124-131. doi:10.1016/j.jbi.2015.04.003
33. Gsaxner C, Pepe A, Li J, et al. Augmented Reality for Head and Neck Carcinoma Imaging: Description and Feasibility of an Instant Calibration, Markerless Approach. *Comput Methods Programs Biomed*. November 2020:105854. doi:10.1016/j.cmpb.2020.105854
34. Rahman R, Wood ME, Qian L, Price CL, Johnson AA, Osgood GM. Head-Mounted Display Use in Surgery: A Systematic Review. *Surg Innov*. 2020;27(1):88-100. doi:10.1177/1553350619871787
35. Battaglia S, Badiali G, Cercenelli L, et al. Combination of CAD/CAM and Augmented Reality in Free Fibula Bone Harvest. *Plast Reconstr Surg - Glob Open*. 2019;7(11):e2510. doi:10.1097/GOX.0000000000002510
36. Tepper OM, Rudy HL, Lefkowitz A, et al. Mixed reality with hololens: Where virtual reality meets augmented reality in the operating room. *Plast Reconstr Surg*. 2017;140(5):1066-1070. doi:10.1097/PRS.0000000000003802
37. Rose AS, Kim H, Fuchs H, Frahm JM. Development of augmented-reality applications in otolaryngology–head and neck surgery. *Laryngoscope*. 2019;129(S3):S1-S11. doi:10.1002/lary.28098
38. Meulstee JW, Nijsink J, Schreurs R, et al. Toward Holographic-Guided Surgery. *Surg Innov*. 2019;26(1):86-94. doi:10.1177/1553350618799552
39. Chan JYK, Holsinger FC, Liu S, Sorger JM, Azizian M, Tsang RKY. Augmented reality for image guidance in transoral robotic surgery. *J Robot Surg*. 2020;14(4):579-583. doi:10.1007/s11701-019-01030-0
40. Mamone V, Ferrari V, Condino S, Cutolo F. Projected Augmented Reality to Drive Osteotomy Surgery: Implementation and Comparison With Video See-Through Technology. *IEEE Access*. 2020;8:169024-169035. doi:10.1109/ACCESS.2020.3021940

# Optimization of the hybrid platform through projection of planned osteotomy lines: a preclinical study on phantom-based tumor models

*Chan et al., Oral Oncol 2022; doi: 10.1016/j.oraloncology.2022.105775*

## Introduction

Margin control is a fundamental in head and neck, and the only surgeon-controlled variable. In the maxilla, the complex anatomy and limited exposure represent a major challenge to obtain negative margins. Thus, positive margins have been reported as high as 72%-80% in advanced maxillary cancers.[1,2] Intraoperative navigation (IN) has been employed as a strategy to improve margins in maxillectomies.[3] This approach allows point tracking of instruments to intraoperatively orient surgeons using co-registration with patient imaging. The main drawbacks of IN are that it provides a two-dimensional view of a registered instrument/pointer tool without anticipating any cutting directions, and the information is displayed in monitors far from the table, which results in gaze-switching by the surgeon. Moreover, navigation is utilized intraoperatively, with no preoperative planning of the procedure. By merging navigation information within the surgical field, augmented reality (AR) enhances the surgeons' natural vision while addressing the gaze-toggling drawback of IN. This was confirmed by our group in an AR preclinical experience with advanced sinonasal tumours.[4] Our AR system used projected high-definition three-dimensional (3D) tumour reconstructions onto skull models to delineate tumoral extension during virtual resections. The projector-based AR eliminates the need for heavy wearable computers that may be cumbersome during a real surgical procedure,[5] while minimizing the surgeon's peri-spatial visual distortion that occurs with these "see-through" AR devices.[6] Moreover, we tracked the projector and the projection surface with optical navigation markers to enable repositioning of both components without losing accuracy.[7,8] Despite solving the gaze-toggling issue and with the AR being superior to control margins compared to the unguided approach, the intratumoral cutting rates rate we obtained using the AR technology was 9.4%. In addition, we found that the use of our AR approach was quite challenging for surgeons, which was reflected by workload questionnaires.

Our AR system is integrated with a surgical navigation platform that localizes the direction of the cutting instrument in 3D planes with respect to the tumor improving accuracy.[9,10] By exploiting this platform, we modified our AR approach; we implemented preoperative-planned osteotomies needed to perform a maxillectomy using the surgical navigation platform, and intraoperatively projected those osteotomies on the surgical field using AR. Our objective was to specifically to optimize negative margin rates and reduce the workload of the technology, while retaining the benefits of concentrating the surgeon's view in the operating field using projected navigation information.

## Materials and methods

### *Tumor models*

Three Sawbones® skulls and mouldable material mixed with acrylic glue were employed to build 6 locally advanced maxillary tumor models with orbital cavity, infratemporal fossa and/or skull base invasion. To prevent direct external exposure of tumours, skull surfaces were covered. We delineated four to five

different osteotomy regions to complete virtual resections: palate (Pa), fronto-maxillary junction (FMJ), lateroinferior orbital rim (LIOR), zygomatic arch (Zy) and pterygomaxillary junction (PMJ).

***Image acquisition and tumor contouring***

Cone-beam computed tomography (CBCT) scans acquired 3D images of the skull models.[11] Tumors showed higher x-ray attenuation than the artificial bone and contouring was performed semi-automatically.[12] A global threshold was applied to provide a quick, coarse segmentation, and then manual refinement was used to smooth the segmentation.

***Integrated augmented reality - surgical navigation platform***

Our AR system consists of a portable high-definition projector (PicoPro, Celluon Inc, Federal Way, WA), a stereoscopic infrared camera (Polaris Spectra, NDI, Waterloo, Ontario, Canada), a USB 2.0 M pixel camera (ICAN Webcam 2MP, China), and a laptop (M4500, Precision laptop, Dell, Round Rock, Texas). A custom-made 3D printed case was fabricated to anchor a 4-sphere navigation reference tool and contain the other elements of the AR system. The AR system was registered into a single coordinate system by pairing correspondent landmarks using fiducial markers identifiable in both the images and projection surface. The more complex technicalities of this system were previously described. The AR is integrated and projects information of a surgical navigation platform provided by an in-house software, the "GTx-Eyes". This software has been validated in pre-clinical and clinical studies in head and neck[9,13,14] and orthopaedic oncology.[15-17] Tumor and margin segmentations were superimposed on tri-planar views and also shown as 3D surface renderings. The same stereoscopic camera used in the AR system was used for tracking the surgical tool. Image-to-tracker registration was obtained by paired-point matching of pre-drilled divots in the skull by means of a tracked pointer. A 4-sphere reference tool was drilled to the skull. A fiducial registration error of $\leq 1$ mm was deemed acceptable. A 3-sphere reference was attached to an osteotome and calibrated using a custom stainless-steel jig. This advanced surgical navigation system allows visualization of the entire trajectory of the cutting instrument with respect to the tumor in 3D views.

Before the virtual resections, an "ideal" resection plan was predetermined using the navigation software aiming to: i) have no positive margins ($\leq$0 mm); ii) minimize close (<5 mm) and excessive (>15mm) margins; and iii) maximize adequate (5–15 mm) margins. After contouring the 3D tumours, a semi-transparent wireframe was generated 5 mm from the outer surface using MATLAB software (MathWorks, Mass.) to help visualize intended surgical margins during cut planning. Here, we focused on planning and guiding only the "straight cut" sections of tumor resection, as would be performed by a planar/straight cutting tool (osteotome/saw). As such, it is important to note that the "ideal" planes will necessarily contain regions of excessive distance as the tool straight shape does not perfectly match the irregular shape of the tumour. Based on the same concept of straightness of the cutting instrument and irregularity of the tumour surface, it is also not possible corresponding to the "ideal" resection plans, were projected onto the skulls using the AR system in order to guide the surgeons. Additional numerical cutting parameters, specifically distance to the osteotomy

line and pitch and roll angles of the osteotome were projected onto the surgical field along with the 3D reconstructions of the tumours to indicate the surgeon the virtual osteotomy direction with respect to the predetermined resection plan (Figure 1). Information on these parameters was provided with a color-coded scale, green indicating adequate direction.

As mentioned, the osteotome was tracked throughout the procedures to guide its positioning relative to the planned resection (Figure 2). The optical sensor mounted to the projector case facilitated real-time tracking of the AR device, to allow the projector and/or skull to be repositioned during tasks without compromising projection accuracy, with a registration error <1 mm.

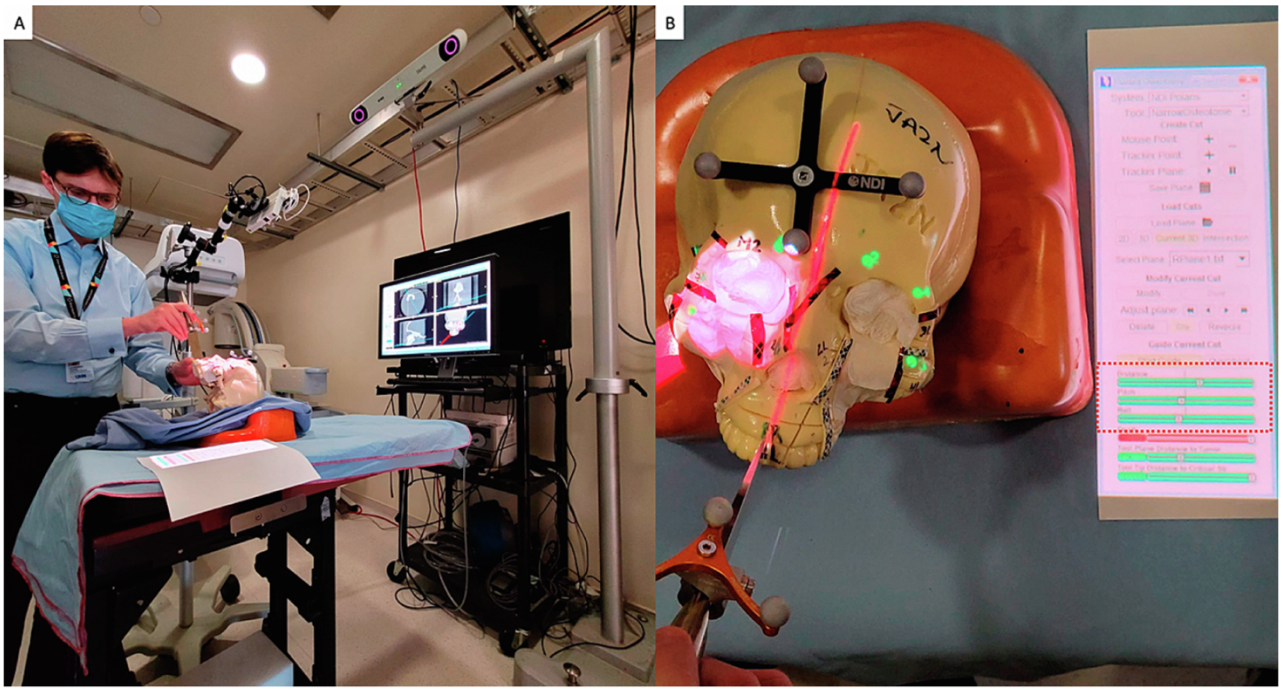


**Figure 1**. AR system experimental setup. **A**. The portable high-definition projector displaying images onto the surgical field. A stereoscopic infrared camera tracking the projector, the osteotome and the skull, all of which are attached with sphere navigation tools. The tracked information is integrated on the surgical navigation software, which is displayed in the monitor only for demonstration purposes. The surgeon maintains his view on the surgical field throughout the entire procedure. **B**. Surgeons' view of the AR system, with the osteotomy line projected over the skull along with the right maxillary sinus tumour and the cutting trajectory information showing distance, pitch, and roll parameters (red dotted rectangle).

### *Simulations*

Five fellowship-trained surgeons with 3 to 5 years of experience in oncologic ablations participated in the maxillectomy simulations. Instead of cutting the skulls, virtual cuts were performed to allow reusing the models. Surgeons were instructed to position the osteotome between the delineated areas of the different osteotomy sites in a sequential order (Pa-FMJ-LIOR-Zy-PMJ) to complete a maxillectomy. Two procedures were performed: i) unguided virtual resections using axial, sagittal, coronal images of CT images displayed on a screen; and ii) AR-guided virtual resections. In the AR simulations, pre-planned osteotomy lines and cutting parameters were projected over the skulls and surgical field to guide the participants. Once the participant placed the osteotome and provided confirmation of obtaining the proposed cut, the virtual cutting trajectory was recorded and analyzed. The order of the simulations was randomized to prevent the "learning effect" from

participants. Analysis of cutting planes was performed using MATLAB software. An area of 4 cm × 2 cm (1 cm on both sides with respect to the longitudinal axis) along the longitudinal axis of the cut was isolated from each plane. The minimal distance with respect to the tumor surface was calculated for each point making up the isolated area and reproduced as a distribution of distances shown as a 4 cm × 2 cm color-scaled image. Distance from the tumor surface was classified as "intratumoral" (≤0 mm), "close" (>0mm and ≤ 5 mm), "adequate" (>5 mm and ≤ 15 mm), and "excessive" (>15 mm). The percentages of points at intratumoral, close, adequate, and excessive distances were calculated for each simulation plane. Distance, pitch and roll angles were also computed.

The NASA Task Load Index (NASA-TLX) questionnaire was completed by the participants after the simulations. This questionnaire assesses the workload of a task in six scales; mental, physical and temporal demand, performance, effort and frustration.[18,19]

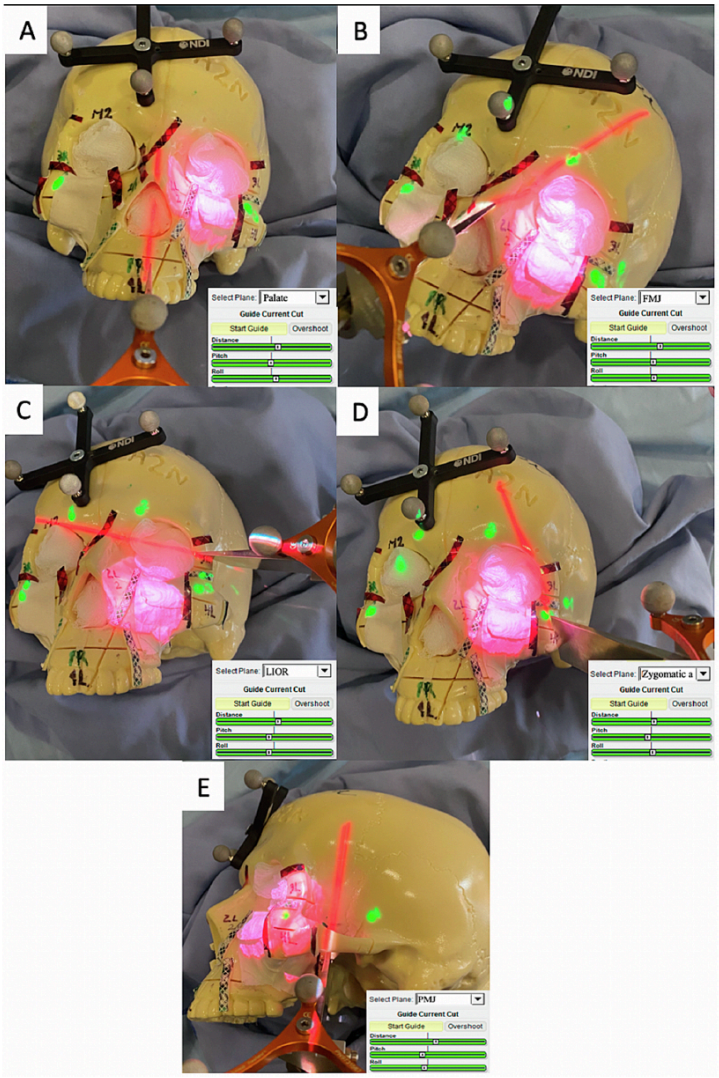


**Figure 2**. Example of the different AR-projected osteotomies required to resect a left-sided maxillary tumour in sequence, with zoom-ins into the distance pitch and roll cutting parameters projected onto the surgical field; **A**. Palate osteotomy. **B**. Fronto-maxillary osteotomy. **C**. Lateral orbital osteotomy. **D**. Zygomatic arch osteotomy. **E**. Pterygomaxillary osteotomy.

***Statistical analysis***

Statistical analysis was run through XLSTAT® (Addinsoft®, New York). Simulations were grouped in two categories: unguided and AR. Both categories were compared in terms of intratumoral virtual cuts, which was the main outcome, and was assessed with the Fisher exact test. The groups were also compared in terms of percentage of intratumoral, close, adequate, and excessive distances from the tumor, through the bilateral Kruskal-Wallis test and Steel-Dwass-Critchlow-Fligner post-hoc test. Multivariable analysis adjusting for surgeon was performed through logistic regression analysis. A comparison between the "ideal" cutting plan and the AR-guided virtual osteotomies was also performed by means of a two-way random-effects interclass correlation index (ICC) model (targets = planned osteotomies, raters = surgeons). This was done in order to establish the similarities between the predetermined cut plan and the actual result with AR, with values closer to 1 indicating more similitude. The NASA-TLX scores were analyzed with the Kruskal-Wallis test. Student t-test was also used. Level of significance was set at 0.05 for all statistical tests.

**Results**

***Comparison between AR and unguided osteotomies***

A total of 115 virtual osteotomies were analyzed. Intra-tumoral and "close" margins were lower for the AR-assisted osteotomies compared to the unguided ones (0.0% vs 1.9%, $p < 0.0001$; and 0.8% vs 7.9%, $p < 0.0001$ respectively). Furthermore, the proportion of osteotomies located within "adequate" margins was higher in the AR-assisted than in the unguided, (25.3% vs 18.6%, $p = 0.018$). Regarding the "excessive" margin, no differences were noticed between AR-assisted and unguided osteotomies (73.7% vs 70.9%, p = NS) (Table 1). AR simulations showed better performance than the unguided ones in replicating the preoperative osteotomy planning with regards to distance, pitch, and roll ($0.73 \pm 0.05$ mm vs $6.44 \pm 0.42$ mm, $p < 0.0001$; $1.16 \pm 0.07°$ vs $13.04 \pm 1.05°$, $p < 0.0001$; and $0.98 \pm 0.07°$ vs $11.7 \pm 1.14°$, $p < 0.0001$ respectively) (Figure 3). The AR gain to prevent intratumoral virtual cuts did not vary significantly when stratified by surgeon ($p = 0.400$). The time required to complete the tasks was similar between the AR and the unguided simulations ($76.3 \pm 4.1$ s vs $81.6 \pm 5.8$ s; $p > 0.05$).

***Comparison of subjective task load between AR and unguided osteotomies***

NASA-TLX scores (mean ± SD) were higher for unguided simulations compared with AR-assisted ones for the domains of mental demand ($74.0 \pm 11.3$ vs $32.6 \pm 12.8$; $p = 0.009$), performance ($50.6 \pm 20.0$ vs $19.4 \pm 7.3$; $p = 0.0088$), effort ($69.0 \pm 8.7$ vs $33.0 \pm 11.7$; $p = 0.009$), and frustration ($57.2 \pm 19.5$ vs $23.6 \pm 11.8$; $p = 0.009$). No differences were observed between simulations regarding physical and temporal demand domains (Table 1).

***Comparison between "ideal" pre-planned and AR osteotomies***

No intratumoral virtual osteotomies were observed when using AR. The mean area of osteotomies lying within "close" margins did not differ for AR virtual cuts, compared to the pre-determined ones (0.8% vs 0.0%, $p = 0.06$). The average ICC for the area of "adequate" margins between the pre-determined and AR

osteotomies was 0.893 (95% CI: 0.804–0.949). Similarly, the average ICC for the area of "excessive" margins was 0.885 (95% CI: 0.787–0.946) (Table 1).

| **CUTTING ACCURACY** | | | | | | |
|---|---|---|---|---|---|---|
| **Margin delineation distribution** | **AR** | **Unguided** | **p-value*** | **Planning** | **AR** | **p-value*** |
| **Intratumoral cut (%)** | 0.0 | 1.9 | **<0.0001** | 0.0 | 0.0 | 1.000 |
| **Close margins (%)** | 0.8 | 7.9 | **<0.0001** | 0.0 | 0.8 | 0.060 |
| **Adequate margins (%)** | 25.3 | 18.6 | **0.018** | 41.8 | 25.3 | **0.001** |
| **Excessive margins (%)** | 73.7 | 70.9 | 0.859 | 58.1 | 73.7 | **0.003** |
| **NASA TASK LOAD INDEX SCORES** | | | | | | |
| **Mental demand Mean (SD)** | 32.6 (12.9) | 74 (11.3) | **0.0090** | – | 32.6 (12.9) | – |
| **Physical demand Mean (SD)** | 23.2 (12.9) | 44.2 (24.8) | 0.1732 | – | 23.2 (12.9) | – |
| **Temporal demand Mean (SD)** | 25 (8.3) | 47 (25.4) | 0.1745 | – | 25 (8.3) | – |
| **Performance Mean (SD)** | 19.4 (7.3) | 50.6 (20.0) | **0.0088** | – | 19.4 (7.3) | – |
| **Effort Mean (SD)** | 33 (11.7) | 69 (8.7) | **0.0088** | – | 33 (11.7) | – |
| **Frustration Mean (SD)** | 23.6 (11.8) | 57.2 (19.5) | **0.0090** | – | 23.6 (11.8) | – |

**Table 1**. Comparison between AR-guided and unguided simulations in terms of margin delineation accuracy and task load. Comparison between planned and simulated cutting in terms of margin delineation accuracy. *Kruskal-Wallis test

**Discussion**

By adjusting our AR method, we avoided intratumoral margins during simulated maxillectomies. The AR had significantly lower positive and close margins compared with the unguided simulations. We found no difference in close margins between the ideal pre-determined osteotomies and the AR approach and almost equal cutting trajectories in adequate and excessive margins, with ICC scores approaching 1. Finally, the NASA-TLX scores suggest that the technology was intuitive and easily utilized by the surgeons, with improved scores in Mental Demand, Performance, Effort and Frustration with respect with the unguided virtual resections. There was no difference in intratumoral cuts when stratified by surgeon which suggests that the system use was operator-independent. Importantly, the information of the cutting trajectory was projected within the surgical field, maintaining one of the most significant advantages of the AR technology.

The maxillary region is ideal to capitalize on the benefits of computer-assisted surgery (CAS). The relatively immobile components of the midface facilitate co-registration of the images and the patient anatomy, as deformation of tissue is minimal. Moreover, contrary to other head and neck sites such as the oral cavity, the maxillary sinuses vital structures can be located in very close contact to the resection, and exposure can be limited. In many cases, surgeons perform "blind" cuts during maxillectomies, especially at the posterior margin, which can explain the high-rate of incomplete resections.[20,21] The ability of CAS/surgical navigation to co-register preoperative images with the intraoperative "on-the-table" patient anatomy to enhance surgical precision, adds a valuable tool to the surgeons' armamentarium. Nevertheless, the most widely used surgical navigation systems consist of point-tracking an instrument on two-dimensional tri-planar views of CT/MRI

images to provide the surgeon with better spatial orientation. In contrast, our navigation platform enables visualization of the entire cutting trajectory of a tracked planar tool (*e.g.*, osteotome, saw) oriented to a 3D reconstruction of the tumour. This real-time intraoperative feedback on 3D cutting trajectories, as opposed to point-based localization, facilitates more accurate resection in initial pre-clinical and clinical studies.[9,13,15,16]

AR has gained recent interest in the CAS research community, as enables integration of imaging information within the surgical field. One goal of this technology is to potentially solve the "switching focus problem" that occurs when the surgeon has to look away from the operative field to consult image data on a 2-dimensional screen away from the patient. Wearable commercial computers have been utilized for AR in head and neck surgery, especially for educational purposes.[22] Despite the novelty of the approach, there are inherent limitations of head mounted displays (HMD) including device weight, patient information breeches, battery life, potential lag time secondary to preoperative image processing, and signal interference with wireless internet/Bluetooth connections.[23] Also, there are perceptual limitations with HMD, that use the "see-through" AR principle, to support high-precision manual tasks, as they reduce the user performance due to focus errors and visual discomfort.[24,25] Thus, we believe that projector-based technology is a more plausible option, retaining the benefits of the AR without peri-spatial distortion of the surgeon.[6] Our group has very recently reported the use of AR in a pre-clinical study specifically for head and neck oncology.[4] The AR approach consisted of projecting 3D tumour reconstructions directly on the surgical field (*i.e.*, skull models) to guide surgeons during virtual resections.

That study had several innovations, including the projector-based AR approach described for head and neck surgical oncology and a quantitative assessment of visual attention using a gaze-tracking device. One of the novelties of our system is the tracking of the AR projector as well as the projection surface, which allowed us to reposition those components without losing accuracy, which is fundamental in CAS, and which also minimizes the parallax issue.[6] However, when the resection margins were compared to unguided resections we reported a suboptimal 9.4% intratumoral virtual resection rate. The explanations for this "high" rate were the loss of the sense of depth when projecting a 3D image onto a two-dimension surface, and the need of having a 90° angle between the projector and the surface to prevent image distortion. These issues were also reflected with poor NASA-TLX scores.

Projecting pre-planned osteotomy lines over the skulls, along with the cutting trajectory parameters (distance, pitch and roll) on the surgical field, greatly simplified and improved our previous approach by achieving negative margins and improving NASA-TLX workload scores. The workflow described in this study, which intraoperatively executes a preoperative plan designed by a navigation software has several advantages in the maxillary region. To begin with, pre-operative planning facilitates 3D visualization of the surgical cases, in which more experienced surgeons can provide their input about the surgical strategy. It can also anticipate and precisely outline areas that will inevitably have close/positive margins due to the need to spare vital structures. Radiation oncologists may benefit from information on the planned resection, to adjust adjuvant radiotherapy doses to certain areas at risk, possibly sparing unaffected sub-sites and reducing the total

radiation dosing. Benefits of virtual surgical planning (VSP), which comprise planning sessions, cutting-guides, 3D printed models and custom plate manufacturing, have been reported for maxillectomy defects, with promising facial projection and bony-union results.[26] Despite these guides being commercially available, they can only assist the surgeon in certain osteotomies, usually the palatal, fronto-maxillary junction and orbital osteotomies. The more posterior cuts, which are the ones made with less exposure and the ones that carry a higher positive margin rate,[20] are unguided and made blindly. Our AR approach enables guidance for all osteotomies, regardless of anatomical location, through the use of projected-navigation guides. Furthermore, since osteotomy lines are projected, soft tissues do not represent a limiting factor as in cases of placing 3D printed guides on bone. Pre-operative planning can also be used to predict the postoperative defect more accurately as well. We therefore envision the possibility of a "hybrid AR-printed approach" for maxillary resections, where the entire surgery is planned; AR technology used to guide the ablative portion of the procedure, while printed cutting guides are used to shape the bony free flap reconstruction, as surgical access and placing cutting guides are less of an issue in the donor sites used for reconstruction.

We are well aware that the obvious limitation of our study is the preclinical nature. The skull exposure differs greatly from a real maxillectomy scenario. Moreover, we did not consider vital structures during the pre-planning of the virtual osteotomies nor during the exercises, although this can be easily included in the planning. Finally, as stated in the methods section, no actual cuts were performed in the skulls, which would more accurately represented a surgical resection. This would have increased the validity of our study.

## Conclusions

Continued development of our projector-based AR method improved margin delineation and was more easily utilized by the surgeons, while retaining the benefits of the technology. We hope to soon be able to translate our AR experience to the operating room and consolidate our preclinical findings to improve outcomes.

## References


1. Ferrari M, Ioppi A, Schreiber A, Gualtieri T, Mattavelli D, Rampinelli V, et al. Malignant tumors of the maxillary sinus: prognostic impact of neurovascular invasion in a series of 138 patients. Oral Oncol 2020;106:104672. https://doi.org/10.1016/j.oraloncology.2020.104672.
2. Arosio AD, Turri-Zanoni M, Sileo G, Tirloni M, Volpi L, Lambertoni A, et al. Maxillary sinus floor infiltration: results from a series of 118 maxillary sinus cancers. The Laryngoscope 2022;132(1):26–35.
3. Catanzaro S, Copelli C, Manfuso A, Tewfik K, Pederneschi N, Cassano L, et al. Intraoperative navigation in complex head and neck resections: indications and limits. Int J Comput Assist Radiol Surg 2017;12(5):881–7. https://doi.org/10.1007/s11548-016-1486-0.
4. Sahovaler A, Chan HHL, Gualtieri T, Daly M, Ferrari M, Vannelli C, et al. Augmented reality and intraoperative navigation in sinonasal malignancies: a preclinical study. Front Oncol 2021;11. https://doi.org/10.3389/fonc.2021.723509.
5. Scherl C, Stratemeier J, Karle C, Rotter N, Hesser J, Huber L, et al. Augmented reality with HoloLens in parotid surgery: how to assess and to improve accuracy. Eur Arch Oto-Rhino-Laryngology 2021;278(7):2473–83. https://doi.org/10.1007/s00405-020-06351-7.
6. Mamone V, Ferrari V, Condino S, Cutolo F. Projected augmented reality to drive osteotomy surgery: implementation and comparison with video see-through technology. IEEE Access 2020;8:169024–35. https://doi.org/10.1109/ACCESS.2020.3021940.
7. Meulstee JW, Nijsink J, Schreurs R, Verhamme LM, Xi T, Delye HHK, et al. Toward holographic-guided surgery. Surg Innov 2019;26(1):86–94. https://doi.org/10.1177/1553350618799552.

8. Chan HHL, Haerle SK, Daly MJ, Zheng J, Philp L, Ferrari M, et al. An integrated augmented reality surgical navigation platform using multi-modality imaging for guidance. PLoS ONE 2021;16(4):e0250558. https://doi.org/10.1371/journal.pone.0250558.
9. Hasan W, Daly MJ, Chan HHL, Qiu J, Irish JC. Intraoperative cone-beam CT-guided osteotomy navigation in mandible and maxilla surgery. Laryngoscope 2020;130(5):1166–72. https://doi.org/10.1002/lary.28082.
10. Muhanna N, Douglas CM, Daly MJ, Chan HHL, Weersink R, Townson J, et al. Evaluating an image-guided operating room with cone beam CT for skull base surgery. J Neurol Surg Part B Skull Base 2021;82(S 03):e306–14. https://doi.org/10.1055/s-0040-1701211.
11. King E, Daly MJ, Chan H, Bachar G, Dixon BJ, Siewerdsen JH, et al. Intraoperative cone-beam CT for head and neck surgery: feasibility of clinical implementation using a prototype mobile C-arm. Head Neck 2013;35(7):959–67. https://doi.org/10.1002/hed.23060.
12. Jermyn M, Ghadyani H, Mastanduno MA, Turner W, Davis SC, Dehghani H, et al. Fast segmentation and high-quality three-dimensional volume mesh creation from medical images for diffuse optical tomography. J Biomed Opt 2013;18(8):086007. https://doi.org/10.1117/1.JBO.18.8.086007.
13. Ferrari M, Daly MJ, Douglas CM, Chan HHL, Qiu J, Deganello A, et al. Navigationguided osteotomies improve margin delineation in tumors involving the sinonasal area: a preclinical study. Oral Oncol 2019;99:104463. https://doi.org/10.1016/j.oraloncology.2019.104463.
14. Muhanna N, Douglas CM, Daly MJ, Chan HHL, Weersink R, Qiu J, et al. The image-guided operating room—utility and impact on surgeon's performance in the head and neck surgery. Head Neck 2019;41(9):3372–82. https://doi.org/10.1002/hed.25864.
15. Sternheim A, Rotman D, Nayak P, Arkhangorodsky M, Daly MJ, Irish JC, et al. Computer-assisted surgical planning of complex bone tumor resections improves negative margin outcomes in a sawbones model. Int J Comput Assist Radiol Surg 2021;16(4):695–701. https://doi.org/10.1007/s11548-021-02337-w.
16. Sternheim A, Daly M, Qiu J, Weersink R, Chan H, Jaffray D, et al. Navigated pelvic osteotomy and tumor resection. J Bone Jt Surg 2015;97(1):40–6.
17. Sternheim A, Kashigar A, Daly M, Chan H, Qiu J, Weersink R, et al. Cone-beam computed tomography-guided navigation in complex osteotomies improves accuracy at all competence levels: a study assessing accuracy and reproducibility of joint-sparing bone cuts. J Bone Joint Surg Am 2018;100(10):e67. https://doi.org/10.2106/JBJS.16.01304.
18. Rainieri G, Fraboni F, Russo G, Tul M, Pingitore A, Tessari A, et al. Visual scanning techniques and mental workload of helicopter pilots during simulated flight. Aerosp Med Hum Perform 2021;92(1):11–9. https://doi.org/10.3357/AMHP.5681.2021.
19. Devos H, Gustafson K, Ahmadnezhad P, Liao Ke, Mahnken JD, Brooks WM, et al. Psychometric properties of NASA-TLX and index of cognitive activity as measures of cognitive workload in older adults. Brain Sci 2020;10(12):994. https://doi.org/10.3390/brainsci10120994.
20. Kreeft AM, Smeele LE, Rasch CRN, Hauptmann M, Rietveld DHF, Leemans CR, et al. Preoperative imaging and surgical margins in maxillectomy patients. Head Neck 2012;34(11):1652–6. https://doi.org/10.1002/hed.21987.
21. Likhterov I, Fritz MA, El-Sayed IH, Rahul S, Rayess HM, Knott PD. Locoregional recurrence following maxillectomy: implications for microvascular reconstruction. Laryngoscope 2017;127(11):2534–8. https://doi.org/10.1002/lary.26620.
22. Wong K, Yee HM, Xavier BA, Grillone GA. Applications of augmented reality in otolaryngology: a systematic review. Otolaryngol - Head Neck Surg (United States) 2018;159(6):956–67. https://doi.org/10.1177/0194599818796476.
23. Rahman R, Wood ME, Qian L, Price CL, Johnson AA, Osgood GM. Head-mounted display use in surgery: a systematic review. Surg Innov 2020;27(1):88–100. https://doi.org/10.1177/1553350619871787.
24. Condino S, Carbone M, Piazza R, Ferrari M, Ferrari V. Perceptual limits of optical see-through visors for augmented reality guidance of manual tasks. IEEE Trans Biomed Eng 2020;67(2):411–9. https://doi.org/10.1109/TBME.2019.2914517.
25. Ferrari V, Carbone M, Condino S, Cutolo F. Are augmented reality headsets in surgery a dead end? Expert Rev Med Devices 2019;16(12):999–1001. https://doi.org/10.1080/17434440.2019.1693891.
26. Swendseid BP, Roden DF, Vimawala S, Richa T, Sweeny L, Goldman RA, et al. Virtual surgical planning in subscapular system free flap reconstruction of midface defects. Oral Oncol 2020;101:104508. https://doi.org/10.1016/j.oraloncology.2019.104508.

# Final considerations

The research activities completed in the context of this PhD course demonstrated that surgical navigation with 3-dimensional rendering confers a higher quality to oncologic ablations in the head and neck, irrespective of the open or endoscopic surgical technique. The benefits deriving from this implementation come with no relevant drawbacks from a logistical and practical standpoint, nor were major adverse events observed. Thus, implementation of this technology into the standard care is the logical proposed step forward. However, the genuine presence of a prognostic advantage needs longer and larger study to be formally addressed.

On the other hand, pico projector-based augmented reality showed no sufficient advantages to encourage translation into the clinical setting. Although observing a clear practical advantage deriving from the projection of osteotomy lines onto the surgical field, no substantial benefits were measured when comparing this technology with surgical navigation with 3-dimensional rendering. Yet recognizing a potential value of this technology from an educational standpoint, the performance displayed in the preclinical setting in terms of surgical margins optimization is not in favor of a clinical translation with this specific aim.

# Publications (November 2019-October 2022)

1. **Ferrari M**, Daly MJ, Douglas CM, Chan HHL, Qiu J, Deganello A, Taboni S, Thomas CM, Sahovaler A, Jethwa AR, Hasan W, Nicolai P, Gilbert RW, Irish JC. ***Navigation-guided osteotomies improve margin delineation in tumors involving the sinonasal area: A preclinical study***. Oral Oncol (epub ahead of print), 2019.
2. Serioli S, Doglietto F, Fiorindi A, Biroli A, Mattavelli D, Buffoli B, **Ferrari M**, Cornali C, Rodella L, Maroldi R, Gasparotti R, Nicolai P, Fontanella MM, Poliani PL. ***Pituitary Adenomas and Invasiveness from Anatomo-Surgical, Radiological, and Histological Perspectives: A Systematic Literature Review***. Cancers (Basel) 4;11(12), 2019.
3. Mattavelli D, **Ferrari M**, Rampinelli V, Schreiber A, Buffoli B, Deganello A, Rodella LF, Fontanella MM, Nicolai P, Doglietto F. ***Development and validation of a preclinical model for training and assessment of cerebrospinal fluid leak repair in endoscopic skull base surgery***. Int Forum Allergy Rhinol 10:89-96, 2020.
4. Agosti E, Saraceno G, Qiu J, Buffoli B, **Ferrari M**, Raffetti E, Belotti F, Ravanelli M, Mattavelli D, Schreiber A, Hirtler L, Rodella LF, Maroldi R, Nicolai P, Gentili F, Kucharczyk W, Fontanella MM, Doglietto F. ***Quantitative anatomical comparison of transnasal and transcranial approaches to the clivus***. Acta Neurochir (Wien) 162:649-660, 2020.
5. Saraceno G, Agosti E, Qiu J, Buffoli B, **Ferrari M**, Raffetti E, Belotti F, Ravanelli M, Mattavelli D, Schreiber A, Hirtler L, Rodella LF, Maroldi R, Nicolai P, Gentili F, Kucharczyk W, Fontanella MM, Doglietto F. ***Quantitative Anatomical Comparison of Anterior, Anterolateral and Lateral, Microsurgical and Endoscopic Approaches to the Middle Cranial Fossa***. World Neurosurg 134:e682-e730, 2020.
6. Belotti F, Tengattini F, Mattavelli D, **Ferrari M**, Fiorentino A, Agnelli S, Schreiber A, Nicolai P, Fontanella MM, Doglietto F. ***Transclival approaches for intradural pathologies: historical overview and present scenario***. Neurosurg Rev 44:279-287, 2020.
7. **Ferrari M**, Bossi P, Mattavelli D, Ardighieri L, Nicolai P. ***Management of sinonasal adenocarcinomas with anterior skull base extension***. J Neurooncol 150:405-417, 2020.
8. Zappa F, Mattavelli D, Madoglio A, Rampinelli V, **Ferrari M**, Tampalini F, Fontanella M, Nicolai P, Doglietto F; PEER Research Group. ***Hybrid Robotics for Endoscopic Skull Base Surgery: Preclinical Evaluation and Surgeon First Impression***. World Neurosurg 134:e572-e580, 2020.
9. **Ferrari M**, Schreiber A, Mattavelli D, Rampinelli V, Bertazzoni G, Tomasoni M, Gualtieri T, Nicolai P. ***How aggressive should resection of inverted papilloma be? Refinement of surgical planning based on the 25-year experience of a single tertiary center***. Int Forum Allergy Rhinol 10:619-628, 2020.
10. **Ferrari M**, Sahovaler A, Chan HHL, Nicolai P, Irish JC, Gilbert RW. ***Scapular tip-thoracodorsal artery perforator free flap for total/subtotal glossectomy defects: Case series and conformance study***. Oral Oncol (epub ahead of print), 2020.
11. **Ferrari M**, Ioppi A, Schreiber A, Gualtieri T, Mattavelli D, Rampinelli V, Taboni S, Tomasoni M, Bossi P, Deganello A, Nicolai P. ***Malignant tumors of the maxillary sinus: Prognostic impact of neurovascular invasion in a series of 138 patients***. Oral Oncol (epub ahead of print), 2020.
12. Accorona R, Colombo G, **Ferrari M**, Fazio E, Bolzoni-Villaret A. ***Inverted Supernumerary Intranasal Teeth as Unusual Indications of Endoscopic Surgery***. Iranian Journal of Otorhinolaryngology 32(3), 2020.
13. Lombardi D, **Ferrari M**, Paderno A, Taboni S, Rampinelli V, Barbara F, Schreiber A, Mattavelli D, Tomasoni M, Farina D, Ravanelli M, Maroldi R, Nicolai P. ***Selection of the surgical approach for lesions with parapharyngeal space involvement: A single-center experience on 153 cases***. Oral Oncol (epub ahead of print), 2020.
14. Mattavelli D, **Ferrari M**, Taboni S, Morello R, Paderno A, Rampinelli V, Del Bon F, Lombardi D, Grammatica A, Bossi P, Deganello A, Piazza C, Nicolai P. ***The 8th TNM classification for oral squamous cell carcinoma: What is gained, what is lost, and what is missing***. Oral Oncol (epub ahead of print), 2020.
15. **Ferrari M**, Paderno A, Giannini L, Cazzador D, Ciardiello C, Carretta G, Piazza C, Nicolai P. ***COVID-19 screening protocols for preoperative assessment of head and neck cancer patients candidate for elective surgery in the midst of the pandemic: A narrative review with comparison between two Italian institutions***. Oral Oncol (epub ahead of print), 2020.
16. Lombardi D, Tomasoni M, Paderno A, Mattavelli D, **Ferrari M**, Battocchio S, Missale F, Mazzola F, Peretti G, Mocellin D, Borsetto D, Fussey JM, Nankivell P, Skalidi N, Bussi M, Giordano L, Galli A, Arrigoni G, Raffetti E, Pracy P, Vander Poorten V, Nicolai P. ***The impact of nodal status in major salivary gland carcinoma: A multicenter experience and proposal of a novel N-classification***. Oral Oncol (epub ahead of print), 2020.

17. Schreiber A, Ravanelli M, **Ferrari M**, Mattavelli D, Rampinelli V, Bolzoni Villaret A, Bertazzoni G, Tomasoni M, Gualtieri T, Zorza I, Farina D, Maroldi R, Nicolai P. ***Early Postoperative Magnetic Resonance in the Diagnosis of Persistent Juvenile Angiofibroma***. Laryngoscope 131(8):E2436-E2441, 2020.
18. Rampinelli V, **Ferrari M**, Zorzi S, Berlucchi M. ***Treatment of congenital nasolacrimal duct cyst: the role of endoscopic marsupialisation***. Acta Otorhinolaryngol Ital 40(5):377-382, 2020.
19. Schreiber A, Ravanelli M, Rampinelli V, **Ferrari M**, Vural A, Mattavelli D, Mataj E, Mazza V, Zorza I, Bonù ML, Signorini L, Chiari E, Sorrentino T, Doglietto F, Farina D, Maroldi R, Nicolai P. ***Skull base osteomyelitis: clinical and radiologic analysis of a rare and multifaceted pathological entity***. Neurosurg Rev 44:555-569, 2021.
20. Rampinelli V, Mattavelli D, **Ferrari M**, Schreiber A, Ravanelli M, Farina D, Deganello A, Fontanella MM, Doglietto F, Nicolai P. ***Management of anterior fossa cephaloceles: an overview***. J Neurosurg Sci 65:140-150, 2021.
21. Sahovaler A, Berania I, **Ferrari M**, Ziai H, Jethwa A, Goldstein DP, de Almeida JR, Gilbert R. ***Temporal Artery Posterior Auricular Skin Free Flap for Secondary Oral Cavity Reconstruction***. Laryngoscope 131:1297-1300, 2021.
22. Sahovaler A, **Ferrari M**, Athayde J, Mendez A, Fung K, Yoo J, Nichols AC, MacNeil SD. ***Investigating the Sources of Heterogeneity in Systematic Review of Recurrence Rate after Hemithyroidectomy for Low-Risk Well-Differentiated Thyroid Cancer***. Eur Thyroid J 10:179-182, 2021.
23. Sahovaler A, **Ferrari M**, Chan H, Ziai H, Gilbert R, Irish J. ***Comparing contour restoration of mandibular body defects with fibula, iliac crest, and scapular tip flaps: a conformance virtual study***. J Oral Maxillofac Surg 79:1345-1354, 2021.
24. Vural A, Carobbio ALC, **Ferrari M**, Rampinelli V, Schreiber A, Mattavelli D, Doglietto F, Buffoli B, Rodella LF, Taboni S, Tomasoni M, Gualtieri T, Deganello A, Hirtler L, Nicolai P. ***Transorbital endoscopic approaches to the skull base: a systematic literature review and anatomical description***. Neurosurg Rev 44(5):2857-2878, 2021.
25. Gualtieri T, Verzeletti V, **Ferrari M**, Perotti P, Morello R, Taboni S, Palumbo G, Ravanelli M, Rampinelli V, Mattavelli D, Paderno A, Buffoli B, Rodella LF, Nicolai P, Deganello A. ***A new landmark for lingual artery identification during transoral surgery: Anatomic-radiologic study***. Head Neck 43:1487-1498, 2021.
26. **Ferrari M**, Migliorati S, Tomasoni M, Crisafulli V, Nocivelli G, Paderno A, Rampinelli V, Taboni S, Schreiber A, Mattavelli D, Lancini D, Gualtieri T, Ravanelli M, Facchetti M, Bozzola A, Ardighieri L, Maroldi R, Bossi P, Farina, D, Battocchio S, Deganello A, Nicolai P. ***Sinonasal cancer encroaching the orbit: Ablation or preservation?***. Oral Oncol (epub ahead of print), 2021.
27. Gualtieri T, Taboni S, **Ferrari M**, Gilbert R. ***Bioengineering for head and neck reconstruction: the role of customized flaps***. Curr Opin Otolaryngol Head Neck Surg 29:156-160, 2021.
28. **Ferrari M**, Orlandi E, Bossi P. ***Sinonasal cancers treatments: state of the art***. Curr Opin Oncol 33:196-205, 2021.
29. Sahovaler A, Chan HHL, **Ferrari M**, Gualtieri T, Zhang C, Taboni S, Irish JC, Gilbert RW. ***Objective evaluation of orbito-zygomatic reconstruction with scapular tip free flaps to restore facial projection and orbital volume***. Oral Oncol (epub ahead of print), 2021.
30. Schreiber A, Mattavelli D, Accorona R, Rampinelli V, **Ferrari M**, Grammatica A, Tomacelli GL, Verzeletti V, Fazio E, Abousiam M, Nebiaj A, Deganello A, Nicolai P, Buffoli B, Rezzani R, Piazza C, Calabrese L. ***Endoscopic-assisted multi-portal compartmental resection of the masticatory space in oral cancer: Anatomical study and preliminary clinical experience***. Oral Oncol (epub ahead of print), 2021.
31. Grammatica A, Piazza C, **Ferrari M**, Verzeletti V, Paderno A, Mattavelli D, Schreiber A, Lombardi D, Fazio E, Gazzini L, Giorgetti G, Buffoli B, Rodella LF, Nicolai P, Calabrese L. ***Step-by-Step Cadaver Dissection and Surgical Technique for Compartmental Tongue and Floor of Mouth Resection***. Front Oncol 11:613945, 2021.
32. Romani C, Bignotti E, Mattavelli D, Bozzola A, Lorini L, Tomasoni M, Ardighieri L, Rampinelli V, Paderno A, Battocchio S, Gurizzan C, Castelnuovo P, Turri-Zanoni M, Facco C, Sessa F, Schreiber A, **Ferrari M**, Ravaggi A, Deganello A, Nicolai P, Buglione M, Tomasini D, Maroldi R, Piazza C, Calza S, Bossi P. ***Gene Expression Profiling of Olfactory Neuroblastoma Helps Identify Prognostic Pathways and Define Potentially Therapeutic Targets***. Cancers (Basel) 13:2527, 2021.
33. **Ferrari M**, Cazzador D, Taboni S, Trimarchi MV, Emanuelli E, Nicolai P. ***When is a multidisciplinary surgical approach required in sinonasal tumours with cranial involvement?*** Acta Otorhinolaryngol Ital 41:S3-S17, 2021.
34. Chan HHL, Haerle SK, Daly MJ, Zheng J, Philp L, **Ferrari M**, Douglas CM, Irish JC. ***An integrated augmented reality surgical navigation platform using multi-modality imaging for guidance***. Plos One 16:e0250558, 2021.
35. Rampinelli V, Agosti E, Saraceno G, **Ferrari M**, Taboni S, Mattavelli D, Schreiber A, Tomasoni M, Gualtieri T, Ravanelli M, Buffoli B, Rezzani R, Fontanella MM, Nicolai P, Piazza C, Deganello A, Doglietto F. ***Endoscopic***

***Subtemporal Epidural Key-Hole Approach: Quantitative Anatomical Analysis of Three Surgical Corridors***. World Neurosurg 152:e128-e137, 2021.

36. **Ferrari M**, Taboni S, Carobbio ALC, Emanuelli E, Maroldi R, Bossi P, Nicolai P. ***Sinonasal Squamous Cell Carcinoma, a Narrative Reappraisal of the Current Evidence***. Cancers (Basel) 13:2835, 2021.
37. Rampinelli V, **Ferrari M**, Poli P, Lancini D, Mattavelli D, Timpano S, Redaelli de Zinis LO, Badolato R, Padoan R, Berlucchi M. ***Paranasal mucoceles in children with cystic fibrosis: Management of a not so rare clinical condition***. Am J Otolaryngol 42(6):103107, 2021.
38. Mattavelli D, Fiorentino A, Tengattini F, Colpani A, Agnelli S, Buffoli B, Ravanelli M, **Ferrari M**, Schreiber A, Rampinelli V, Taboni S, Verzeletti V, Deganello A, Rodella LF, Maroldi R, Ceretti E, Sartore L, Piazza C, Fontanella MM, Nicolai P, Doglietto F. ***Additive Manufacturing for Personalized Skull Base Reconstruction in Endoscopic Transclival Surgery: A Proof of Concept***. World Neurosurg 155:e439-e452, 2021.
39. Vural A, Carobbio ALC, **Ferrari M**, Rampinelli V, Schreiber A, Mattavelli D, Doglietto F, Buffoli B, Rodella LF, Taboni S, Tomasoni M, Gualtieri T, Deganello A, Hirtler L, Nicolai P. **Response to Letter to the Editor: Nuancing the role of transorbital endoscopic approaches in skull base surgery**. Neurosurg Rev 45(1):913-914, 2021.
40. Agosti E, Turri-Zanoni M, Saraceno G, Belotti F, Karligkiotis A, Rocca G, Buffoli B, Raffetti E, Hirtler L, Rezzani R, Rodella LF, **Ferrari M**, Nicolai P, Bresson D, Herman P, Dallan I, Castelnuovo P, Locatelli D, Fontanella MM, Doglietto F. ***Quantitative Anatomic Comparison of Microsurgical Transcranial, Endoscopic Endonasal, and Transorbital Approaches to the Spheno-Orbital Region***. Oper Neurosurg (Hagerstown) 21(6):E494-E505, 2021.
41. Muhanna N, Douglas CM, Chan HHL, Daly MJ, Townson JL, **Ferrari M**, Eu D, Akens M, Chen J, Zheng G, Irish JC. ***Rabbit VX2 head and neck squamous cell models for translational head and neck theranostic technology development***. Clin Transl Med 11:e550-554.
42. Zappa F, Madoglio A, **Ferrari M**, Mattavelli D, Schreiber A, Taboni S, Ferrari E, Rampinelli V, Belotti F, Piazza C, Fontanella MM, Nicolai P, Doglietto F. ***Hybrid Robotics for Endoscopic Transnasal Skull Base Surgery: Single-Centre Case Series***. Oper Neurosurg (Hagerstown) 21(6):426-435, 2021.
43. Sahovaler A, Chan HHL, Gualtieri T, Daly MJ, **Ferrari M**, Vannelli C, Eu D, Manojlovic-Kolarski M, Orzell S, Taboni S, de Almeida J, Goldstein D, Deganello A, Nicolai P, Gilbert RW, Irish JC. ***Augmented reality and intraoperative navigation in sinonasal malignancies: A preclinical study***. Front Oncol 11:723509, 2021.
44. Taboni S, **Ferrari M**, Daly MJ, Chan HHL, Eu D, Gualtieri T, Jethwa AR, Sahovaler A, Sewell A, Hasan W, Berania I, Qiu J, de Almeida J, Nicolai P, Gilbert RW, Irish JC. ***Navigation-guided transnasal endoscopic delineation of the posterior margin for maxillary sinus cancers: A preclinical study***. Front Oncol 11:747227, 2021.
45. Lechner M, Takahashi Y, Turri-Zanoni M, Liu J, Counsell N, Hermsen M, Kaur RP, Zhao T, Ramanathan Jr. M, Schartinger VH, Emanuel O, Helman S, Varghese J, Dudas J, Riechelmann H, Sprung S, Haybaeck J, Howard D, Engel NW, Stewart S, Brooks L, Pickles JC, Jacques TS, Fenton T, Williams L, Vaz FM, O'Flynn P, Stimpson P, Wang S, Hannan SA, Unadkat S, Hughes J, Dwivedi R, Forde CT, Randhawa P, Gane S, Joseph J, Andrews PJ, Royle G, Franchi A, Maragliano R, Battocchio S, Bewicke-Copley H, Pipinikas C, Webster A, Thirlwell C, Ho D, Teschendorff A, Zhu T, Steele C, Pillay N, Vanhaesebroeck B, Mohyeldin A, Fernandez-Miranda J, Park KW, Le Q, West RB, Saade R, Manes RP, Omay SB, Vining EM, Judson BL, Yarbrough WG, Sansovini M, Nicolini S, Grassi I, Bongiovanni A, Capper D, Schueller U, Thavaraj S, Sandison A, Surda P, Hopkins C, **Ferrari M**, Mattavelli D, Rampinelli V, Facchetti F, Nicolai P, Bossi P, Henriquez OA, Magliocca K, Solares CA, Wise SK, Llorente JL, Patel Z, Nayak J, Hwang PH, Lacy P, Woods R, O'Neill JP, Jay A, Carnell D, Forster MD, Ishii M, London Jr. NR, Bell DM, Gallia GL, Castelnuovo P, Severi S, Lund VJ, Hanna EY. ***Clinical Outcomes, Kadish-INSICA Staging and Therapeutic Targeting of SSTR2 in Olfactory Neuroblastoma***. Eur J Cancer 162:221-236, 2021.
46. Orlandi E, **Ferrari M**, Lafe E, Preda L, Benazzo M, Vischioni B, Bonora M, Rampinelli V, Schreiber A, Licitra L, Nicolai P. ***When everything revolves around internal carotid artery: analysis of different management strategies in patients with very advanced cancer involving the skull base***. Front Oncol 11:781205, 2021.
47. **Ferrari M**, Taboni S, Carobbio ALC, Buffoli B, Rampinelli V, Mattavelli D, Schreiber A, Verzeletti V, Ravanelli M, Daly MJ, Chan HHL, Sahovaler A, Franz L, Gualtieri T, Rezzani R, Maroldi R, Signoroni A, Deganello A, Irish JC, Nicolai P. ***Development of a cadaveric head and neck cancer model and three-dimensional analysis of margins in surgical navigation-aided ablations***. Eur J Surg Oncol (epub ahead of print), 2021.
48. **Ferrari M**, Zanoletti E, Taboni S, Cazzador D, Tealdo G, Schreiber A, Mattavelli D, Rampinelli V, Doglietto F, Fontanella MM, Buffoli B, Vural A, Verzeletti V, Carobbio ALC, Mardighian D, Causin F, Orlandi E, Cenzato M,

Rezzani R, Nicolai P. ***Resection of the internal carotid artery in selected patients affected by cancer of the skull base***. Head Neck 44(4):1030-1042, 2022.

49. Chan HHL, Sahovaler A, Daly MJ, **Ferrari M**, Franz L, Gualtieri T, Tzelnick S, Eu D, Manojlovic-Kolarski M, Berania I, Orzell S, de Almeida JR, Goldstein DP, Nicolai P, Gilbert RW, Irish JC. ***Projected cutting guides using an augmented reality system to improve surgical margins in maxillectomies: A preclinical study***. Oral Oncol (epub ahead of print), 2022.
50. Schreiber A, Mattavelli D, Ravanelli M, Rampinelli V, **Ferrari M**, Maroldi R, Piazza C, Nicolai P. ***In Response to Early Functional Imaging in Juvenile Angiofibroma***. Laryngoscope 132(6):E23-E24, 2022.
51. Sartore L, Pasini C, Pandini S, Dey K, **Ferrari M**, Taboni S, Chan HHL, Townson J, Viswanathan S, Mathews S, Gilbert RW, Irish JC, Re F, Nicolai P, Russo D. ***Hybrid Core-Shell Polymer Scaffold for Bone Tissue Regeneration***. Int J Mol Sci 23(9):4533, 2022.
52. Mattavelli D, Tomasoni M, **Ferrari M**, Compagnoni A, Schreiber A, Taboni S, Rampinelli V, Marazzi E, Raffetti E, Redaelli de Zinis LO, Deganello A, Maroldi R, Bossi P, Piazza C, Nicolai P. ***Salvage surgery in recurrent sinonasal cancers: Proposal for a prognostic model based on clinicopathologic and treatment-related parameters***. Head Neck (epub ahead of print), 2022.
53. **Ferrari M**, Mattavelli D, Schreiber A, Gualtieri T, Rampinelli V, Tomasoni M, Taboni S, Ardighieri L, Battocchio S, Bozzola A, Ravanelli M, Maroldi R, Piazza C, Bossi P, Deganello A, Nicolai P. ***Does reorganization of clinicopathological information improve prognostic stratification and prediction of chemoradiosensitivity in sinonasal carcinomas? A retrospective study on 145 patients***. Front Oncol 12:799680, 2022.
54. **Ferrari M**, Mattavelli D, Tomasoni M, Raffetti E, Bossi P, Schreiber A, Orlandi E, Taboni S, Rampinelli V, Gualtieri T, Turri-Zanoni M, Battaglia P, Arosio AD, Bignami M, Tartaro T, Molteni M, Bertazzoni G, Fiaux-Camous D, Jourdaine C, Verillaud B, Eu D, Nair D, Moiyadi A, Shetty P, Ghosh-Laskar S, Budrukkar A, Magrini SM, Guillerm S, Faivre S, Piazza C, Gilbert RW, Irish JC, de Almeida JR, Pai P, Herman P, Castelnuovo P, Nicolai P. ***The MUSES⁎: a prognostic study on 1360 patients with sinonasal cancer undergoing endoscopic surgery-based treatment: ⁎MUlti-institutional collaborative Study on Endoscopically treated Sinonasal cancers***. Eur J Cancer 171:161-182, 2022.
55. Alessandrini L, **Ferrari M**, Taboni S, Sbaraglia M, Franz L, Saccardo T, Del Forno BM, Agugiaro F, Frigo AC, Dei Tos AP, Marioni G. ***Tumor-stroma ratio, neoangiogenesis and prognosis in laryngeal carcinoma. A pilot study on preoperative biopsies and matched surgical specimens***. Oral Oncol (epub ahead of print), 2022.
56. Mondin A, Manara R, Voltan G, Tizianel I, Denaro L, **Ferrari M**, Barbot M, Scaroni C, Ceccato F. ***Pasireotide-Induced Shrinkage in GH and ACTH Secreting Pituitary Adenoma: A Systematic Review and Meta-Analysis***. Front Endocrinol (Lausanne) 13:935759, 2022.
57. Giammalva GR, Dell'Aglio L, Guarrera B, Baro V, Calvanese L, Schiavo G, Mantovani G, Rinaldi V, Iacopino DG, Causin F, Nicolai P, **Ferrari M**, Denaro L. ***Transnasal Endoscopic Approach for Osteoid Osteoma of the Odontoid Process in a Child: Technical Note and Systematic Review of the Literature***. Brain Sci 13;12(7):916, 2022.
58. Lechner M, Takahashi Y, Turri-Zanoni M, **Ferrari M**, Liu J, Counsell N, Mattavelli D, Rampinelli V, Vermi W, Lombardi D, Saade R, Park KW, Schartinger VH, Franchi A, Facco C, Sessa F, Battocchio S, Fenton TR, Vaz FM, O'Flynn P, Howard D, Stimpson P, Wang S, Hannan SA, Unadkat S, Hughes J, Dwivedi R, Forde CT, Randhawa P, Gane S, Joseph J, Andrews PJ, Dave M, Fleming JC, Thomson D, Zhu T, Teschendorff A, Royle G, Steele C, Jimenez JE, Laco J, Wang EW, Snyderman C, Lacy PD, Woods R, O'Neill JP, Saraswathula A, Kaur RP, Zhao T, Ramanathan Jr. M, Gallia GL, London Jr. NL, Le QT, West RB, Patel ZM, Nayak JV, Hwang PH, Hermsen M, Llorente J, Facchetti F, Nicolai P, Bossi P, Castelnuovo P, Jay A, Carnell D, Forster MD, Bell DM, Lund VJ, Hanna EY. ***International Multicenter Study of Clinical Outcomes of Sinonasal Melanoma Shows Survival Benefit for Patients Treated with Immune Checkpoint Inhibitors and Potential Improvements to the Current TNM Staging System***. J Neurol Surg B Skull Base (epub ahead of print), 2022.
59. Arosio AD, Bernasconi DP, Valsecchi MG, Pacifico C, Battaglia P, Bignami M, **Ferrari M**, Mattavelli D, Rampinelli V, Tomasoni M, Schreiber A, Gualtieri T, Piazza C, Magrini SM, Tartaro T, Molteni M, Lambertoni A, Sileo G, Bossi P, Orlandi E, Bertazzoni G, Fiaux-Camous D, Jourdaine C, Verillaud B, Herman P, Nicolai P, Castelnuovo P, Turri-Zanoni M. ***Patterns of recurrences in sinonasal cancers undergoing an endoscopic surgery-based treatment: Results of the MUSES* on 940 patients: *MUlti-institutional collaborative Study on Endoscopically treated Sinonasal cancers***. Oral Oncol (epub ahead of print), 2022.
60. Bertazzoni G, Testa G, Tomasoni M, Mattavelli D, Del Bon F, Montalto N, **Ferrari M**, Andreoli M, Morello R, Sbalzer N, Vecchiati D, Piazza C, Nicolai P, Deganello A. ***The Enhanced Recovery After Surgery (ERAS) protocol***

***in head and neck cancer: a matched-pair analysis***. Acta Otorhinolaryngol Ital 42(4):325-333, 2022.

61. Mattioli F, Serafini E, Lo Manto A, Mularoni F, Abeshi A, Lionello M, **Ferrari M**, Paderno A, Lancini D, Mattavelli D, Confuorto G, Marchi F, Ioppi A, Sampieri C, Mercante G, De Virgilio A, Petruzzi G, Crosetti E, Pellini R, Giuseppe S, Giorgio P, Piazza C, Molteni G, Bertolin A, Succo G, Nicolai P, Alicandri-Ciufelli M, Marchioni D, Presutti L, Fermi M. ***The role of adjuvant therapy in pT4N0 laryngectomized patients: A multicentric observational study***. Head Neck (epub ahead of print), 2022.

# Conferences, courses, and masters (November 2019-October 2022)

| | |
|---|---|
| • December 2nd-4th, 2019 | He participated as LECTURER and TUTOR to the course "**Joint European Diploma of Endoscopic Skull Base Surgery**" (Presidents: Prof. Castelnuovo P, Prof. Herman P, Prof. Nicolai P), in Paris (France), with the presentation entitled "***Paranasal sinus and anterior skull base anatomy with special reference to vascular anatomy***". |
| • December 6th-7th, 2019 | He participated to the course **"[Techniques of Oral Cavity Reconstruction: Myomucosal and Locoregional Flaps]"** (President: Prof. Nocini PF; Course Director: Prof. Ferrari S), in Verona (Italy). |
| • January 19th-21st, 2020 | He participated as LECTURER to the course **"[Paranasal sinuses and anterior skull base]"** (Course Directors: Prof. Presutti L, Prof. Marchioni D), in Modena (Italy), with the lecture entitled ***"Endoscopic Trans Nasal Corridors: Beyond the Sinuses"***. |
| • June 22nd, 2020 | He participated as LECTURER to the "**[2nd Master of 2nd level – Otoneurosurgery: an interdisciplinary view of skull base surgery]**" (Director: Dr. Zanoletti E), at the University of Padua, in Padua (Italy), with the lecture entitled "***[Techniques of endoscopic transnasal reconstruction and their use in complex defects of the skull base]***". |
| • October 9th, 2020 | He participated as INVITED SPEAKER and MEMBER OF THE SCIENTIFIC SECRETARIAT to the conference – webinar **"2nd International Conference Bioengineering and Cell Therapy"**, in Brescia (Italy), with the presentation entitled "***Preliminary experience with in vivo bone regeneration through bio-engineered poly-hydrogel scaffolds***". |
| • September 12th – December 31st, 2020 | He participated as LECTURER to the online course **"[Hadrontherapy and the importance of multidisciplinarity for a personalized therapy]"** (Scientific Director: Dr. Orlandi E), in Pavia (Italy), with the lecture entitled "***Multidisciplinary approach for the treatment of major salivary gland cancers***". |
| • October 13th, 2020 | He participated as LECTURER at the "**17th Master of 2nd level in aesthetic plastic surgery**" (Director: Prof. Bassetto F), at the University of Padua, in Padua (Italy), with the lecture entitled "***[Preliminary experience in bone regeneration in the animal model]***". |
| • October 15th, 2020 | He participated as LECTURER to the seminar **"[Laryngeal resections and post-surgical physiology of the hypopharyngeal-laryngeal axis]**" in the context of educational activities of the Degree Course in Speech Therapy of the University of Padua (President: Prof. Trevisi P), in Padua (Italy). |
| • January 22nd, 2021 | He participated as LECTURER to the online master **"Disease of the nose, maxillofacial area and cranial base"**, in Patras (Greece), with the lecture entitled "***Current strategies of skull base reconstruction***". |
| • May 20th, 2021 | He participated as LECTURER to the webinar **"International summer school spring webinar, ent and neurosurgeon: key partners in endoscopic transsphenoidal surgery"**, at the University of Brescia, Brescia (Italy), with the presentation "***Approaches to the cavernous sinus***". |
| • May 26th-29th, 2021 | He participated as LECTURER and SPEAKER to the congress **"[107th National Congress of the Italian Society of Otorhinolaryngology – Head and Neck Surgery]"** (President: Prof. Bussi M), in Milan (Italy). |
| • May 28th, 2021 | He participated as DISCUSSANT to the webinar round table **"[The role of hadrontherapy in the multidisciplinary management of rare diseases of the head and neck]"** (Scientific Director: Dr. Orlandi E), in Pavia (Italy). |
| • June 15th, 2021 – June 15th, 2022 | He participated as LECTURER to the online course **"[Hadrontherapy and the importance of multidisciplinarity for a personalized therapy]"** (Scientific Director: Dr. Orlandi E), in Pavia (Italy), with the lecture entitled "***Multidisciplinary approach for the treatment of major salivary gland cancers***". |
| • July 22nd-25th, 2021 | He participated as POSTER PRESENTER to the **"American Head and Neck Society 10th International Conference on Head and Neck Cancer"** (Program Chair: Dr. Rosenthal E; Conference Chair: Dr. Ferris R; President of the Society: Dr. Nathan CA), in Chicago (United States). |
| • July 25th, 2021 | He participated as LECTURER to the webinar **"[SCCH&N: recurrent/metastatic disease. How the clinical practice changed]"** (Scientific Director: Dr. Ghi MG), in |

Padua, Italy, with the presentation "***A case of locally advanced recurrence of nasal vestibule***".

• September 20th-22nd, 2021 — He participated as LECTURER to the course **"7th International Summer School «Transnasal Endoscopic Surgery: from Sinuses to Skull Base»"** (Course Directors: Prof. Fontanella MM, Prof. Nicolai P, Prof. Rezzani R), at the University of Brescia, in Brescia (Italy).

• October 26th, 2021 — He participated as LECTURER to the seminar **"[Clinical scenarios of multidisciplinary collaboration between otorhinolaryngologist and speech therapist in high-volume head and neck oncological center]**" in the context of educational activities of the Degree Course in Speech Therapy of the University of Padua (President: Prof. Trevisi P), in Padua (Italy).

• November 2nd-4th, 2021 — He participated as TUTOR to the course **"[1st Head and neck surgical anatomy course of the «Scuola triVeneta di discipline Otorinolaringoiatriche»]"** (Presidents: Prof. Nicolai P, Dr. Spinato R; Course Directors: Dr. Emanuelli E, Dr. Pelucchi S), in Verona (Italy).

• November 11th-12th, 2021 — He participated as DISCUSSANT to the congress **"[XVI national congress of the Italian Skull Base Society]"** (President: Prof. Castelnuovo P), in Varese (Italy).

• November 24th-26th, 2021 — He participated as LECTURER and TUTOR to the course "**Joint European Diploma of Endoscopic Skull Base Surgery**" (Presidents: Prof. Castelnuovo P, Prof. Herman P, Prof. Nicolai P), in Paris (France), with the presentation entitled "***Paranasal sinus and anterior skull base anatomy with special reference to vascular anatomy***".

• December 13th-16th, 2021 — He participated as LECTURER to the course **"AUORL dissection course"** (President: Dr. Scotti C), in Cremona (Italy).

• February 21st-23rd, 2022 — He participated as TUTOR to the course **"[2nd Head and neck surgical anatomy course of the «Scuola triVeneta di discipline Otorinolaringoiatriche»]"** (Presidents: Prof. Nicolai P, Dr. Spinato R; Course Directors: Dr. Emanuelli E, Dr. Pelucchi S), in Verona (Italy).

• February 21st-23rd, 2022 — He participated as INVITED SPEAKER and TUTOR to the course "**Joint European Diploma of Endoscopic Skull Base Surgery**" (Presidents: Prof. Castelnuovo P, Prof. Herman P, Prof. Nicolai P), in Paris (France), with the presentation entitled "***Endoscopic anatomy for ventral posterior skull base approaches, from tuberculum sellae to odontoid***".

• March 22nd-27th, 2022 — He participated as LECTURER to the congress "**8th World Federation of Skull Base Societies Meeting**" (Presidents: Prof. Borba LA, Dr. Landeiro JA, Dr. Misra BK, Dr. Dias F), in Rio de Janeiro (Brazil)

• April 20th-23rd, 2022 — He participated as LECTURER to the congress "**14th Congress of the European Skull Base Society**" (Presidents: Prof. Danesi G, Prof. Locatelli D), in Riva del Garda (Italy)

• May 2nd-4th, 2022 — He participated as LECTURER and TUTOR to the course "**Joint European Diploma of Endoscopic Skull Base Surgery**" (Presidents: Prof. Castelnuovo P, Prof. Herman P, Prof. Nicolai P), in Paris (France), with the presentations entitled "***Orbital anatomy in relation to skull base approaches***", "***Endoscopic endonasal anatomy of infratemporal fossa and upper parapharyngeal space***", and "***Modular approach to the infratemporal fossa***".

• May 25th-28th, 2022 — He participated as LECTURER to the congress "**108th Congress of the Italian Society of Otorhinolaryngology and Head and Neck Surgery**" (President: Prof. Paludetti G), in Rome (Italy)

• May 28th-29th, 2022 — He participated as LECTURER and TUTOR to the course "**Endoscopic transnasal skull base surgery @ Gemelli hands-on course for ENT- and neuro-surgeons**" (Directors: Prof. Galli J, Prof. Olivi A, Prof. Paludetti G), in Rome (Italy)

• June 11th, 2022 — He participated as LECTURER to the conference "**Hong Kong International Head and Neck Conference – Survivorship and Innovation**" (Chair: Dr. Chow V), in Hong Kong (Hong Kong).

• June 6th-10th, 2022 — He participated as FACULTY MEMBER and TUTOR to the course **"7th International Summer School «Transnasal Endoscopic Surgery: from Sinuses to Skull Base»"** (Course Directors: Prof. Fontanella MM, Prof. Nicolai P, Prof. Rezzani R, Prof. Piazza C), at the University of Brescia, in Brescia (Italy).

• June 23rd-24th, 2022 — He participated as LECTURER and TUTOR to the course **"[Theoretical and practical course of neuro-oncology – from the dissection laboratory to the operating room]**" (Organizers: Dr. Ius T, Dr. Panciani PP), in Brescia (Italy).

| | |
|---|---|
| • July 1st – December 31st, 2022 | He participated as LECTURER to the congress **"[Hadrontherapy and the importance of multidisciplinarity for a personalized therapy]"** (Scientific Director: Dr. Orlandi E), in Pavia (Italy), with the lecture entitled "***Multidisciplinary approach for the treatment of major salivary gland cancers***". |
| • September 22nd-23rd, 2022 | He participated as LECTURER to the online course **"[XI Annual conference of the G.L.O. ("Gruppo Lombardo Otorinolaringoiatri")]"** (Scientific Director: Prof. Piazza C), in Milan (Italy), with the lecture entitled "***Augmented Reality***". |
| • September 30th, 2022 | He participated as CASE PRESENTER to the **8th National Congress of the AIOCC ("Associazione Italiana di Oncologia Cervico-Cefalica" – Italian Head and Neck Oncology Society)**, in Bologna (Italy). |
| • September 30th – October 2nd, 2022 | He participated as LECTURER to the "**Hungarian Society of Oto-Rhino-Laryngology, Head & Neck Surgery annual congress**" (President: Prof. Tamas L), in Eger (Hungary), with the lectures entitled "***Endoscopic transnasal reconstruction of post-ablative defects: not just the naso-septal flap***" and "***Multidisciplinary, histology-driven management of sinonasal cancers: state of the art***" |
| • October 23rd-25th, 2022 | He participated as TUTOR to the course **"[3rd Head and neck surgical anatomy course of the «Scuola triVeneta di discipline Otorinolaringoiatriche»]"** (Presidents: Prof. Nicolai P, Dr. Spinato R; Course Directors: Dr. Emanuelli E, Dr. Pelucchi S), in Verona (Italy). |
| • October 29th – November 2nd, 2022 | He participated as LECTURER, CHAIR, and MODERATOR to the "**6th Congress of the Confederation of European Otorhinolaryngology - Head and Neck Surgery**" (President: Prof. Nicolai P), in Milan (Italy), within the contributes entitled "***Lateral neck cystic lesions***", "***Skull base pathologies: choosing the best approach***", "***Salivary gland surgery: basic, step-by-step video lessons***", "***What is new in the management of juvenile angiofibroma?***", "***Septal perforation from diagnosis to treatment options***", "***Future of skull base surgery***", and "***Endoscopic anatomy of the sinonasal tract and anterior central skull base***". |